2015

Potential for Geothermal Energy in Northern Louisiana: Analysis of the Subsurface Environment in Union and Morehouse Parishes

Tessa Shizuko Hermes
Louisiana State University and Agricultural and Mechanical College

POTENTIAL FOR GEOTHERMAL ENERGY IN NORTHERN LOUISIANA: ANALYSIS OF THE SUBSURFACE ENVIRONMENT IN UNION AND MOREHOUSE PARISHES

A Thesis

Submitted to the Graduate Faculty of the
Louisiana State University and
Agricultural and Mechanical College
in partial fulfillment of the
requirements for the degree of
Master of Science

in

The Department of Geology and Geophysics

by
Tessa Shizuko Hermes
B.A., Oberlin College, 2009
December 2015

Acknowledgments

I would like to thank my advisors, Drs. Barb Dutrow and Jeff Nunn, for their support, guidance, and patience throughout this endeavor. Dr. Dutrow was the on-campus representative for my advising team, meeting with me at least once a week to discuss my work, progress, and to answer any questions I might have either in person or via email. Dr. Nunn, the remote partner in my advising team, made the drive from Houston to Baton Rouge several times to meet in person to discuss my progress and attend Thesis Committee meetings, and was otherwise available for consultation via email or telephone. I would also like to thank Dr. Karen Luttrell for serving on my Thesis Committee, as well as her advice and support throughout my time at LSU. I am grateful to Dr. Jeff Hanor for answering any questions I sent his way, providing several pieces of reference material, and guiding me in the use of Surfer® software. C. Alex Holston, Undergraduate Researcher, must be acknowledged for his tireless and accurate mining of formation top data from SONRIS. This research was made possible by a grant from the Louisiana Board of Regents, a scholarship from the Southeastern Geophysical Society of New Orleans, and a Geological Society of America Graduate Student Research Grant.

Table of Contents

List of Tables

List of Figures

Abstract

Efforts to mitigate greenhouse gas emissions and reduce dependence on fossil fuels have led to renewed focus on the exploration and development of alternative energy production. One such option is hydrothermal binary geothermal energy production from geothermal reservoirs with temperatures of at least 100 °C at depths no greater than 5 km. In the U.S., such systems have the potential to provide 5,400 % of 2013 total U.S. energy consumption. This study evaluates the potential for geothermal energy systems implementation in Morehouse and Union Parishes, Louisiana, by using publicly available bottom hole temperature (BHT), mud weight (MW), logged formation top depth, and produced brine chemistry data to characterize subsurface conditions. Based on 278 corrected BHT data from 231 wells, geothermal gradients in the study area were found to range from 17.02 to 49.79 °C/km, with an averaged linear geothermal gradient of 30.87 °C/km. West-central Morehouse Parish presents the highest geothermal gradients in the study area, averaging 41.01 °C/km, while Union Parish presents geothermal gradients averaging 31.64 °C/km. The onset of overpressure at approximately 2.82 km, based on 88 MW data, corresponds to the average depth of Upper Jurassic Cotton Valley sediments and is below the 2.42 km average depth to 100 °C. Results from this study indicate that there is potential for implementation of two types of hydrothermal binary geothermal energy production systems. Union Parish would be best considered for geothermal energy production from co-produced fluids, as it hosts wells placed in deeper, hotter hydrocarbon reservoirs that are currently in production and development. West-central Morehouse Parish would be best considered for enhanced geothermal systems development, as it presents the highest geothermal gradients.

Introduction

Total United States (U.S.) energy consumption in 2013 was 102.5 EJ, with 81 % of that energy derived from fossil fuels and 8 % from renewables. Efforts to mitigate GHG emissions and reduce dependence on fossil fuels have led to renewed focus on the exploration and development of renewables. The U.S. Energy Information Association (U.S. EIA) uses the term "renewables" to refer to geothermal, wind, solar, biomass, municipal solid waste and landfill gas (MSW/LFG), and hydropower (U.S. EIA 2015). Of the renewable resources available within the U.S., hydrothermal binary geothermal energy production offers the smallest total amount of life-cycle greenhouse gas (GHG) emissions per kWh (e.g. Sullivan and Wang 2013).

Hydrothermal binary is one of two types of geothermal energy production systems, the other being hydrothermal flash. Hydrothermal flash and binary production systems are applied to high- and low-temperature geothermal systems, respectively. High-temperature geothermal systems have reservoir temperatures above 200 °C, while low-temperature geothermal systems are defined by reservoir temperatures below 150 °C (GTO 2015). Tester et al. (2006) report that the economic limits of low-temperature geothermal systems are reservoir temperatures of 100 °C at 5 km depth. Considering that the average geothermal gradient of continental crust is 25 to 30 °C/km (Tester et al. 2006), the potential for development of low-temperature geothermal resources exists across many regions in the U.S., whereas high-temperature geothermal systems are more limited in extent (e.g. tectonic plate boundaries, volcanic activity, near-surface magma, etc.).

The three necessary components of a geothermal system are heat, fluid, and permeability (GTO 2015). Heat is transported from within the Earth to the surface, in part, via fluid, which flows through permeable rock. Methods for power production depend primarily on the heat content of the fluid because it is possible to engineer fracture permeability and introduce fluid to

a geothermal reservoir using Enhanced Geothermal Systems (EGS) techniques. When fracture permeability is engineered, the limits of an EGS reservoir are determined by the extent of this fracture network, through which the primary fluid flows from injection to production wells. EGS can utilize natural geothermal fluid at depth, injected wastewater, or CO_2 as its primary fluid (GTO 2015). The maximum recoverable EGS resource base is estimated at 5.6 x 10^6 EJ (Tester et al. 2006).

Geothermal resources generated only 0.056 EJ in 2012 and 0.059 EJ in 2013, with a projected generation of 0.096 EJ for 2020 (US EIA 2015; Table 1). Thus, identifying potential low-temperature geothermal reservoirs within the United States is essential for decreasing the production of GHGs and reliance on fossil fuels.

Table 1. Potential for low-temperature geothermal systems to provide for U.S. energy needs.

2013	Exajoules (EJ)
[1]Total geothermal energy generation:	0.059
[1]Total U.S. energy consumption:	102.488
[2]Maximum recoverable EGS resource base:	5,600,000.000

1 (U.S. EIA 2014), 2 (Tester et al. 2006)

A recent U.S.-specific multi-criteria decision analysis (MCDA) of the sustainability of utility-scale electricity generation options ranks both flash and binary geothermal, alongside biopower, as the most sustainable sources of energy (e.g. Klein and Whalley 2015). The binary method allows production of reliable emission-free power from reservoirs with temperatures as low as 100°C (e.g. Tester et al. 2006). Binary cycle power production systems operate as a closed-loop system that utilizes two working fluids: one primary and one secondary (Figure 1). The Earth heats a primary fluid at depth, which is then either pumped to the surface or driven naturally to the surface by the force of an overpressured reservoir or buoyancy. The primary fluid

is used at surface for heat transfer to a secondary, or binary, fluid. Binary fluids, typically refrigerants, must have a lower boiling point than water in order to flash to vapor as a result of this heat exchange. The vapor then drives a turbine-generator, producing electricity (e.g. Reinhardt 2013).

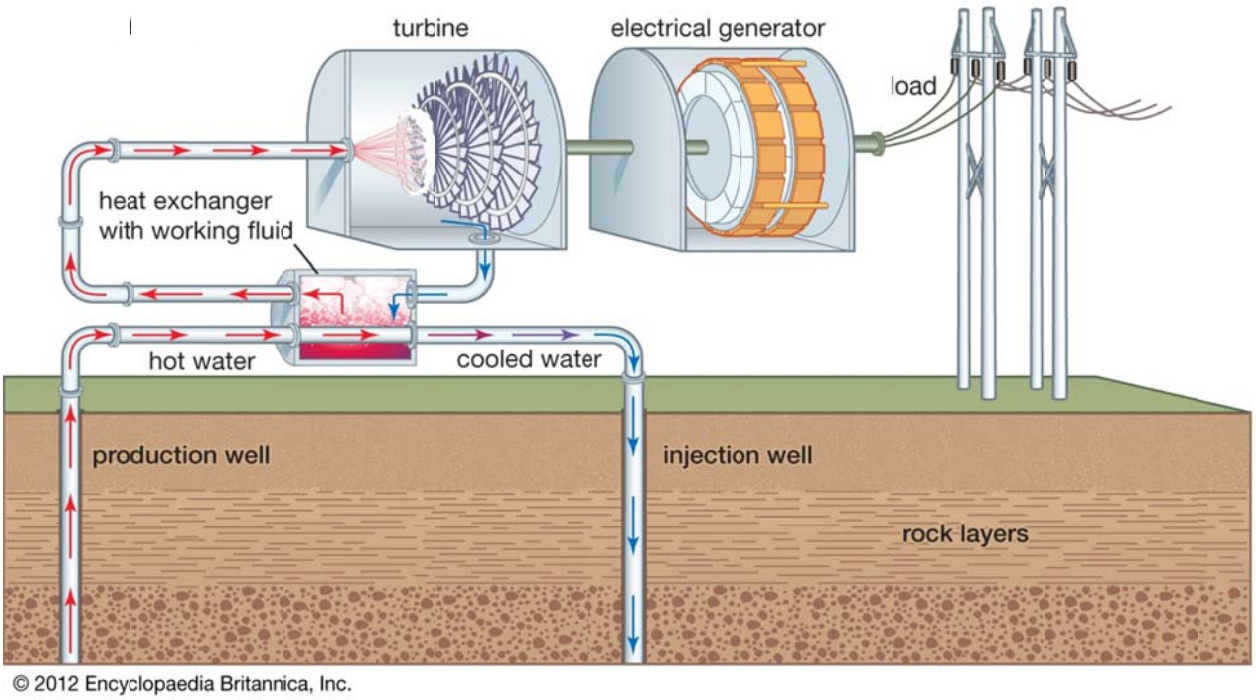

Figure 1. Simple illustration of a typical closed loop binary cycle geothermal power production system. Primary fluid (e.g. hot water) is brought from within the Earth to heat a binary fluid in a heat exchanger, which flashes to steam, driving a turbine to produce electricity. After heat exchange, the cooled water is injected into the geothermal reservoir to begin the cycle again.

These closed loop systems also offer solutions for wastewater disposal from oil and gas production. In some oil and gas wells, ten or more barrels of water are produced for every barrel of oil or gas. Many wells are shut in because the costs of operation and wastewater disposal outweigh the value of the produced hydrocarbons (Tester et al. 2006). Binary cycle technology

allows the generation of geothermal electricity from coproduced wastewater, offering the potential to make otherwise uneconomic oil and gas wells economic (GTO 2015).

The majority of geothermal electricity generation in the United States is sourced from high-temperature geothermal systems in the West, such as The Geysers Geothermal Field in Sonoma and Lake Counties, California, which has a reservoir temperature range of 260-316 °C and an average well depth of 2.6 km (Calpine Corporation 2012). These high-temperature system reservoirs are defined by temperatures above 200 °C, and have fluid at depth with natural permeability allowing sufficient flow of geothermal fluids. Such locations are not widely available in the United States.

Low-temperature geothermal systems are defined as having temperatures below 150 °C and, unlike high-temperature reservoirs, potential exists across the United States for the development of low-temperature geothermal systems by the creation of enhanced – or engineered – geothermal systems (EGS), geothermal power coproduction from active wells' wastewater, redevelopment of uneconomic oil and gas fields as geothermal fields, and direct use of geothermal fluids for heating and cooling on a municipality-wide scale (GTO 2015). Low-temperature EGS must present temperatures above 100 °C, the boiling point of freshwater at 1 bar of pressure, ideally between 1 and 5 km depth. Shallower than 1 km, groundwater is more likely to be involved in near-surface hydrologic cycles. The maximum depth limit of 5 km is because drilling deeper than 5 km is not economic for most low-temperature geothermal systems (GTO 2015).

When identifying geographic areas for geothermal energy potential, a reliable starting point is investigation of areas with elevated surface heat flow, which can be an indicator of

elevated geothermal gradients and higher temperatures at shallow depths. Average surface heat flow of continental crust is 59 mW/m^2 (e.g. Tester et al. 2006). The most recent surface heat flow map of the United States shows an area of surface heat flow consistently above 65 mW/m^2 in north-central Louisiana (Blackwell and Richards 2011). Some of the highest surface heat flow values here (75-80 mW/m^2) appear in Union and Morehouse Parishes, Louisiana (Figure 2). These values range from 10 to 36 % above the average for continental crust.

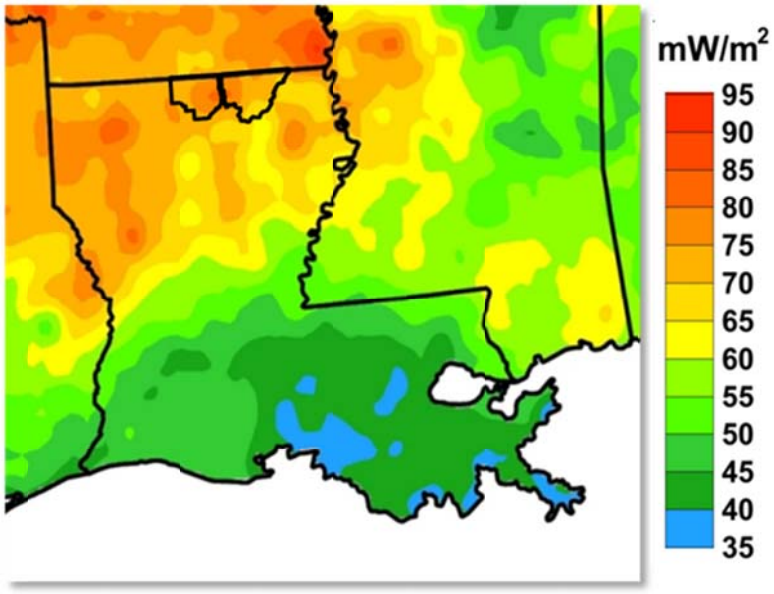

Figure 2. Surface heat flow map taken from Blackwell and Richards (2011). Union (left) and Morehouse (right) Parishes are outlined within Louisiana. Note the area of higher heat flow shared by the two Parishes.

It is also apparent in Figure 2 that there are areas of anomalously high surface heat flow in northwest Louisiana and northeast Louisiana. D'Aquin (2010) focused on the part of the northwestern anomaly that coincides with Bossier Parish. His findings included the determination of onset of geopressure, evidence of a reservoir cap, at approximately 2.75 km depth and a linear geothermal gradient of 35 °C/km for south Bossier Parish. D'Aquin's findings complement Puckette's (2009) determination of the onset of geopressure at between 2.7 and 3.0

km in northern Louisiana. The presence of geopressure is not a requirement for the development of EGS, but it can indicate the top of a section of increased porosity and coincide with an increased geothermal gradient (Jones 1969). The work presented here evaluates the potential for geothermal energy systems in north-central Louisiana, focusing on Union and Morehouse Parishes, by investigating subsurface conditions to determine if sufficient heat energy exists to provide temperatures of at least 100 °C at depths shallower than 5 km, and also determines the existence of geopressure.

Geologic Setting

Northern Louisiana lies within the Inner Gulf Coastal Plain (e.g. U.S. Army Corps of Engineers 2010) and the Gulf of Mexico Basin (Figure 3). This northern edge of the Gulf of Mexico Basin marks the Eastern bound of a failed rift system that extends West and South adjacent to the Gulf Coast (e.g. Johnson 1958). Notable structural features in this region are the North Louisiana Salt Basin and The Monroe Uplift, located at the northern edge of the Gulf of Mexico basin on the easternmost edge of the Arkansas fault zone (Figure 3), coincides with the area of highest surface heat flow in northeast Louisiana, which Morehouse and Union Parishes split (Figure 2). The Parishes lie between the salt diapir provinces of North Louisiana and Mississippi, with Union Parish bordering the northern edge of the North Louisiana Salt basin (Figure 3).

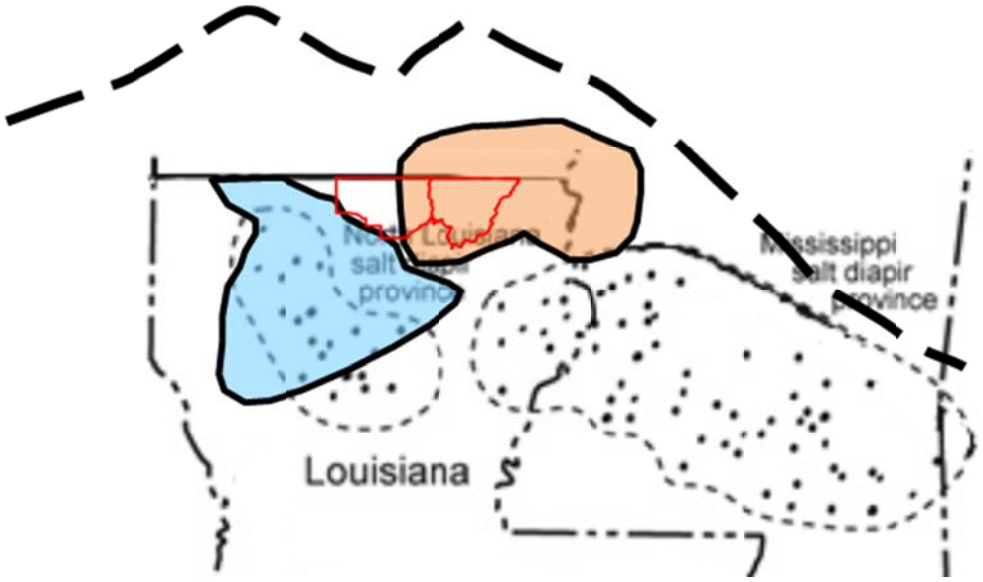

Figure 3. Heavy black dashed line marks the Northern limit of the Gulf of Mexico Basin; light dashed black outlines define the North Louisiana and Mississippi salt diapir provinces, with diapirs indicated as black dots; light blue shape is the North Louisiana Salt Basin; light orange shape is the Monroe Uplift; and Union (left) and Morehouse (right) Parishes are outlined in red (modified from Jackson and Galloway 1984, Li 2006, and Galloway 2009).

The Monroe Uplift has experienced several episodes of uplift and erosion, with its most recent episode of uplift occurring in the Eocene (e.g. Johnson 1958). Evidence of pre-Eocene uplift is presented by a series of arcuate, elongated gravity minima interpreted as evidence of crustal attenuation during Triassic and Jurassic rifting. These rift areas cooled, subsided, filled with sediment, lithified, and were subsequently faulted and subjected to igneous intrusions as well as intrusions of salt bodies (e.g. Kruger and Keller, 1986). Figure 3 shows that although salt diapirs exist within this region, they did not develop in Morehouse or Union Parishes.

It is estimated that more than 2 km of sediment were eroded during the Cretaceous, resulting in an unconformity between the top of the Cotton Valley group sandstone formations and base of the overlying Hosston fine-grained sandstone (Figure 4). This unconformity acts as a trap in some Cotton Valley hosted hydrocarbon reservoirs in the region (Johnson 1958). Within Union and Morehouse Parishes, the target Cotton Valley sandstone packages are the gas bearing Blanket and Massive Sandstones, as well as the Updip Cotton Valley section that bears oil and gas. Deposition of the Cotton Valley group occurred during a time when the Monroe Uplift was not a positive structural feature (Dyman and Condon 2006).

The Cotton Valley sand packages are not the only thick, laterally extensive targets for hydrocarbon production in this region. The underlying Bossier Shale, also a member of the Cotton Valley group, and Smackover formations have been explored and developed as well (e.g. Collins 1980 and Goddard et al. 2008). The thickness of the sediments between the Cotton Valley and Smackover tops is approximately 1 km in Union and Morehouse Parishes (Dyman and Condon 2006). The deepest wells in Union and Morehouse Parishes were drilled to produce from the Upper Smackover, and the shallowest wells were drilled to produce from the Monroe

Gas Rock, an Upper Cretaceous shallow platform carbonate approximately 40 m thick, which overlies a late Cretaceous unconformity (Washington 2004).

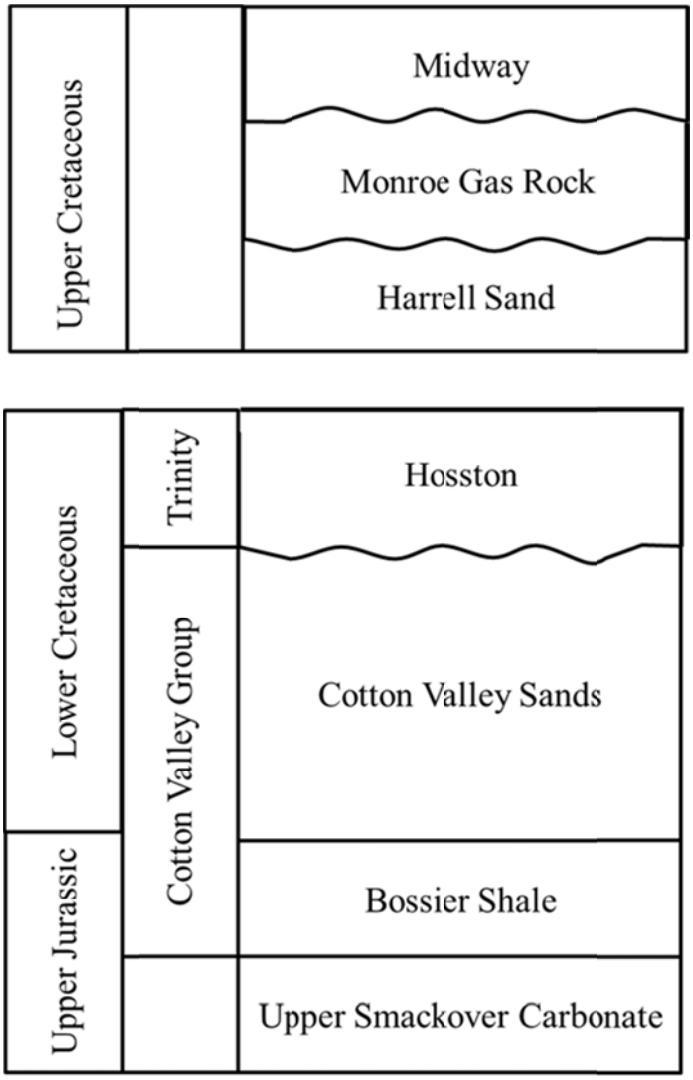

Figure 4. Simplified stratigraphic column for Union and Morehouse Parishes, Louisiana. The Upper Smackover Carbonate, Cotton Valley Sands, and Monroe Gas Rock are the most extensively developed oil and gas target formations.

The Upper Smackover is a laterally extensive blanket ooid grainstone, ranging in thickness from 91-122 m and covering an area of at least 10,400 km^2. Reservoirs within the Smackover are associated with stratigraphic traps, with diagenesis as the likely dominant control on porosity variation from the northeast to the southwest (e.g. Moore and Druckman 1981). The

producing zones of these reservoirs generally have 15-20% porosity with water saturation up to 65% (Collins 1980). Thermal conductivity of a rock depends mainly on mineralogy, porosity, and fluid content. Thus, water saturation and formation fluid chemistry can alter the thermal conductivity of a reservoir. For example, the thermal conductivity of limestone decreases linearly with increasing porosity if the pores are filled with air, but thermal conductivity of the rock can be increased by water saturation (Brigaud and Vasseur 1989). Further affecting the thermal conductivity within a reservoir is the chemistry of the pore fluid; thermal conductivity of water decreases with increasing salinity (e.g. Sharqaway et al. 2010).

Methods

Extensive exploration and development of the Monroe Gas Rock, Cotton Valley group, and Smackover formation for liquid and gas hydrocarbons in northern Louisiana has produced a considerable amount of data for the subsurface environment and physical properties of these formations. Accessing data that is available to the public for Morehouse and Union Parishes allowed bottom hole temperature (BHT), mud weight (MW), and fluid chemistry of produced brines to be used to assess the potential for production of geothermal electricity. If such potential exists in these Parishes, it could open the possibility for development of geothermal power production.

A metadata set containing geothermal data for oil and gas wells in Louisiana is available through the National Geothermal Database, but was received directly from its author, Brian Harder of the Louisiana Geological Survey, for use in this study. Raw data for BHT and MW were extracted from this metadata set (Harder 2013) and used to calculate corrected BHT (T_c), geothermal gradient, depth to 100°C, depth to 150°C, expected temperatures at 5 km depth, hydrostatic pressure, and geostatic ratio (Appendices A and D). The information contained in the metadata set was sourced from the Louisiana Department of Natural Resources SONRIS database well history files.

Two ways of reporting depth in the oilfield are measured depth (MD) and true vertical depth (TVD), either of which can be converted to a depth subsea (SS) by subtracting the elevation at zero depth. MD is the actual length of the wellbore and TVD is the well's surface-hole elevation minus its bottom-hole elevation. The majority of depths reported in the metadata used for this study are MD, not TVD, and none were reported as SS. The difference between MD and TVD in vertical wells is, for example: A vertical well drilled to 1.34 km MD with a steady

5° deviation from vertical and a consistent azimuthal direction will have a TVD only 0.01 km less than the resulting MD. All wells considered in this study were reported as vertical wells, which means that while drilling was in progress surveys were performed to determine the well's deviation from vertical, and efforts were made to keep this deviation as close to 0° as possible. Therefore, all reported depths are treated as TVD in this study.

It is also important to note that the depths reported and used in this study were not consistently identified in well documents as being Kelly bushing elevation or ground level elevation referenced measurements, which are referred to as KBMD or GLMD, respectively, in the oilfield. Thus, this study did not adjust for KB height, which is most often reported in these documents as being between 11 and 25 ft (0.003-0.008 km) above GL, and has a negligible effect on this study's calculations.

Bottom-hole temperature (BHT)

BHTs extracted from the metadata were corrected for the cooling effect of drilling fluid circulation (Appendix A). Drilling fluid is utilized to maintain wellbore stability, as well as to cool and lubricate the drill bit as it progresses through the subsurface. In 1971, the Geothermal Survey of North America project group developed a statistically-determined third order empirical equation (Equation 1) based on data from 336 wells located in south Louisiana and 266 from west Texas, to correct for this cooling effect (Kehle 1972):

$$T_E = T_L - 8.819\text{x}10^{-12}\, D^3 - 2.143\text{x}10^{-8}\, D^2 + 4.375\text{x}10^{-3}\, D - 1.018$$

(Equation 1)

Where $T_E \equiv$ equilibrium temperature (°F), $T_L \equiv$ BHT (°F), and $D \equiv$ BHT depth (ft)

T_E was calculated for all reported BHTs and then converted to °C, which is hereafter defined as T_c. Although reported BHTs themselves can have errors of +/- 5 °C (Blackwell and

Richards 2011), the Kehle-corrected T_c is representative of the actual temperature at depth, and the temperature correction factor increases with depth up to 3.68 km, after which it begins to decrease (Kehle 1972). The Kehle correction was chosen for this study over the correction introduced by Harrison et al. (1983) because the Harrison correction is based on a majority of wells located in Oklahoma, whereas the Kehle correction is based on a majority of wells in Louisiana. It should also be noted that the Harrison correction is unreliable at depths greater than 3.05 km (Harrison et al. 1983), whereas the Kehle correction is reliable up to at least 4 km depth (Kehle 1972).

To determine geothermal gradient for each well, it is necessary to determine if change in T_c with depth is linear. For several wells there were multiple associated T_c's, reported at varying depths. For these wells, the geothermal gradient was determined by establishing a line of best fit anchored to a mean annual surface temperature (MAST) of 20 °C (Figure 5). After establishing the geothermal gradient for each well, those that exhibited gradients above 80 °C/km or below 10 °C/km were assumed to be erroneous and eliminated from further study, as in Weides and Majorowicz (2014).

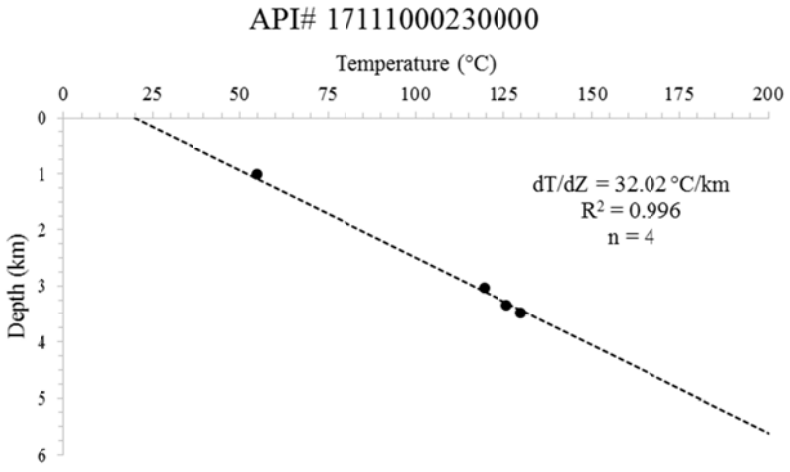

Figure 5. An example of temperature plotted against depth for a well with multiple T_c's. An R^2 value nearing 1 indicates that a linear geothermal gradient is a reliable assumption. Lines of best fit were anchored to 20 °C MAST.

For wells with only one BHT, the geothermal gradient (dT/dZ) was calculated as:

$$dT/dZ = (T_C\text{-}20°C)/D_{km} \quad \text{(Equation 2)}$$

Where T_C is the Kehle-corrected BHT in degrees Celsius, 20°C is the assumed mean annual surface temperature (as in Blackwell and Richards 2011), and D_{km} is the depth of T_c in kilometers.

Depth to 100 °C and 150 °C isotherms was either extrapolated or interpolated based on the maximum T_c for that well (Equations 3a and 3b). For example, if the maximum T_c in a well is above 100 °C, the depth to 100 °C is interpolated. If not, the depth to 100 °C is extrapolated. The same is true for depth to 150 °C.

$$Z_{100} = 80 / (dT/dZ) \quad \text{(Equation 3a)}$$

$$Z_{150} = 130 / (dT/dZ) \quad \text{(Equation 3b)}$$

Where a mean annual surface temperature of 20 °C has been incorporated, Z_x = depth to x °C isotherm, and dT/dZ = calculated geothermal gradient.

A plot of multiple T_c against depth enables the identification of possible changes in geothermal gradient with depth as well as the averaged geothermal gradient for the Parishes. The mean annual surface temperature (MAST) of Union and Morehouse Parishes was assumed as 20°C (Blackwell and Richards 2011), and the slope of a line of best fit to all T_c, anchored to MAST, was established as the average geothermal gradient for the study area. Uncorrected BHT, in °C, was plotted against depth as well, in order to observe the difference between corrected and uncorrected values.

Isothermal surfaces of 100 °C and 150 °C were mapped and contoured with Surfer® 7.0 using the natural neighbor gridding algorithm, as were all other contour maps in this study. The natural neighbor gridding algorithm was chosen because it does not extrapolate values beyond the limits x, y, or z found in the source data and, when compared with other gridding algorithms

offered by Surfer®, results in the most accurate contours for large data sets with inconsistent data density (Golden Software 2002). Also, unlike kriging, the natural neighbor method does not combine the high points of a surface into a ridge or other unified body, but will leave these highs as individual high points for the mapper to vet and potentially contour by hand. Blackwell and Richards (2011) used Surfer's® minimum curvature gridding algorithm to contour their surface heat flow map. This is because their data was relatively less dense and covered a significantly larger geographic area than the data here associated with only Union and Morehouse Parishes. The spatial resolution of thermal anomalies in Morehouse and Union Parishes is too fine for the application of the minimum curvature algorithm.

In order to determine whether temperatures above 100 °C consistently occur at 5 km depth, temperature at 5 km depth was calculated using Equation 4 and used to create a temperature contour map.

$$((5\text{ km}) \times (dT/dZ)) + 20 = T_5$$

(Equation 4)

Mud weight (MW)

While drilling, wellbore stability is maintained by adjusting the density of drilling fluid. This ensures that hydraulic pressure exerted by the contents of the wellbore either equals or slightly exceeds the natural pore fluid pressure at depth. Drilling fluid density is known as mud weight (MW), and the conversion from MW to equivalent pore fluid pressure at depth is as follows, with pressure in Pascals (Pa):

$$\text{Pressure} = 119.826427 \cdot MW \cdot g \cdot z$$

(Equation 5)

Where Pressure ≡ equivalent pore fluid pressure at depth (Pa), MW ≡ mud weight (lbs/gal), g = 9.8 m/s^2, z ≡ depth (m) of MW measurement, and 119.826427 converts lbs/gal to kg/m^3.

This study treats this indirect measurement of pore fluid pressure as direct, such that "equivalent pore fluid pressure" is shortened to "fluid pressure". When plotted against depth, this fluid pressure data can reveal changes in hydrostatic gradient if the data do not follow a linear equation of best fit (e.g. Hanor 1987). An average fluid pressure gradient across Union and Morehouse Parishes was established as the slope of a best fit line anchored to surface.

Geostatic ratio is the ratio of the observed fluid pressure at depth to the overburden for that depth (Jones 1969). Overburden is the pressure exerted by overlying sediments and fluids together. Although geostatic ratio is unitless, if two assumptions are made, the ratio of fluid pressure (kPa) to depth (m) can be used as a proxy for geostatic ratio. These assumptions are an average formation fluid density of 1.04 g/cm^3 and an average bulk rock density of 2.3 g/cm^3. The assumption for fluid density is derived from the Gulf Coast region's 10.2 kPa/m hydrostatic gradient, which relies on a fluid density of 1.04 g/cm^3. An overburden pressure gradient can be calculated as 22.5 kPa/m if a bulk rock density of 2.3 g/cm^3 is assumed. If the fluid density and bulk rock density are much different than 1.04 and 2.3 g/cm^3, respectively, then the geostatic ratio cannot be assumed as the numerical equivalent of P(kPa)/D(m) (Hanor 1987). The utility of geostatic ratio comes from the relationship between hydrostatic pressure and overburden. Overburden relies on the pressure of the grains upon each other. If pore fluid pressure (numerator) increases disproportionately with overburden pressure (denominator), the geostatic ratio will increase non-linearly with depth. This departure from linearity indicates either a change in lithology (e.g. an increase in porosity, mineralogy, or permeability with depth), temperature (a cause of pore fluid expansion), or formation fluid chemistry (salinity).

Historically, in the Gulf Coast region, geostatic ratios greater than 10.52 kPa/m define what is known as geopressure and indicate the presence of a reservoir cap or seal (e.g. Jones 1969). However, due to the tendency of MW to be slightly higher than is necessary to match the natural pore fluid pressure at depth, fluid pressure calculated with Equation 5 can be greater than the actual fluid pressure at depth and MW-based geostatic ratios may be higher than what is defined as geopressure. Understanding of the error associated with MW-derived fluid pressures compared to actual fluid pressures at depth is not established in the literature. Despite this, converting the calculated fluid pressures into geostatic ratio allows for the establishment of a median geostatic ratio, standard deviation of the data, and compartmentalization of hydrostatic pressure zones within the depth range studied. The occurrence of these zones can be compared with changes in lithology, temperature gradient, or fluid chemistry to examine the cause of the observed changes in fluid pressure gradient. In such cases, a departure from a linear increase in geostatic ratio with depth, in addition to being higher than 10.52 kPa/m, can be indicative of a confining layer or seal which has resulted in a geopressured reservoir.

Fluid Composition

Changes in geothermal gradient and fluid pressure are influenced by formation fluid chemistry. In addition, geothermal fluids can contain elements with mining value, as well as mineral precipitates that form scale in the reservoir, down hole, and in equipment at surface. Therefore, chemistry of produced brines data (Appendix F) are sourced from the U.S. Geological Survey National Produced Waters Geochemical Database (Blondes et al. 2015). Samples in this data set were sourced from brines associated with oil and gas production and did not include data from previous studies, found in the literature. Wells with a charge balance error (CBE) greater than 5% were not considered for further analysis.

Concentration of total dissolved solids (ppm) was plotted against depth (km) to observe changes in salinity with depth, and the average salinity of the produced brines was used to confirm that the use of P(kPa)/D(m) as a proxy for geostatic ratio is appropriate for the study area. Concentrations of major ions are also noted (Appendix F).

Formations at Depth

A primary control on geothermal gradient and formation fluid pressure is lithology. Extensively explored and developed hydrocarbon bearing reservoirs in Union Parish include the Upper Smackover carbonate and multiple Cotton Valley sand packages. In Morehouse Parish, the major hydrocarbon bearing formation targeted for oil and gas development is the Monroe Gas Rock. The depths at which a wellbore encountered the tops of the Smackover, Cotton Valley and Monroe Gas Rock were sourced from Driller's and Geologist's Logs in well history files available through the LDNR's SONRIS database (Figure 6). Because the potential for geothermal energy systems is found within 5 km of the land's surface, formation tops were mapped and contoured as depth from surface, not structure in depth sub-sea, contours after conversion to kilometers from feet.

The error range associated with formation top depths reported in this study is not well constrained. This is because the physical source of data is inconsistently reported. If reported formation tops are picked by the geologist by gamma data, or by the driller using drilling parameters, the error is likely to be no more than 1-5 ft (0.3-1.5 m). If the reported formation tops are picked using cuttings, error might range from 1-30 ft (0.3-9.1 m) depending on the length of stands (i.e. how often fluid circulation is stopped in order to make pipe connections),

proper calculation of lag time (how long it takes the cuttings to reach the surface after being dislodged from the formation by the drill bit), or and skill level of the person reporting.

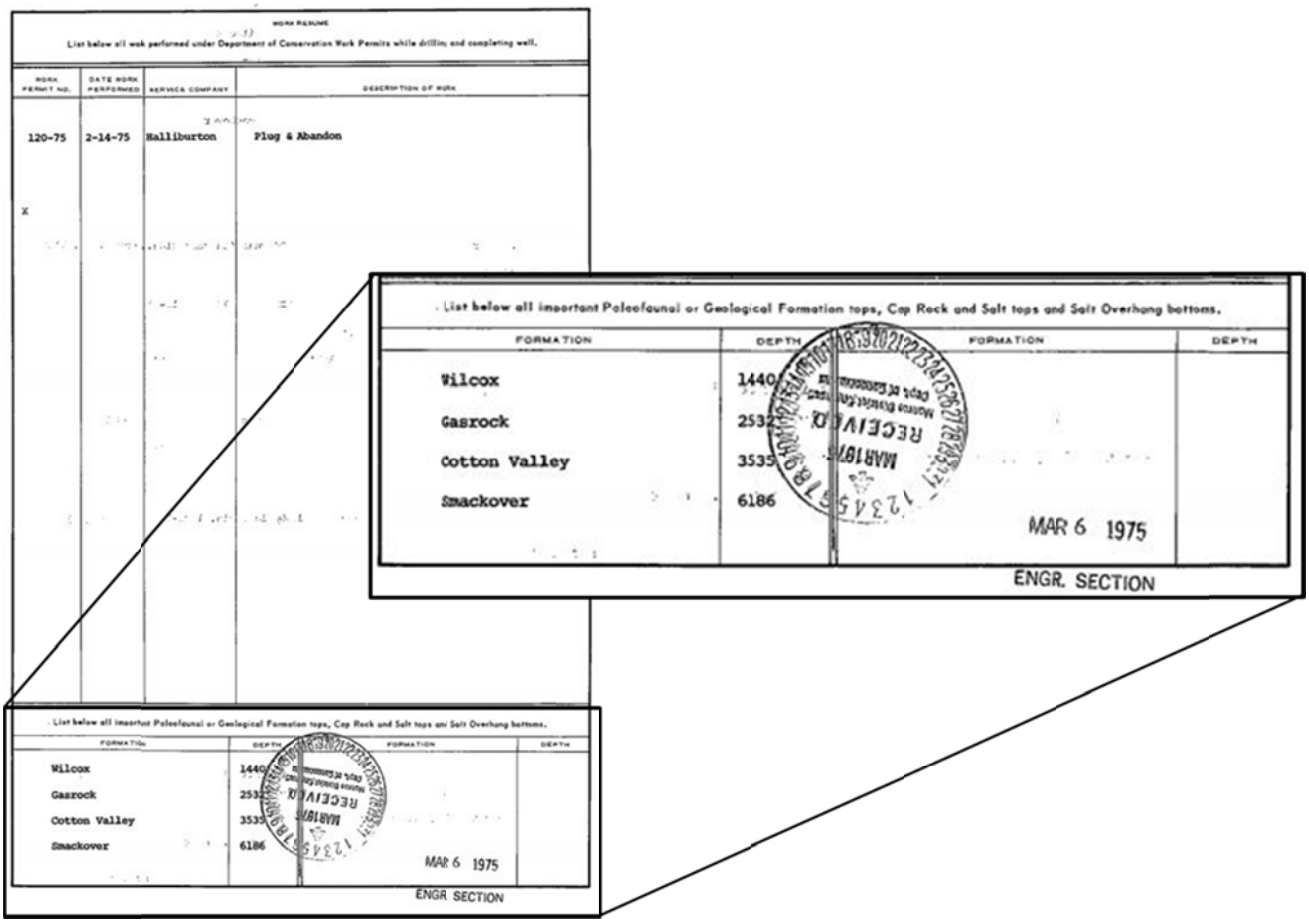

Figure 6. Scan of a Geologist's log with formation names and depths in well API#17067206960000, in Morehouse Parish. This log reports the Cotton Valley top at 3,535 ft and the Smackover top at 6,186 ft (LDNR 2015).

Results

To evaluate geothermal potential, the metadata (Harder 2014)-derived well data for Morehouse and Union Parishes was checked for duplicate well data, resulting in an initial data set of 280 bottom hole temperatures (BHTs) and 88 mud weights (MWs) from 233 individual wells. Further analysis excluded wells with geothermal gradients above 80 °C/km and below 10 °C/km, resulting in a refined data set of 278 T_c derived from 231 individual wells, and a well distribution of 19.35 km^2/well (United States Census Bureau 2010). The number of MW data was not influenced by the exclusion of wells with erroneous geothermal gradients.

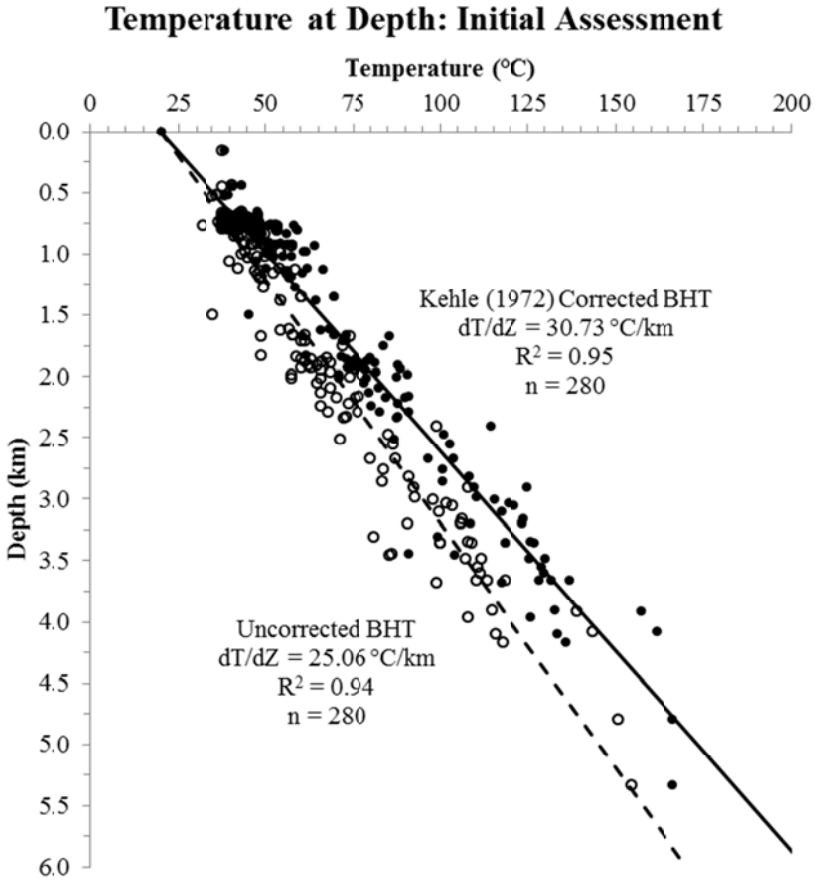

Figure 7. Increasing effect of the Kehle correction with depth can be seen in the increased distance between the data sets, and the overall effect of the correction is expressed in the higher geothermal gradient (dT/dZ) of the Corrected BHTs when compared to that of the Uncorrected BHTs. Uncorrected BHTs are represented by open circles and Corrected BHTs (T_c) by solid circles. The lines of best fit are anchored to 20 °C MAST.

Temperature

The Kehle correction (Equation 1) was applied to the 280 BHTs. The resulting T_c are compared to the uncorrected BHTs in Figure 7. Differences between corrected and uncorrected BHTs range from 0.68–18.42 °C, with larger differences as depth increases. Based on these data, the average geothermal gradient for Union and Morehouse Parishes is 25.06 °C/km using uncorrected BHT values, and rises to 30.73 °C/km after correcting for the cooling effect of drilling fluid.

The number of T_c's per well range from one to six. Well temperature profiles, also anchored at MAST, were created for the 26 wells with more than one T_c (Figure 8; full data in Appendix B). The depth of T_c in these wells ranges from 0.44 to 5.33 km, with the range of T_c being 38.55–166.51 °C. Although the deepest T_c has the highest temperature, the shallowest well does not have the lowest T_c. A line of best fit was used to establish a linear geothermal gradient for each well, with R^2 values for the lines of best fit ranging from 0.42 to 0.99.

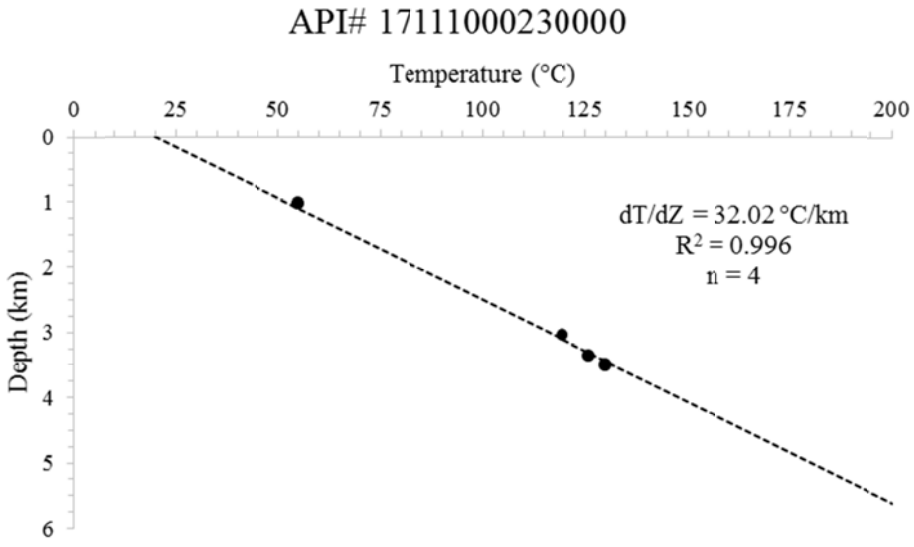

Figure 8. A line of best fit, anchored to 20 °C MAST, was used to determine linear geothermal gradients for wells with multiple T_c. Plots for analysis of the remaining 25 such wells may be found in Appendix B.

Plotting the 278 T_c against depth results in a linear best fit equation with an R^2 value of 0.96 (Figure 9). Figure 9 and the well profile plots (Appendix B) confirm that a linear geothermal gradient is an appropriate assumption for the 231 wells. The averaged linear geothermal gradient for the study area as a whole is 30.87 °C/km (Figure 9).

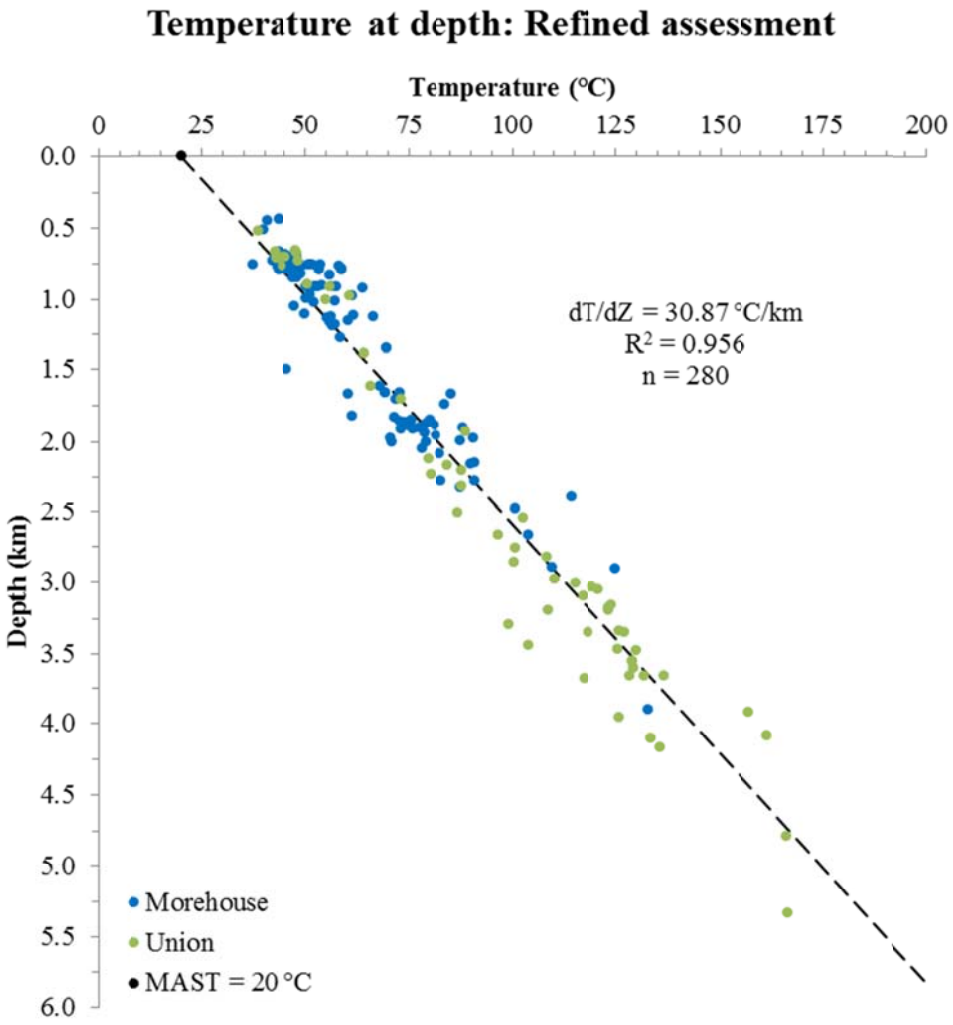

Figure 9. The 279 T_c from Morehouse and Union Parishes are represented by blue and green circles, respectively. Mean annual surface temperature (MAST) is represented by a black dot, and the line of best fit is anchored to it. There are several Union Parish data that fall below the line of best fit, and at depths shallower than 1.25 km data from both Parishes clusters above the line.

The contoured linear geothermal gradient map, created using all 231 wells for which linear geothermal gradients were established (Figure 10). The range in calculated linear

geothermal gradient within the study area is 17.02 to 49.79 °C/km, and the average of these calculated linear geothermal gradients is 33.57 °C/km. Establishing a linear geothermal gradient for each individual well allows for calculation of the depth to a specific temperature as well as the calculation of temperatures at a specific depth. For wells with BHTs above or equal to 100 °C, the depth to 100 °C is an interpolated datum. For wells with BHTs lower than 100 °C, the depth to 100 °C is an extrapolated datum (Appendix C).

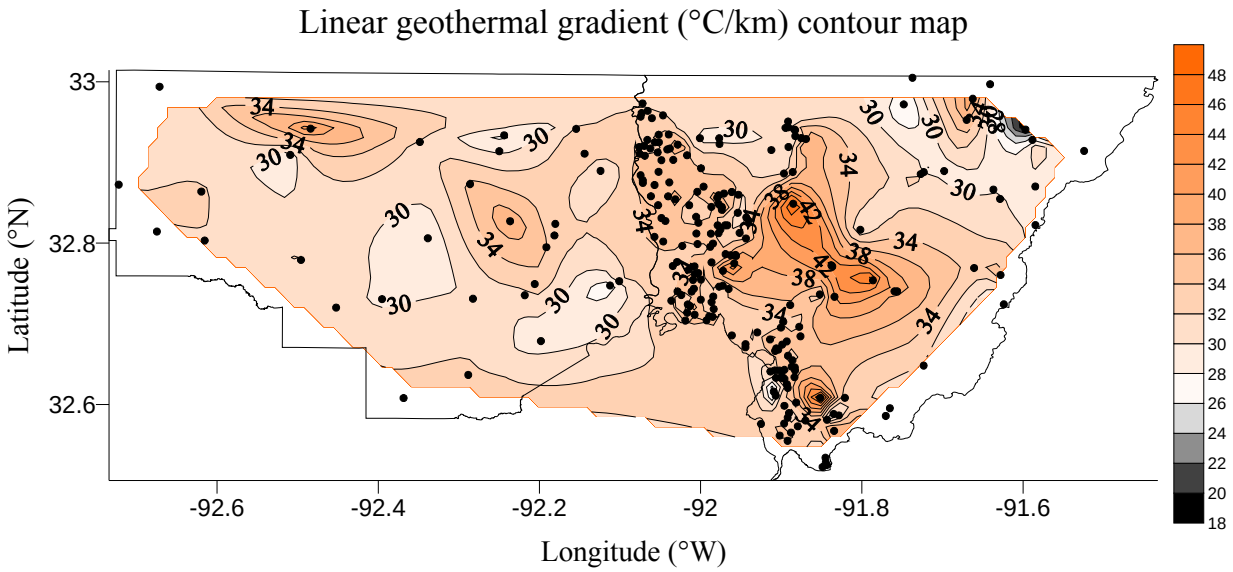

Figure 10. Contour fill for linear geothermal gradients below the average for continental crust are in gray scale, and those above are in orange scale. The majority of the study area has geothermal gradients above 25 °C/km, with an area of highest gradients in west central Morehouse Parish. Data have been vetted.

Considering both interpolated and extrapolated data from the 229 wells for which linear geothermal gradients were calculated, the depth to 100 °C in Morehouse and Union Parishes is found to range from 1.61 to 4.70 km. The average depth to 100 °C is 2.42 km, and the median depth is 2.36 km. The interpolated and extrapolated data were used to contour a depth to 100 °C isothermal surface within Union and Morehouse Parishes (Figure 11). The results of this map indicate the shallowest depths to 100 °C are in west central Morehouse Parish.

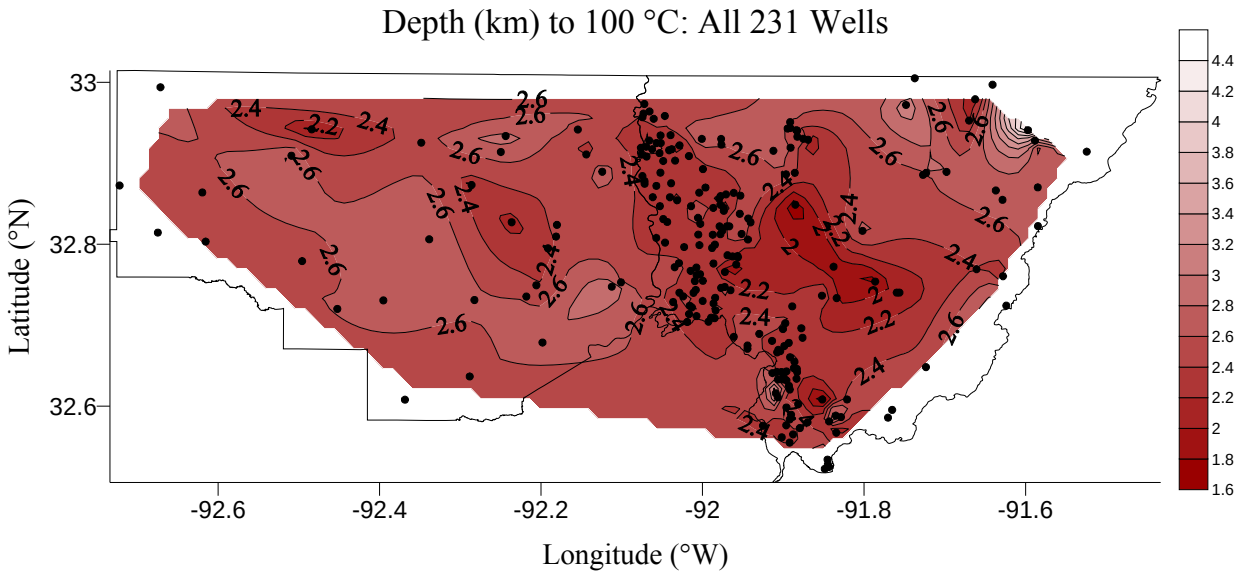

Figure 11. Both extrapolated and interpolated depths to the 100 °C isotherm were used to contour this 100 °C isotherm depth surface. Note the shallowest depths to 100 °C in west central Morehouse Parish.

This 100 °C isotherm was then gridded and contoured using only either extrapolated or interpolated data (Figure 12). The range of interpolated depths to 100 °C is 1.95 to 3.58 km, and the average is 2.60 km. The range of extrapolated depths to 100 °C is 1.61 to 4.70 km, and the average is 2.40 km (Appendix C).

Using the same gradients and wells as in the calculation of depth to 100 °C, the depth to a 150 °C was calculated for each well and the 150 °C isotherm was contoured (Figure 13). The range in depth to 150 °C is 2.61 to 7.64 km. The average depth to 150 °C is 3.93 km and the median depth is 3.83 km. Only 3 wells considered in this study had T_c greater than or equal to 150 °C. Thus, a separate map of interpolated values was not created for the 150 °C isotherm. These three wells are located in Union Parish and indicated in Figure 13.

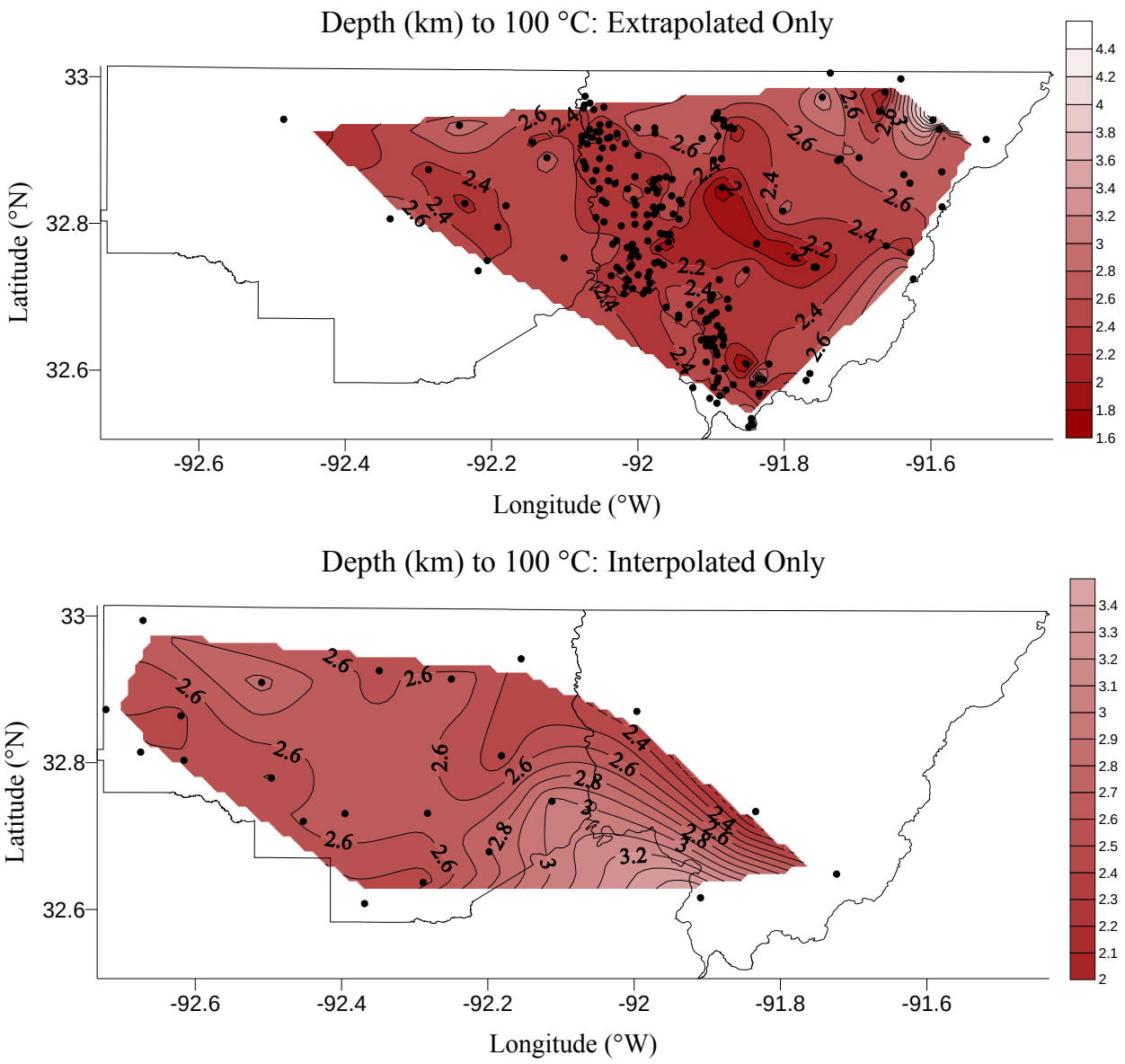

Figure 12. Contoured 100 °C isotherm using extrapolated (top) and interpolated (bottom) and depths to show difference in spatial distribution of values, as well as their influence on the combined depth to 100 °C isotherm contour map.

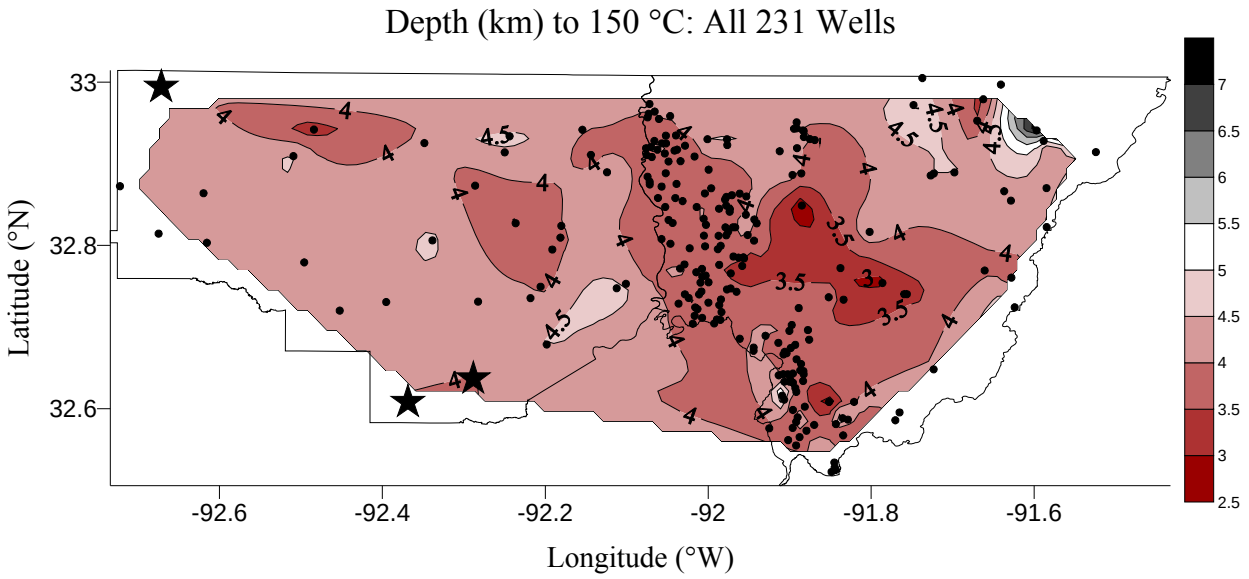

Figure 13. Both extrapolated and interpolated depths to the 150 °C isotherm were used to contour this 150 °C isotherm depth surface. Note the shallowest depths to 150 °C in west central Morehouse Parish. Black stars mark wells with T_c above 150 °C; black circles mark the remaining 228 wells. Contour depths greater than 5 km are presented in gray scale and occur only in northeast Morehouse Parish.

Because the limit for economic production of emission-free geothermal power for enhanced geothermal systems is a depth of 5 km (GTO 2015), the linear geothermal gradients for the 231 wells were used to calculate temperature at 5 km depth; extrapolated for 230 wells and interpolated for one. The resulting temperature contour map shows that the temperature at 5 km is above 100 °C for all wells, with relatively higher temperatures forming a feature of note in western central Morehouse Parish (Figure 14). The range of temperatures at 5 km depth is 105.12 to 268.97 °C, the average is 187.86 °C, and the median is 189.68 °C (Appendix A).

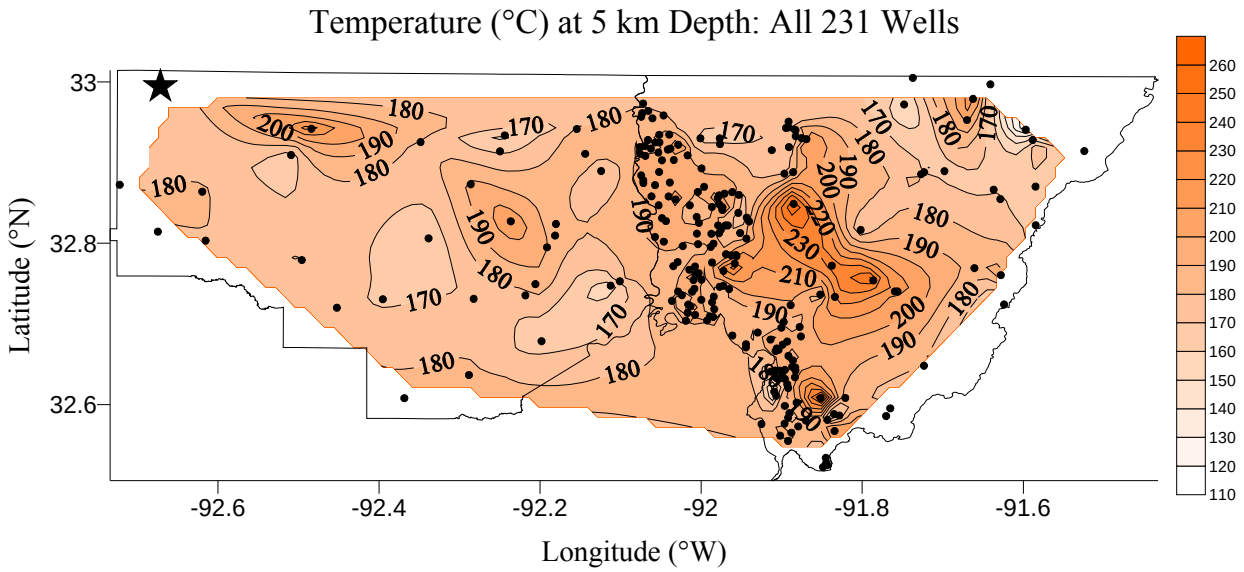

Figure 14. Temperature contour at 5 km depth in Union and Morehouse Parishes. A black star marks the well drilled deeper than 5 km; black circles mark the remaining 230 wells. Temperature exceeds 100 °C for all data points, with the highest temperatures creating a feature of note in west central Morehouse Parish.

Formations at Depth

To establish the target reservoir for a geothermal system, an understanding of the lateral and vertical occurrence of the formations at depth is necessary. The Smackover and Cotton Valley formations exist at depth throughout Union and Morehouse Parishes and their surfaces have been mapped in depth sub-sea (e.g. Dyman and Condon 2006, Li 2006). Unfortunately, the BHT and MW data could not be converted to sub-sea depths. Thus, it was necessary to create original maps of the Smackover and Cotton Valley formation tops as depth from surface within Union and Morehouse Parishes. The majority of formation top data for the Smackover and Cotton Valley come from Union Parish because the majority of wells existing in Morehouse Parish were drilled to target the hydrocarbon-bearing Monroe Gas Rock formation, which is stratigraphically above both the Cotton Valley and Smackover formations. Wells drilled to target the hydrocarbon-bearing Smackover and Cotton Valley formations most consistently

encountered temperatures above 100 °C. Thus, these formations became this study's focus for a potential geothermal target reservoir.

Table 2. Location of the Smackover formation top in three dimensions. Shaded API #'s indicate wells with Smackover, Cotton Valley, and BHT data.

Smackover	API #	lat (°N)	lon (°W)	depth (km)
Union	17111000230000	32.87254	-92.7221	3.35
Union	17111222940000	32.96674	-92.6834	2.82
Union	17111250240000	32.80324	-92.6154	3.14
Union	17111224580000	32.90488	-92.5544	2.87
Union	17111223960000	32.76629	-92.5257	3.13
Union	17111225010000	32.78898	-92.5199	3.07
Union	17111223070000	32.78949	-92.5171	3.09
Union	17111224890000	32.78617	-92.5073	3.07
Union	17111229800000	32.77918	-92.4959	3.09
Union	17111206660000	32.72014	-92.4523	3.53
Union	17111024390000	32.73064	-92.3953	3.15
Union	17111238810000	32.91399	-92.2499	2.46
Union	17111248970000	32.94165	-92.1545	2.29
Union	17111244540000	32.88958	-92.1243	2.28
Morehouse	17067206960000	32.88813	-91.7231	1.89

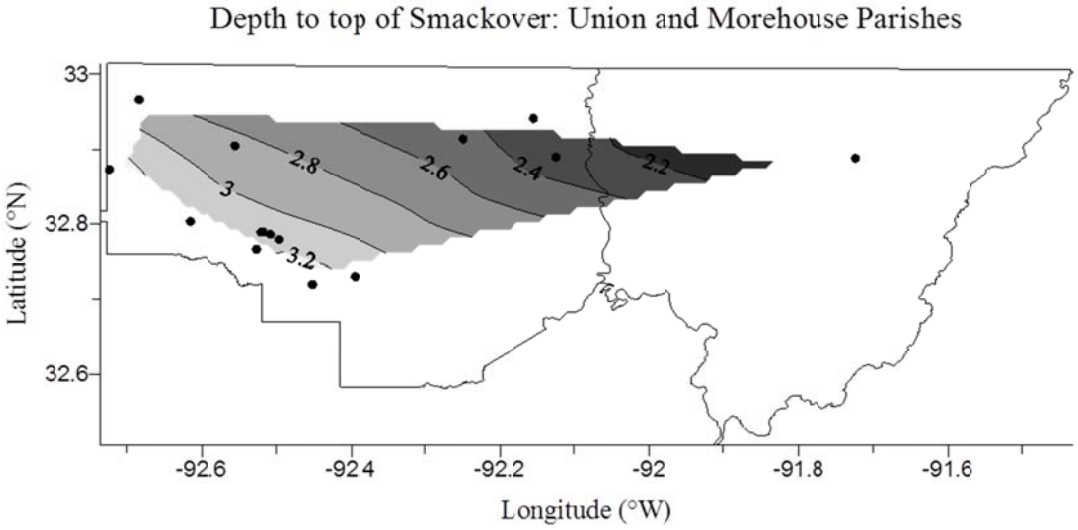

Figure 15. Contoured depth to the top of the Smackover formation in Union and Morehouse Parishes ranges from 1.89 to 3.53 km. The 15 well spots are indicated by black dots.

Depth to the Smackover formation, based on 15 wells, ranges from 1.89 km in north central Morehouse Parish to 3.53 km in southwest Union Parish (Table 2; Figure 15). The average depth to the top of the Smackover formation is 2.88 km.

Depth to the Cotton Valley formation, based on 18 wells, ranges from 0.82 km in north central Morehouse Parish to 2.50 km in northwest Union Parish (Table 3; Figure 16). The average depth to the top of the Cotton Valley formation is 1.69 km.

Table 3. Location of the Cotton Valley formation top in three dimensions. Shaded API #'s indicate wells with Smackover, Cotton Valley, and BHT data.

Cotton Valley	API #	lat (°N)	lon (°W)	depth (km)
Union	17111221700000	32.95544	-92.7036	2.07
Union	17111222940000	32.96674	-92.6834	2.50
Union	17111227360000	32.86395	-92.6196	2.06
Union	17111224580000	32.90488	-92.5544	1.95
Union	17111223070000	32.78949	-92.5171	2.13
Union	17111222980000	32.69451	-92.5076	2.48
Union	17111224890000	32.78617	-92.5073	2.06
Union	17111024390000	32.73064	-92.3953	2.15
Union	17111228630000	32.608	-92.3686	2.46
Union	17111238810000	32.91399	-92.2499	1.55
Union	17111248970000	32.94165	-92.1545	1.39
Union	17111244540000	32.88958	-92.1243	1.38
Morehouse	17067205460000	32.92833	-91.8903	1.08
Morehouse	17067206220000	32.94093	-91.888	1.05
Morehouse	17067001810000	32.73524	-91.8306	1.22
Morehouse	17067000440000	32.88283	-91.8125	0.82
Morehouse	17067208430000	32.98603	-91.8111	0.94
Morehouse	17067206960000	32.88813	-91.7231	1.08

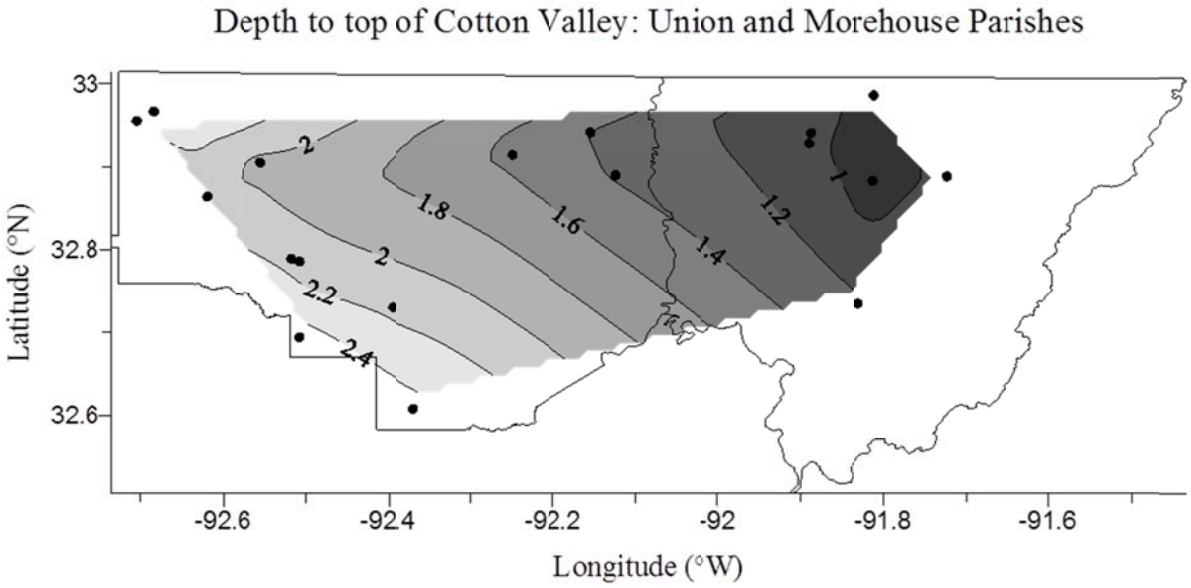

Figure 16. Contoured depth to the top of the Cotton Valley formation in Union and Morehouse Parishes ranges from 0.82 to 2.50 km. The 18 well spots are indicated by black dots.

Fluid Composition

The Blondes et al. (2015) data set did not contain formation fluid data for Morehouse Parish. After the exclusion of erroneous data, concentration of total dissolved solids (TDS) in the produced brines from Union Parish fit a linear gradient of 76,395 ppm/km, the R^2 value of which is 0.85 (Figure 17; Appendix F).

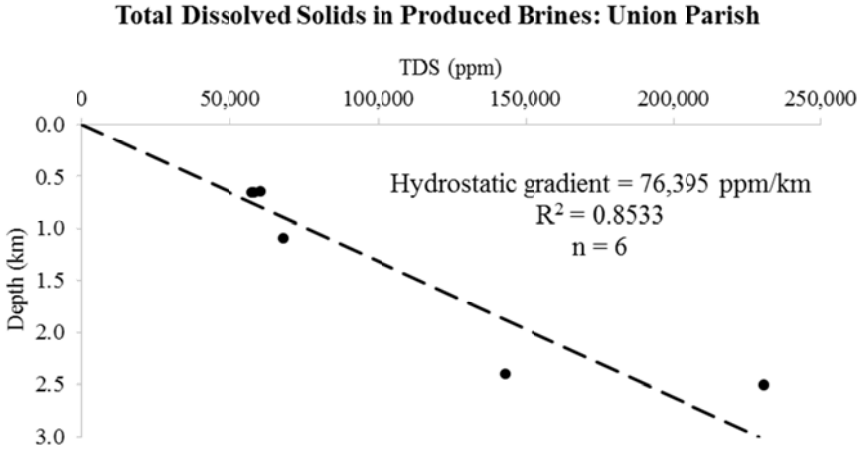

Figure 17. Black dots represent data used to calculate the linear gradient (dashed black line) of 76,395 ppm/km in Union Parish.

Pressure

The linear fluid pressure gradient for Union and Morehouse Parishes combined is 12.8 kPa/m, with an R^2 value of 0.94 (Figure 18). Although a high R^2 value indicates that this linear equation is an appropriate fit, an apparent change in gradient begins between 2.5 and 3 km depth. Equivalent pore fluid pressure profiles for wells with MWs reported at more than one depth can be found in Appendix E. These pressure profiles also display a change in gradient near 3 km depth.

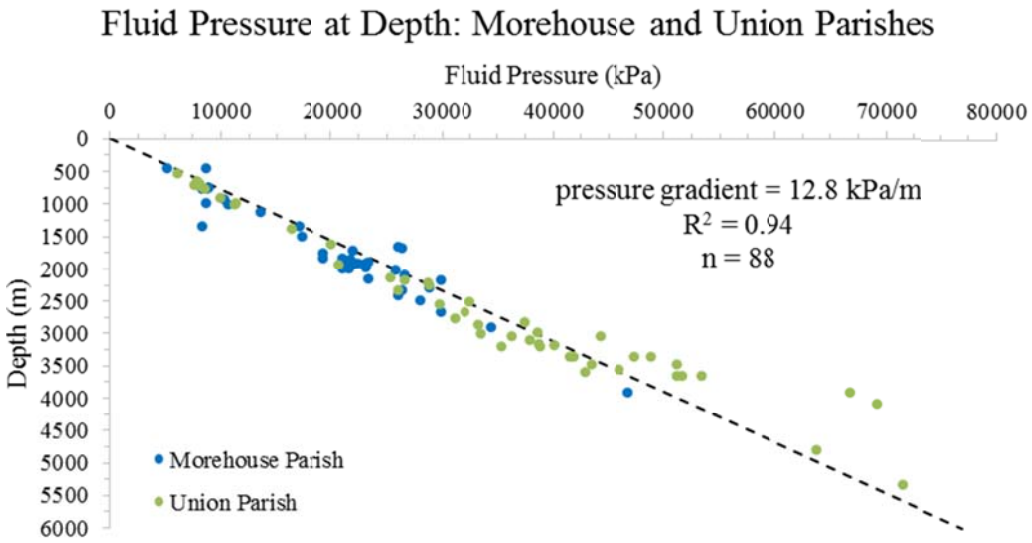

Figure 18. Pressure at depth, as calculated from 88 mud weight (MW) values. Line of best fit is anchored at zero.

The assumed geostatic ratio for the Gulf Coast Region is 10.2 kPa/m (Hanor 1987). The average geostatic ratio for Morehouse and Union Parishes is 12.23 kPa/m, while the median geostatic ratio for these Parishes is 11.88 kPa/m. Because geostatic ratio is a representation of hydrostatic pressure gradient at depth, the change in hydrostatic pressure gradient beginning at approximately 3 km depth is reflected in the geostatic ratio plotted against depth (Figure 19). The standard deviation for the entire set of geostatic ratios is 1.71 kPa/m. The first point to lie outside

of one standard deviation from the median is at 2.17 km, and geostatic ratios rise distinctly and as a group from the median beginning at 2.82 km.

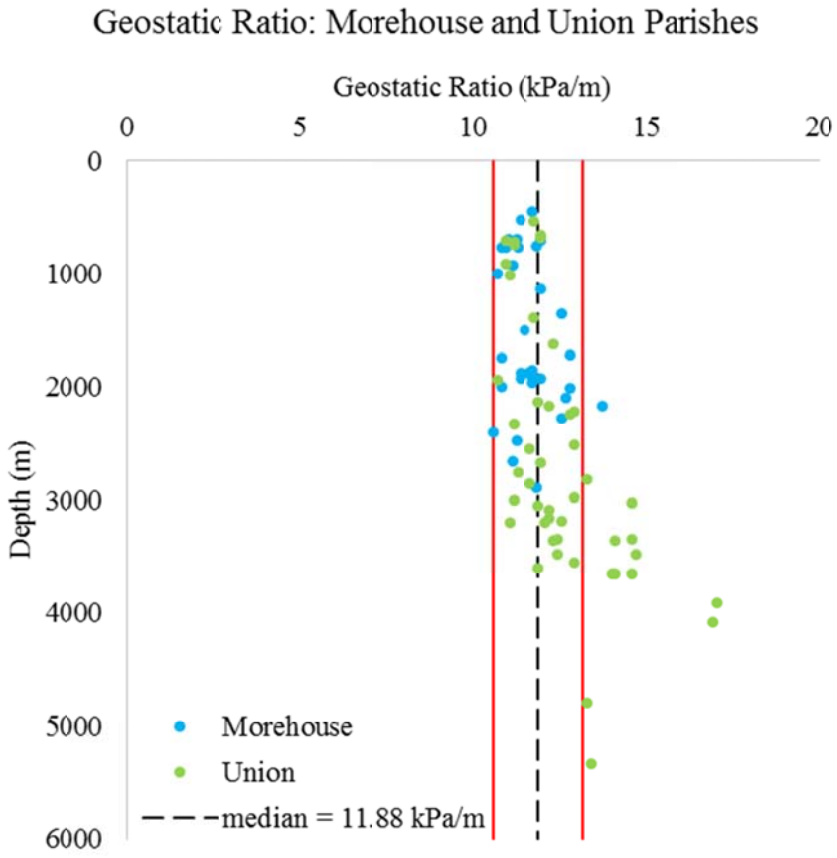

Figure 19. Geostatic ratios from 47 wells within Union and Morehouse Parishes, plotted against depth. The vertical dashed black line presented is the median 11.88 kPa/m value for all 88 data points and the solid red lines indicate one standard deviation from this median.

Discussion

This study used the economic lower limit of 100 °C at 5 km depth for determination of the potential for geothermal energy development (Tester et al. 2006, GTO 2015). All 231 wells in the data set fulfill these requirements. The Gulf of Mexico basin was identified by Anderson (2012) as having commercial geothermal development potential based on the occurrence of sedimentary reservoirs with porosities above 10 % and temperatures greater than 125 °C at depths shallower than 4 km. Only seven wells in the Union and Morehouse Parish data set failed to fulfill Anderson's (2012) temperature and depth requirements.

Areas in the northwest and southern portions of Louisiana have been investigated for their potential for commercial geothermal energy development based on surface heat flow calculations (e.g. D'Aquin 2010) as well as the occurrence of high temperatures at depth, associated with geopressured hydrocarbon reservoirs, in areas where surface heat flow is not elevated (e.g. Gray 2010). This study investigated an area of elevated surface heat flow in north central Louisiana, shared by Union and Morehouse Parishes, with a higher resolution data set than that used to create the contours for Figure 2. Results of this higher resolution mapping show that the area with the highest geothermal gradients, and therefore surface heat flow, is to the east of what was expected based on the Geothermal Map of the United States (Blackwell and Richards 2011). This high is within the limits of the Monroe Uplift structure and includes the town of Bastrop, which is the parish seat of Morehouse Parish and has a population of more than 13,000 people (The City of Bastrop 2015).

Surface heat flow values within the study area range from 10 to 36 % above average for continental crust (Blackwell and Richards 2011). An averaged geothermal gradient of

30.87 °C/km is established for the study area of Union and Morehouse Parishes, Louisiana (Figure 9) based on a trend line fit to 278 T_c and anchored to 20 °C MAST. This gradient is 23.5% higher than the 25 °C/km average for continental crust. Local geothermal gradients, established at each of the 231 wells, range from 17.02 °C/km in northeastern Morehouse Parish to 49.79 °C/km in west-central Morehouse Parish (Figure 10; Appendix C).

The 278 T_c values plotted against their reported depths establish whether the assumption of a linear geothermal gradient is appropriate for the study area. It is apparent that T_c shallower than 1.25 km display a slightly higher slope than the trend line (Figure 9). This phenomenon was addressed by Gray et al. (2012) in their assessment of the Western Canadian Sedimentary Basin. Using oil industry data similar to that used for this study, they found that BHTs and geothermal gradients at depths shallower than 1.2 km fell above their line of best fit. Their likeliest explanation is that shallow basin fill can act as an insulator, resulting in higher geothermal gradients at shallower depths. This led Gray et al. (2012) to remove BHTs shallower than 1.2 km from their data set before applying the Harrison correction, although they note that it is important not to discard this shallow data altogether. In Morehouse and Union Parishes, but especially in Morehouse Parish, the likely explanation for the data cluster above the line of best fit is that these BHTs were taken in association with drilling for the Monroe Gas Rock hydrocarbon-bearing target formation, which was heavily explored prior to the introduction of accurate digital downhole thermometers (Gray et al. 2012).

Considering that even with the cluster of shallow T_c a linear equation best describes the pattern displayed by the 278 T_c, the geothermal gradient determined for each well within the study area is treated as linear when used in calculations (e.g. depth to 100 °C, depth to 150 °C, temperature at 5 km, and heat flow). The resulting highest linear geothermal gradients are

located in west-central Morehouse Parish. Hydrostatic pressure, fluid composition, lithology, proximity to salt diapirs, basal heat flow, fluid flow, and radiogenic heat production affect geothermal gradient. Previous studies have correlated elevated geothermal gradients with the presence of salt bodies, as well as the onset of geopressure between 2.7 – 3.0 km in the southern half of Bossier Parish, Louisiana, approximately 106 km West of Union Parish, within the Upper Jurassic section of the Cotton Valley Group (e.g. D'Aquin 2010, Puckette 2009). Union and Morehouse Parishes lie outside both the North Louisiana and Mississippi salt diapir provinces and appear to be independent from the thermo-conductive influence of salt diapirs (Figure 3).

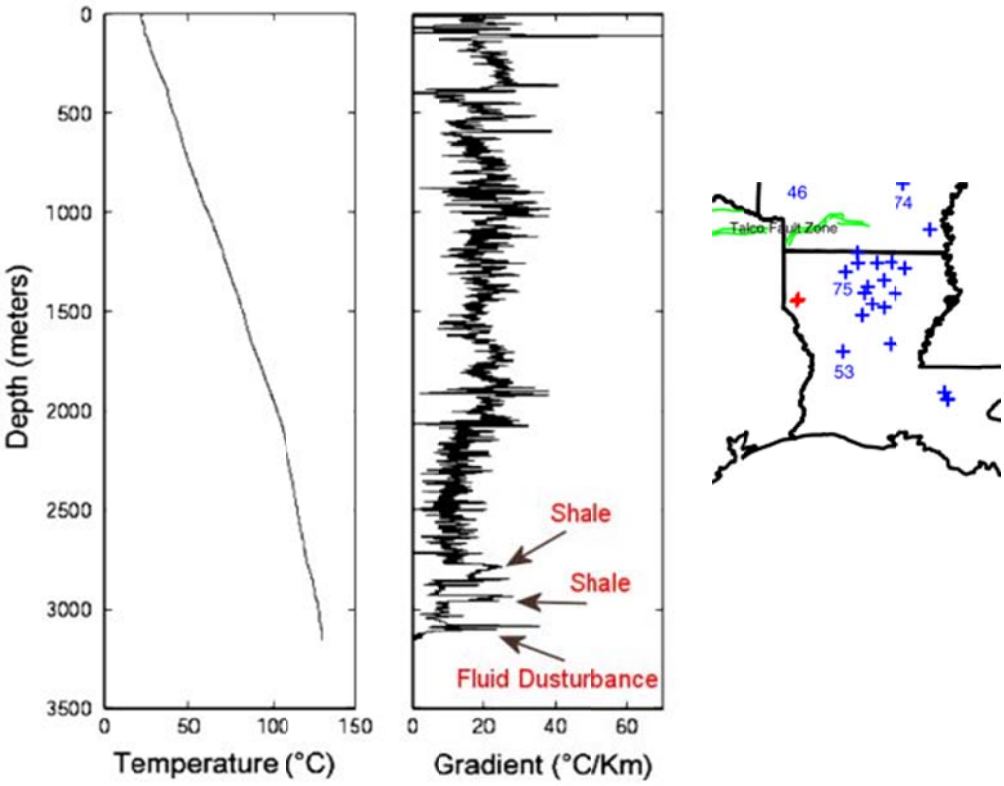

Figure 20. Changes in temperature gradient are not easily identified on a temperature curve alone (left), but can be identified and interpreted when the same data is viewed as a gradient curve (center). Location of these logs is indicated by a red cross on the map of Louisiana (right). Blue crosses represent locations with surface heat flow measurements and green lines indicate the Talco Fault Zone (adapted from Negraru et al. 2008). Shale and fluid disturbance were identified by Blackwell (personal communication 2015).

Negraru et al. (2008) present temperature and gradient curves from two wells 3 km apart in northern DeSoto Parish, Louisiana, approximately 190 km southwest of Union Parish. The curves for the two wells are so similar that it is only necessary to present the logs of one of the wells (Figure 20). The wells lie on the border of D'Aquin's (2010) study area, within which geopressure was determined to occur at approximately 2.75 km depth. This 2.75 km onset of geopressure corresponds with Blackwell's (2015) identification of the first occurrence of shale, as well as Negraru et al.'s (2008) correlation of Jurassic age Cotton Valley sediments (i.e. Bossier Shale) to elevated geothermal gradients. In the temperature log (Figure 20, left) the change in geothermal gradient is easily identifiable. Considering the lower vertical resolution of this study's data, it is not unusual that the depth profile of T_c in Union and Morehouse Parishes does not exhibit an obvious break in trend (Figure 9).

The correlation between changes in hydrostatic gradient, or existence of geopressure, and changes in geothermal gradient is observed in areas of southwest Louisiana as well (e.g. Szalkowski and Hanor 2003, Gray 2010). Uplift and/or an increase in formation temperature can cause overpressure if there is a trap limiting migration of the expanding pore fluid (Beaumont and Fiedler 1999). This trap can be stratigraphic, structural, or both. Such traps, and resulting overpressure, are characteristic of several hydrocarbon reservoirs within Union and Morehouse Parishes (Collins 1980).

Conversion of mud weight (MW) into fluid pressure can be taken one step further, to yield geostatic ratio. If the fluid density and bulk rock density are much different than 1.04 and 2.3 g/cm^3, respectively, then the geostatic ratio cannot be assumed as the numerical equivalent of kPa/m (Hanor 1987). The average density of produced brines from six wells in Union Parish is 1.07 g/cm^3 (Blondes, et al. 2015), which is within 3% error of 1.04 g/cm^3. The study area lies in

a paleo-sedimentary basin, the main constituents of which are shale, sandstone, and limestone. Thus, a bulk rock density of 2.3 g/cm^3 is an appropriate assumption (e.g. Manger 1963). Therefore, this study treats the geostatic ratio as the numerical equivalent of kPa/m.

A non-linear increase in geostatic ratio indicates overpressure; a result of a lack of fluid communication within the water column. The major causes of overpressure are uplift, heat increase, compaction and generation of hydrocarbons (Beaumont and Fiedler 1999). There is an increase in geostatic ratio at approximately 2.82 km, which is reflective of an increase in fluid pressure gradient. According to well logs, the Bossier Shale is approximately 0.2 km thick in western Union Parish (Goddard et al. 2008). The average depth to the Smackover formation in Union Parish is 2.95 km (Table 2). Therefore, the average depth to the Bossier Shale formation top is approximately 2.75 km in Union Parish. This corresponds to the approximated onset of overpressure at 2.82 km, as determined by geostatic ratios (Figure 19).

D'Aquin (2010) concluded that geopressure begins at 2.75 km depth in southern Bossier Parish, in northwestern Louisiana. The depth range of geopressure for D'Aquin's (2010) study area is 2700-3000 km (Figure 21). The depth at which the geostatic ratio rises above 1 standard deviation from the median in Union and Morehouse Parishes, 2.82 km, is indicated by a yellow line on the right side of Figure 21. This rise in geostatic ratio indicates the onset of overpressure. D'Aquin (2010) did not consider the effect of overweighted mud when determining the onset of geopressure. Without being able to determine the error associated with the determination of geostatic ratio via conversion of MW, it is not possible to unequivocally state that this increase in geostatic ratio is geopressure, and it must be referred to simply as overpressure.

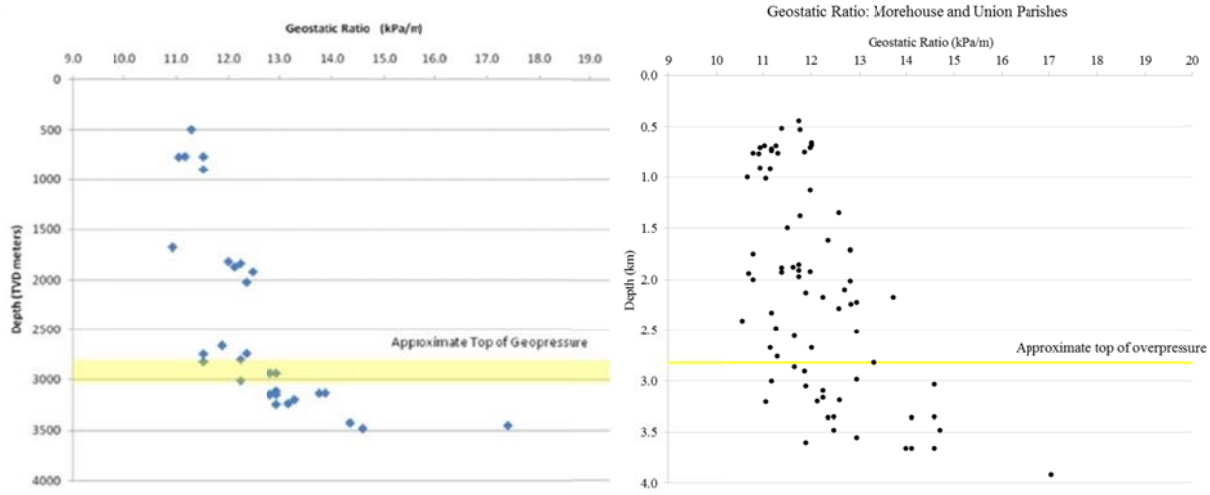

Figure 21. Left is the geostatic ratio plot and indicated depth of geopressure from D'Aquin (2010). Right is the geostatic ratio plot and determined depth of overpressure in Morehouse and Union Parishes. Both plots have the same axis ranges and indicate the top of geo- or overpressure at the same depth, with yellow lines.

The fluid chemistry data do not display a change in salinity gradient across the depths observed, and formation fluid chemistry data used in this study were not from samples at or deeper than the depth at which a change in geostatic ratio is observed (Blondes et al. 2015, Figure 17). Therefore, a relationship between fluid chemistry and change in geostatic ratio cannot be drawn. However, the increase in geostatic ratio at 2.82 km depth does coincide with the transition into Upper Jurassic sediments, from the lower Cotton Valley sandstone formations to the Bossier Shale formation. Correlation of the onset of overpressure with the transition to the Bossier Shale is reported in DeSoto and Bossier Parishes by Negraru et al. (2008), Puckette (2009) and D'Aquin (2010).

The range in depth to the Smackover top is 1.89 to 3.35 km, deepening to the west-southwest across Morehouse and Union Parishes (Table 2, Figure 15). The range in interpolated

depth to 100 °C is 1.95 to 3.58 km (Appendix C). The depth range for the Cotton Valley top is 0.82 to 2.50 km (Table 3), deepening to the west and south, with an average depth of 1.69 km (Figure 16).

In Union Parish, the 100 °C isotherm occurs at depths within the lower part of the Cotton Valley, except in the northeasternmost three wells with interpolated 100 °C depths. In this area, the 100 °C isotherm is interpolated to be below the Smackover top (Figure 22). This is directly related to lower geothermal gradients in this area. Within Union Parish, the 100 °C isotherm generally lies stratigraphically within the lower half of the Cotton Valley group, likely within the Bossier shale, which is produced for gas (Figure 23).

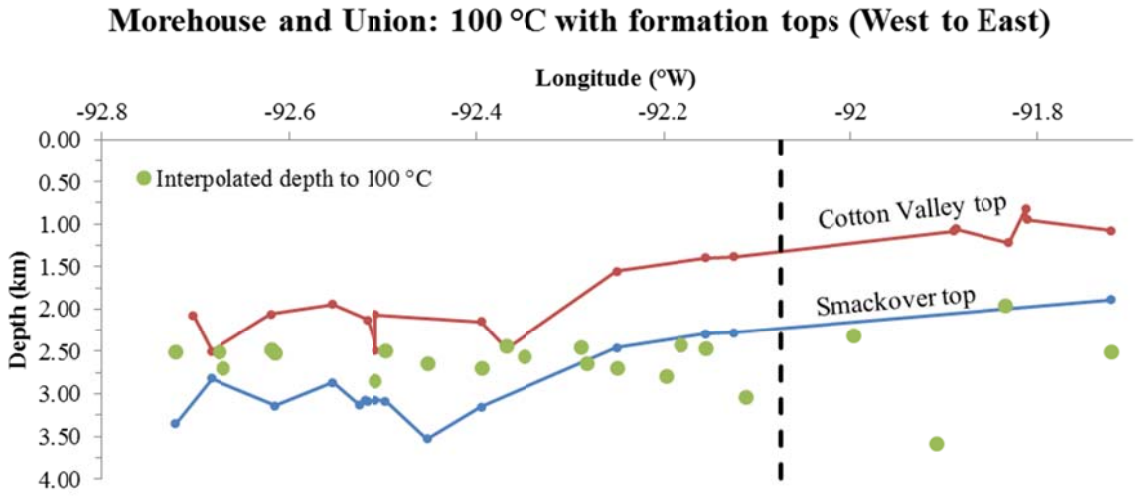

Figure 22. Depth profile of interpolated depths to 100 °C relative to known hydrocarbon producing formations. Dashed black line is the division between Union (West) and Morehouse (East) Parishes. Number of data points are: Cotton Valley (18 points), Smackover (15 points), and interpolated depth to 100 °C (22 points).

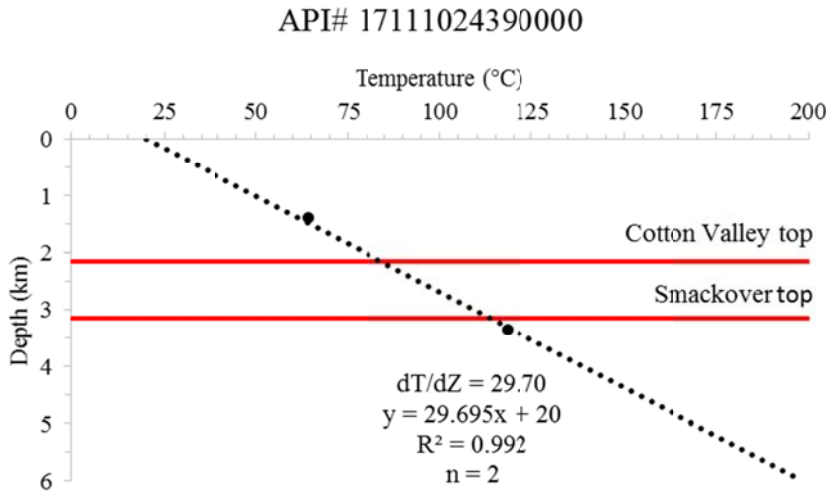

Figure 23. An example of a well in Union Parish with both BHT and formation top data. The dotted black line of best fit is anchored at 20 °C MAST.

Formation fluid chemistry was investigated with the primary purpose of establishing the appropriateness of the assumption that geostatic ratio is equivalent to P(kPa)/D(m). However, formation fluid chemistry can also be used to draw a correlation between changes in salinity, hydrostatic pressure, and geothermal gradient. There are only six fluid chemistry data points in the Blondes et al. (2015) data set for the entirety of the 4,432 km^2 study area, and none of them are at sufficient depths to correlate with a change in hydrostatic or geothermal gradient. Fluid chemistry data between 0 and 1.5 km display a lower gradient than those between 2.5 and 3.0 km, but without data between the two, and without additional data for either group, it cannot be determined whether this is significant or true (Figure 17). In addition, the deeper, higher TDS, brine samples are not located nearer to each other than they are to the shallower, lower TDS, brines (Figure 24). Thus, a linear gradient is assumed for the entire depth range for which there is fluid chemistry data.

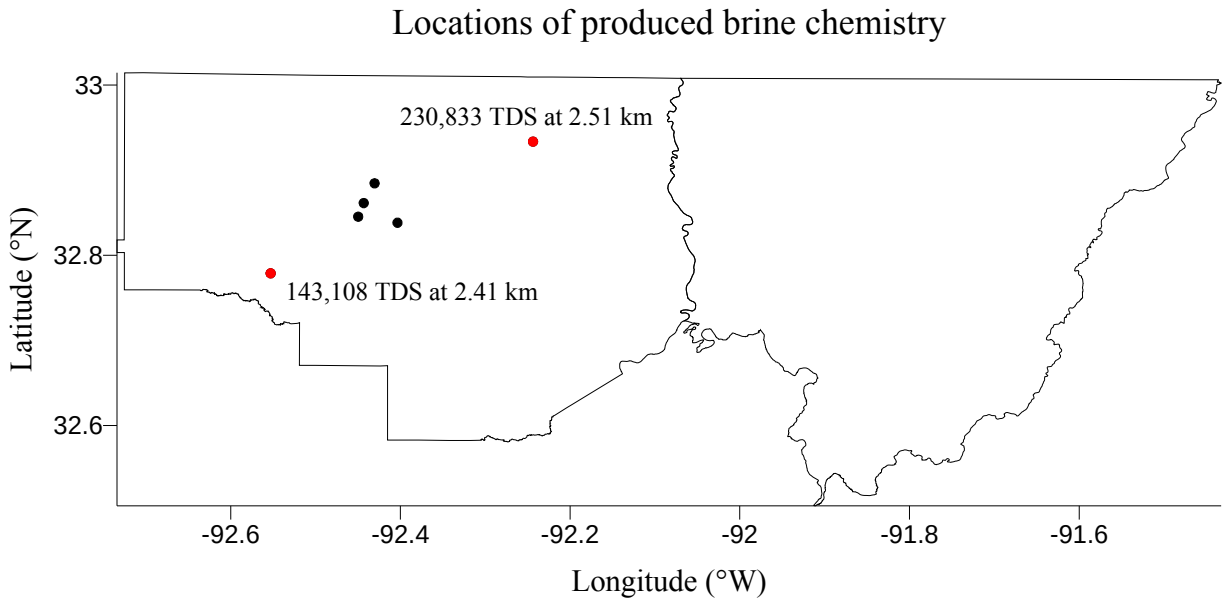

Figure 24. Well locations of the produced brines in the Blondes et al. (2015) data set. The two deeper, higher TDS, wells are indicated with red dots and directly labeled.

Comparisons drawn between this study and its impetus, the heat flow map of Louisiana (Figure 2) adapted from Blackwell and Richards (2011), show differences in the geographic location of a temperature anomaly. In Figure 2, surface heat flow values in Morehouse and Union Parishes range from 65-85 mW/m^2, with the peak of the heat flow anomaly on the border between the two Parishes. This differs from the anomaly presented in the results of this study, which found surface heat flow values from 55-123 mW/m^2, calculated using the same steady state conductive heat flow equation as Blackwell and Richards (2011), with the peak heat flow located in west central Morehouse Parish.

Blackwell and Richards (2011) used Surfer® to map and contour this surface heat flow, using the minimum curvature gridding algorithm and grid interval of 0.08333 ° latitude/longitude. This study of Union and Morehouse Parishes used the natural neighbor gridding algorithm and grid interval of 0.012 ° latitude/longitude. The natural neighbor gridding

algorithm does not allow for a grid interval as large at 0.0833 °, and so the two methods cannot be directly compared. Thus, Figure 25 compares the contoured depth to 100 °C for Union and Morehouse Parishes using minimum curvature with 0.0833 ° spacing (top) and natural neighbor with 0.012 ° spacing (bottom). The location of the anomaly is the same in both cases, suggesting that the difference in geographic location of the anomaly in this study versus Figure 2 is not a result of using different gridding algorithms. Instead, it is likely due to this study having greater data density across Morehouse and Union Parishes.

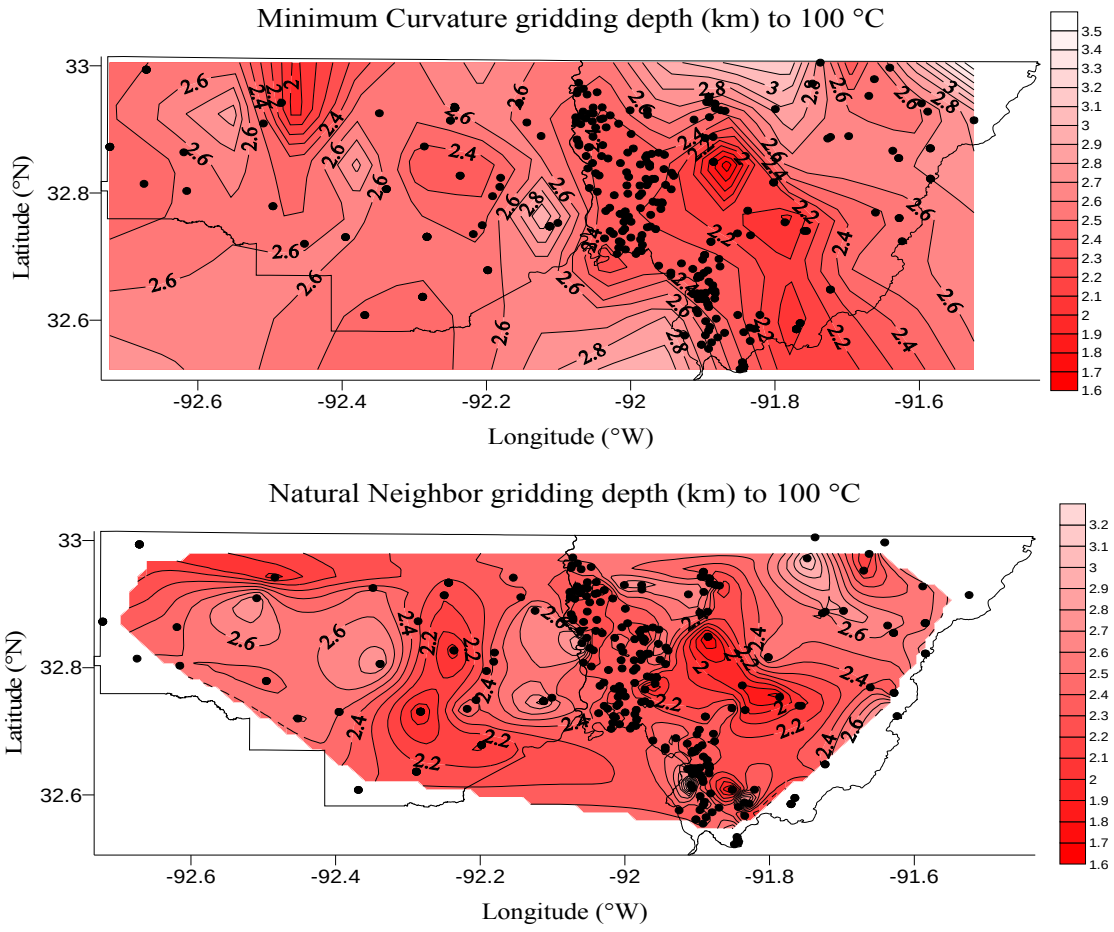

Figure 25. Minimum curvature gridding algorithm with grids spaced 0.0833 ° apart applied to this study's data set to mimic the methods of Blackwell and Richards (top, 2011) is compared to the natural neighbor gridding algorithm used in this study, with grids spaced 0.012 ° apart (bottom). Applying Blackwell and Richards (2011) method to this study's data does not shift the geographic location of the geothermal anomaly.

It is not necessary to calculate surface heat flow using the data in this study in order to compare its results to the surface heat flow map in Figure 2 because the equation for surface heat flow used by Blackwell and Richards (2011) assumes steady state conduction. It is:

$$Q = c * dT/dZ$$

Where Q ≡ heat flow in mW/m^2, c ≡ thermal conductivity of the overlying sediments in W/mK = W/m°C, and dT/dZ ≡ geothermal gradient in °C/km

(Equation 6)

The relationship between dT/dZ and Q is direct and depends only on the thermal conductivity of the overlying sediments. Therefore, if an average thermal conductivity is assumed for the overlying sediment, the features observed in this study's geothermal gradient map (Figure 10) would be preserved in a surface heat flow map created using the same geothermal gradient values. Having established that contouring methods did not play a role, the difference between the location of highest surface heat flow in Figure 2 and Figure 26 is most likely a characteristic of the larger grid spacing and lower data density used to create the surface heat flow map (Blackwell and Richards 2011), although it is also possible for convective heat flow to have an influence. Surface heat flow was calculated for use in Figure 26 by assuming an average thermal conductivity for overlying sediments of 2.47 W/m°C (Blackwell and Steele 1989). A grid spacing of 0.012 ° latitude and longitude was maintained, as was the natural neighbor gridding algorithm.

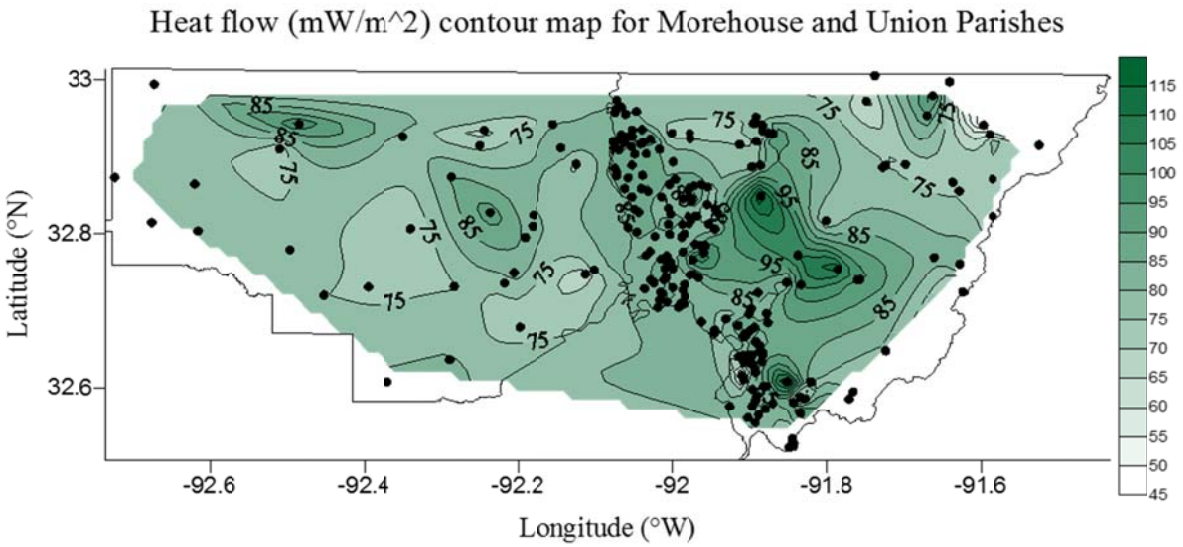

Figure 26. Surface heat flow contour map for Union and Morehouse Parishes, using 231 wells (indicated by black dots). The area of highest surface heat flow is in west central Morehouse Parish.

Conclusion

Union and Morehouse Parishes together cover a geographic area larger than 4,432 km^2, within which geothermal gradients were found to range from 17.02 to 49.79 °C/km. An averaged geothermal gradient of 30.87 °C/km is established for Union and Morehouse Parishes combined, using 278 T_c from 231 wells. This gradient is 23 % higher than the average for continental crust (25 °C/km), with the highest gradients located in western central Morehouse Parish.

Reservoir temperatures adequate for development of geothermal energy production exist within both Morehouse and Union Parishes at economically drillable depths. Based on data from 231 existing wells, extrapolated temperatures for 5 km depth are consistently above 100 °C and the shallowest interpolated depth to 100 °C is 1.59 km. The deepest wells, targeting the Smackover carbonate reservoir, were drilled in Union Parish and have T_c more consistently above 100 °C than those in Morehouse Parish because of their depth. In Morehouse Parish, shallower wells were drilled to target the Monroe Gas Rock, a platform carbonate, and present the highest geothermal gradients in the study area. Thus, Union Parish would be best considered for geothermal energy production from co-produced fluids as a viable option for renewable energy development, and its neighbor to the East, Morehouse Parish, would be best considered for EGS systems development. The separation of the study area into two separate geothermal energy development prospects is necessary because although Morehouse Parish presents the highest geothermal gradients in the study area, it is Union Parish that already hosts wells placed in deeper, hotter hydrocarbon reservoirs that are currently produced for fluids (e.g. hydrocarbons and their associated brines). Although the wells that exist in Morehouse Parish have T_C that result in geothermal gradients up to 49.79 °C/km, only four of these wells were drilled deep enough to encounter temperatures above 100 °C, compared to 18 in Union Parish.

The area found by this study to have maximum geothermal gradients, and therefore maximum heat flow, is East of where the Geothermal Map of North America (Blackwell and Richards 2011) indicates. This is most likely a result of the use of a different data set and a large grid spacing of 0.083 ° latitude and longitude for the Geothermal Map of North America (Blackwell and Richards 2011), but a more dense data set and smaller grid spacing of 0.012 ° in this study (i.e. this study has higher resolution and data density).

The data analyzed in this study does not indicate a correlation between changes in hydrostatic pressure gradient and changes in geothermal gradient. However, if temperature gradient logs could be obtained for wells targeting the Smackover formation in Morehouse or Union Parishes, a change in geothermal gradient with depth would likely be apparent, as lower thermal conductivity rock (s.a. shale) is associated with higher geothermal gradients (e.g. Hanor 1987, Negraru et al. 2008). Nor was a change in fluid chemistry gradient with depth observable given the data set. The onset of overpressure at approximately 2.82 km corresponds to the expected depth of Upper Jurassic Cotton Valley sediments, which include the Bossier Shale and several thick sand packages. These directly overlie the Upper Jurassic Smackover which, with known 15-20% porosity (Collins 1980) and hydrocarbon production, makes an ideal target for the development of geothermal power from co-produced fluids in Union Parish. The highest geothermal gradients in the study area are in western central Morehouse Parish and although few wells here are drilled deep enough to encounter T_c above 100 °C, the Smackover and Cotton Valley formations extend through the area and offer the potential for development of EGS.

References

Anderson, T.C. (2012). Review of permeability characteristics in drilled, sediment-hosted geothermal systems. Report submitted as part of DE-EE5128 "Novel Geothermal Development of Deep Sedimentary Systems in the United States," Energy and Geoscience Institute, 66.

Beaumont, E. A., & Fiedler, F. (1999). Formation Fluid Pressure and Its Applcation. In E. A. and N. H. Beaumont, Foster (Ed.), *Treatise of Petroleum Geology/Handbook of Petroleum Geology: Exploring for Oil and Gas Traps* (pp. 5–1 – 5–64). The American Association of Petroleum Geologists.

Blackwell, D. D., and Richards, M. (2011). Geothermal Map of the United States. American Association of Petroleum Geologists (AAPG), 1 sheet, scale 1:6,500,000.

Blackwell, D. D., & Steele, J. L. (1989). Thermal Conductivity of Sedimentary Rocks: Measurement and Significance. In N. D. Naeser & T. H. McCulloh (Eds.), *Thermal History of Sedimentary Basins: Methods and Case Histories* (pp. 13–36). New York, NY: Springer-Verlag New York. doi:10.1007/978-1-4612-3492-0

Blondes, M. S., Gans, K. D., Thordsen, J. J., Reidy, M. E., Thomas, B., Engle, M. A., … Rowan, E. L. (n.d.). U.S. Geological Survey National Produced Waters Geochemical Database v2.1 (PROVISIONAL). Retrieved March 12, 2015, from http://energy.usgs.gov/EnvironmentalAspects/EnvironmentalAspectsofEnergyProductionandUse/ProducedWaters.aspx#3822349-data

Brigaud, F., & Vasseur, G. (1989). Minerology, Porosity and Fluid Control on Thermal Conductivity of Sedimentary Rocks. *Geophys. J. Int.*, *98*(3), 525–542.

Calpine Corporation. (2012). Geysers by the Numbers. Retrieved from http://www.geysers.com/numbers.aspx June 2015.

Collins, S. E. (1980). Jurassic Cotton Valley and Smackover Reservoir Trends, East Texas, North Louisiana, and South Arkansas. *The American Assocation of Petroleum Geologists Bulletin*, *64*(7), 1004–1013. doi:10.1306/2F91941D-16CE-11D7-8645000102C1865D

D'Aquin, J. A. (2010). *Geothermal Energy Potential of South Bossier Parish, Louisiana*. Louisiana State University, Baton Rouge.

Dickey, P. A. (1969). Increasing concentration of subsurface brines with depth. *Chemical Geology*, *4*(1-2), 361–370. doi:10.1016/0009-2541(69)90055-2

Galloway, W. E. (2009). Gulf of Mexico. *GEO ExPro*, *6*(3).

Geothermal Technologies Office. (2015). *2014 Annual Report Geothermal Technologies Office*. Retrieved from http://energy.gov/sites/prod/files/2015/03/f20/GTO_2014_Annual-web_0.pdf

Goddard, D. A., Mancini, E. A., Horn, M., & Talukdar, S. C. (2008). Hydrocarbon generating potential: Jurassic Cotton Valley-Bossier Group, North Louisiana Salt Basin. *GCAGS Transactions*, *58*, 305–325.

Golden Software. (2002). *Golden Software Surfer Manual*. Golden, Colorado: Golden Software, Inc. Retrieved from http://www.wi.zut.edu.pl/gis/Surfer_8_Guide.pdf

Gray, D. A., Majorowicz, J., & Unsworth, M. (2012). Investigation of the geothermal state of sedimentary basins using oil industry thermal data: case study from Northern Alberta exhibiting the need to systematically remove biased data. *Journal of Geophysics and Engineering*, *9*(5), 534–548. doi:10.1088/1742-2132/9/5/534

Gray, T. A. (2010). *Geothermal Resource Assessment of the Gueydan Salt Dome and the adjacent Southeast Gueydan Field, Vermilion Parish, Louisiana*. Louisiana State University, Baton Rouge. 67 pp.

Hanor, J. S. (1987). *Origin and Migration of Subsurface Sedimentary Brines*. *Lecture Notes for Short Course No. 21*. Retrieved from http://scnotes.sepmonline.org/content/sepscoms/1/local/front-matter.pdf

Harder, B. (personal communication 2014). *Borehole Temperature Observation data for 5,414 oil and gas wells from the Lousiana Department of Natural Resources Office of Conservation online well database*. Metadata set, Louisiana Geological Society. Baton Rouge, LA.

Harrison, W. E., Luza, K. V., Prater, M. L., & Cheung, P. K. (1983). *Geothermal Resource Assessment in Oklahoma*. Special Publication 83-1, Oklahoma Geological Survey. Norman, Oklahoma.

Jackson, M. P. A., & Galloway, W. E. (1984). Structural and depositional styles of Gulf Coast Tertiary continental margins: Applications to hydrocarbon exploration. *AAPG Continuing Education Course Note Series*, *25*(April), 226.

Johnson, O. H. (1958). The Monroe Uplift. *Transactions - Gulf Coast Association of Geological Societies*, *VIII*, 24–32.

Jones, P. (1969). Hydrodynamics of Geopressure in the Northern Gulf of Mexico Basin. *Journal of Petroleum Technology*, *21*. doi:10.2118/2207-PA

Kehle, R. O. (1972). *Geothermal Survey of North America 1971 Annual Progress Report*.

Klein, S. J. W., & Whalley, S. (2015). Comparing the sustainability of U.S. electricity options through multi-criteria decision analysis. *Energy Policy*, *79*, 127–149. doi:10.1016/j.enpol.2015.01.007

Kruger, J. M., & Keller, G. R. (1986). Interpretation of crustal structure from regional gravity anomalies, Ouachita Mountains area and adjacent Gulf coastal plain. *AAPG Bulletin*, *70*(6), 667–689.

Li, P. (2006). Modeling of Thermal Maturity History of Strata in the North Louisiana Salt Basin Area. *56th Annual Meeting of the Gulf Coast Association of Geological Societies*, *56*, 439–454. Retrieved from Data\Published Articles\GCAGS Transactions

Louisiana Department of Natural Resources (LDNR) SONRIS database. Accessed 2015. http://sonris.com/

Moore, C. H., & Druckman, Y. (1981). Burial Diagenesis and Porosity Evolution, Upper Jurassic Smackover, Arkansas and Louisiana. *AAPG Bulletin*, *65*. http://doi.org/10.1306/2F919995-16CE-11D7-8645000102C1865D

Negraru, P. T., Blackwell, D. D., & Erkan, K. (2008). Heat flow and geothermal potential in the South-Central United States. *Natural Resources Research*, *17*(4), 227–243. doi:10.1007/s11053-008-9081-x

Puckette, J. (2009). Preliminary Interpretation of the Pressure Architecture in Parts of Northern Louisiana, Southern Arkansas, and Eastern Texas. *Gulf Coast Association of Geological Societies Transactions*, *59*, 607-620.

Reinhardt, T. (2013, April). New Ways to Produce Geothermal Power at Lower Temperatures. *Power Engineering*, 3. Retrieved from http://www.power-eng.com/articles/print/volume-117/issue-4/departments1/view-on-renewables/new-ways-to-produce-geothermal-power-at-lower-temperatures.html

Sharqaway, Mostafa H., Lienhard V, John H., and Subair, S. (2010). Thermophysical Properties of Seawater: A Review of Existing Correlations and Data, Desalination and Water Treatment, Appendix. *Desalination and Water Treatment*, 1–17. http://doi.org/10.5004/dwt.2010.1079

Szalkowski, S.D. and Hanor, J.S. (2003). Spatial Variations in the Salinity of Produced Waters from Southwestern Louisiana. *GCAGS/GCSSEPM Transactions*, *53*, 798-806.

Tester, J. W., Anderson, B. J., Batchelor, A. S., Blackwell, D. D., & DiPippo, R. (2006). The Future of Geothermal Energy - Impact of Enhanced Geothermal Systems (EGS) on the United States in the 21st Century. *MIT - Massachusetts Institute of Technology*, 358. Retrieved from www1.eere.energy.gov/geothermal/pdfs/future_geo_energy.pdf

The City of Bastrop. (2015). The City of Bastrop. Retrieved from http://www.cityofbastrop.com/ in July 2015.

United States Census Bureau. (2010). State and County QuickFacts. Retrieved April 13, 2015, from http://www.census.gov/quickfacts/table/LND110210/00,22111,22067

U.S. Army Corps of Engineers. (2010). *Regional Supplement to the Corps of Engineers Wetland Delineation Manual: Atlantic and Gulf Coastal Plain Region*. Vicksburg, MS.

U.S. Energy Information Administration. (2015). *Annual Energy Outlook*. Retrieved from http://www.eia.gov/forecasts/aeo/pdf/0383(2015).pdf in March 2015.

Washington, P. A. (2004). Structure of the Eastern Portion of the Monroe Gas Field , NE Louisiana. *Gulf Coast Association of Geological Societies Transactions*, *54*, 729–741.

Weides, S., & Majorowicz, J. (2014). Implications of spatial variability in heat flow for geothermal resource evaluation in large foreland basins: The case of the Western Canada sedimentary basin. *Energies*, *7*(4), 2573–2594. doi:10.3390/en7042573

Appendix A. Wells and their associated temperature data

Parish	WellName	APINo	lat	lon	Funcorr	Cuncorr	Fcorr	Tc	Depth of Measurement (ft)	Depth of Measurement (km)
Morehouse	LOUISVILLE COOPERAGE CO NO. 2	17067000080000	32.94092802	-91.5970207	95	35.00	113.93	45.52	4917	1.50
Morehouse	MCDUFFIE NO. 1	17067001970000	32.58583952	-91.770325	105	40.56	110.26	43.48	1452	0.44
Morehouse	MCDUFFIE NO. 1	17067001970000	32.58583952	-91.770325	140	60.00	157.15	69.53	4422	1.35
Morehouse	NETTIE ROBINSON NO. 1	17067000050000	32.97902753	-91.6624222	137	58.33	151.43	66.35	3699	1.13
Morehouse	CROSSETT NO. 1	17067000090000	32.97202832	-91.7480248	135	57.22	159.38	70.77	6598	2.01
Morehouse	CROSSETT TIMBER & DEV NO. 1	17067000150000	32.94352853	-91.8913283	153	67.22	175.79	79.88	6075	1.85
Morehouse	CROSSETT TIMBER & DEV NO. 1	17067000150000	32.94352853	-91.8913283	167	75.00	190.38	87.99	6263	1.91
Morehouse	HOPE FEE NO. 1	17067000620000	32.82243162	-91.5846203	142	61.11	165.02	73.90	6148	1.87
Morehouse	HOPE FEE NO. B-1	17067000640000	32.76053423	-91.6279214	115	46.11	126.72	52.62	3010	0.92
Morehouse	HOPE FEE C NO. 1	17067000610000	32.87023013	-91.5848201	110	43.33	122.77	50.43	3274	1.00
Morehouse	HOPE FEE C NO. 1	17067000610000	32.87023013	-91.5848201	154	67.78	180.85	82.70	7494	2.28
Morehouse	HOPE FEE C NO. 1	17067000610000	32.87023013	-91.5848201	155	68.33	178.96	81.65	6457	1.97
Morehouse	TENSAS DELTA NO. 1	17067002260000	32.95842806	-92.0467323	168	75.56	193.85	89.92	7115	2.17
Morehouse	L B BARHAM NO. 1	17067000720000	32.81653333	-91.8019256	140	60.00	161.31	71.84	5616	1.71
Morehouse	L B BARHAM NO. 1	17067000720000	32.81653333	-91.8019256	155	68.33	180.20	82.33	6880	2.10
Morehouse	SCHENLEY INDUSTRIES NO. 1	17067201430000	32.85483124	-91.6285212	151	66.11	174.09	78.94	6170	1.88
Morehouse	SCHENLEY INDUSTRIES NO. 1	17067201430000	32.85483124	-91.6285212	145	62.78	168.52	75.85	6311	1.92
Morehouse	MARLATT NO. 1	17067202550000	32.70253675	-91.8975279	165	73.89	189.27	87.37	6560	2.00
Morehouse	MARLATT NO. 1	17067202550000	32.70253675	-91.8975279	198	92.22	229.07	109.48	9513	2.90
Morehouse	E M BARHAM NO. 1	17067203300000	32.64823784	-91.7233239	185	85.00	213.39	100.77	8129	2.48
Morehouse	E M BARHAM NO. 1	17067203300000	32.64823784	-91.7233239	189	87.22	218.71	103.73	8747	2.67
Morehouse	W R HUMPHREYS NO. 1	17067206960000	32.88813091	-91.723124	140	60.00	163.51	73.06	6307	1.92
Morehouse	INTERNATIONAL PAPER BR NO. 3	17067207440000	32.6696377	-91.9062285	105	40.56	114.48	45.82	2460	0.75
Morehouse	CROSSET LBR CO NO. 1	17067000190000	32.93192913	-91.799526	100	37.78	101.22	38.46	513	0.16
Morehouse	CROSSETT TIM & DEV CO NO. 3	17067000360000	32.92912887	-91.8693274	165	73.89	185.84	85.46	5472	1.67

Morehouse	BONITA LUMBER CO NO. 1	17067000600000	32.9143286	-91.5242187	138	58.89	160.61	71.45	6018	1.83
Morehouse	LOUISVILLE COOPERAGE CO NO. 1	17067000590000	32.92802864	-91.5883204	142	61.11	162.76	72.65	5450	1.66
Morehouse	BONNER MEMORIAL NO. 1	17067000540000	32.88563103	-91.7269238	155	68.33	178.19	81.22	6202	1.89
Morehouse	CARTER NO. 1	17067002070000	32.58833946	-91.8350266	120	48.89	142.58	61.43	6008	1.83
Morehouse	MCDUFFIE NO. 1	17067001970000	32.58583952	-91.770325	105	40.56	110.26	43.48	1452	0.44
Morehouse	MCDUFFIE NO. 1	17067001970000	32.58583952	-91.770325	130	54.44	142.51	61.39	3209	0.98
Morehouse	MCDUFFIE NO. 1	17067001970000	32.58583952	-91.770325	140	60.00	157.15	69.53	4422	1.35
Morehouse	R A CARPENTER NO. 1	17067000410000	32.91922911	-91.8910279	148	64.44	171.37	77.43	6261	1.91
Morehouse	W W DOLES NO. 1	17067000030000	32.99702682	-91.6408216	108	42.22	122.25	50.14	3653	1.11
Morehouse	D W PIPES NO. 1	17067002030000	32.62513895	-91.893028	118	47.78	129.59	54.22	2978	0.91
Morehouse	D W PIPES NO. 1	17067002030000	32.62513895	-91.893028	136	57.78	156.75	69.31	5447	1.66
Morehouse	CROSSETT TIMBER & DEV CO NO. A-4	17067000140000	32.95082799	-91.8915283	126	52.22	140.81	60.45	3799	1.16
Morehouse	CROSSETT TIMBER & DEV CO NO. A-4	17067000140000	32.95082799	-91.8915283	144	62.22	167.30	75.17	6239	1.90
Morehouse	CROSSETT NO. 1	17067000010000	33.00502717	-91.7372243	136	57.78	156.75	69.31	5447	1.66
Morehouse	SCHENLEY NO. 1	17067000570000	32.86643094	-91.6368217	145	62.78	167.83	75.46	6088	1.86
Morehouse	CROSSETT TIMBER & DEV CO NO. 2	17067000180000	32.93282867	-91.8826277	119	48.33	133.45	56.36	3706	1.13
Morehouse	TENSAS DELTA NO. B-24	17067002990000	32.91732974	-92.0624326	120	48.89	140.86	60.48	5479	1.67
Morehouse	CARPENTER-CARPENTER NO. 1	17067000170000	32.94012869	-91.8828278	129	53.89	143.28	61.82	3660	1.12
Morehouse	J S CARTER NO. 1	17067002080000	32.58653976	-91.8285264	134	56.67	154.25	67.92	5300	1.62
Morehouse	E E MARLATT NO. 1	17067001820000	32.72333589	-91.8889276	104	40.00	113.25	45.14	2404	0.73
Morehouse	E E MARLATT NO. 1	17067001820000	32.72333589	-91.8889276	226	107.78	257.08	125.05	9521	2.90
Morehouse	DOROTHY W BARHAM NO. 1	17067002140000	32.56734028	-91.8344269	122	50.00	133.67	56.48	2998	0.91
Morehouse	DICKERSON NO. 1	17067001800000	32.73353596	-91.8339262	124	51.11	135.72	57.62	3010	0.92
Morehouse	W S WHITE NO. 1	17067001920000	32.75393549	-91.7862251	135	57.22	146.87	63.82	3048	0.93
Morehouse	VICTOR-ONEAL-WATTS NO. 1	17067000060000	32.95272843	-91.6699226	122	50.00	135.06	57.26	3349	1.02
Morehouse	MOTT NO. 1	17067001960000	32.59543899	-91.7652251	100	37.78	105.32	40.73	1466	0.45
Morehouse	MOTT NO. 1	17067001960000	32.59543899	-91.7652251	150	65.56	174.41	79.12	6609	2.01
Morehouse	GEORGE T YOUNG ESTATE NO. 1	17067001450000	32.71833623	-91.9838302	100	37.78	108.73	42.63	2278	0.69
Morehouse	MRS CHERRIE BERNSTEIN ET AL NO. 14	17067002320000	32.95492838	-92.0605327	100	37.78	108.74	42.63	2280	0.69

Morehouse	MRS CHERRIE BERNSTEIN ET AL NO. 13	17067002230000	32.96132861	-92.073233	100	37.78	108.74	42.63	2280	0.69
Morehouse	MRS. CHERRIE BERNSTEIN ET AL NO. 8	17067002250000	32.96397952	-92.0657217	100	37.78	108.82	42.68	2299	0.70
Morehouse	MRS CHERRIE BERNSTEIN ET AL NO. 9	17067002190000	32.97322818	-92.0721325	102	38.89	111.71	44.29	2516	0.77
Morehouse	BALL NO. 32	17067002370000	32.95682823	-92.0744328	102	38.89	110.82	43.79	2300	0.70
Morehouse	GEORGIA PACIFIC PAPER CORP NO. 2	17067000770000	32.83183231	-91.9434293	100	37.78	109.85	43.25	2550	0.78
Morehouse	D B SPYKER NO. 13	17067001390000	32.74733504	-91.9725296	100	37.78	110.10	43.39	2610	0.80
Morehouse	HARRELL SU 596;PERRY NO. 1	17067005530000	32.7220362	-92.0132307	110	43.33	118.87	48.26	2311	0.70
Morehouse	J B PARKER NO. 1	17067001600000	32.68933714	-91.9297287	100	37.78	109.24	42.91	2402	0.73
Morehouse	BALL NO. 40	17067002900000	32.92802913	-92.0661328	101	38.33	109.92	43.29	2324	0.71
Morehouse	DAVENPORT NO. 1	17067000750000	32.77223475	-91.8377266	122	50.00	132.62	55.90	2739	0.83
Morehouse	ROBINSON NO. 1	17067000450000	32.84883164	-91.8851276	128	53.33	138.17	58.98	2628	0.80
Morehouse	HSU #485-NEWMAN NO. 1	17067000980000	32.80583327	-91.9438293	106	41.11	116.02	46.68	2590	0.79
Morehouse	HARRELL SU 725;SNYDER HEIRS NO. 5	17067001740000	32.67493758	-91.9443288	102	38.89	111.65	44.25	2500	0.76
Morehouse	ROBINSON NO. 1	17067000450000	32.84883164	-91.8851276	128	53.33	138.05	58.92	2598	0.79
Morehouse	HARRELL SU425;GEORGIA PACIFIC NO. 1	17067000830000	32.83763207	-91.9539296	102	38.89	111.85	44.36	2550	0.78
Morehouse	CROSSETT TBR & DEV CO INC J NO. 72	17067004850000	32.77673443	-92.0292314	102	38.89	111.10	43.94	2366	0.72
Morehouse	CROSSETT TBR & DEV CO INC J NO. 79	17067004740000	32.79653365	-92.0228313	103	39.44	112.30	44.61	2415	0.74
Morehouse	CROSSETT TBR & DEV CO INC J NO. 86	17067004090000	32.84703171	-92.0142311	103	39.44	112.79	44.88	2535	0.77
Morehouse	TENSAS-DELTA NO. 44	17067004020000	32.85433135	-92.0315316	111	43.89	120.77	49.31	2529	0.77
Morehouse	HARRELL SU 473;J HILLER NO. 001-A	17067001300000	32.81273299	-91.9516295	101	38.33	110.66	43.70	2502	0.76
Morehouse	HSU 386; GEORGIA PACIFIC NO. 2	17067000270000	32.86153113	-91.97103	103	39.44	113.10	45.05	2610	0.80
Morehouse	CROSSETT TBR & DEV CO INC NO. 95	17067200230000	32.80203339	-92.0464317	106	41.11	115.26	46.25	2405	0.73
Morehouse	HSU GEORGIA PACIFIC NO. 3	17067200410000	32.86003126	-91.9532296	102	38.89	111.73	44.30	2521	0.77
Morehouse	CROSSETT TBR & DEV CO INC NO. 101	17067201330000	32.83263187	-92.0056306	101	38.33	110.48	43.60	2460	0.75
Morehouse	SPEARS-SPYKER NO. 10	17067201120000	32.76573466	-91.9723299	118	47.78	128.09	53.39	2609	0.80
Morehouse	J B MILES NO. F052	17067201190000	32.75443481	-92.0095308	110	43.33	118.64	48.13	2256	0.69
Morehouse	G T MADISON NO. 1	17067201400000	32.78543398	-91.9568295	115	46.11	124.57	51.43	2480	0.76
Morehouse	HARRELL SU410;GA PA NO. 1	17067201470000	32.84483173	-91.9737301	116	46.67	125.68	52.04	2508	0.76
Morehouse	HSU #385; GEORGIA PACIFIC NO. 7	17067201540000	32.85943118	-91.9777302	115	46.11	124.65	51.47	2500	0.76

Morehouse	MC HENRY NO. 1	17067203090000	32.73563584	-92.024031	100	37.78	109.03	42.79	2350	0.72
Morehouse	SNYDER HEIRS C NO. 2	17067203370000	32.6709377	-91.9444291	100	37.78	109.09	42.83	2364	0.72
Morehouse	MC HENRY NO. 13	17067203230000	32.72403615	-92.0160311	100	37.78	109.03	42.79	2350	0.72
Morehouse	HARRELL SU #387; WELLS NO. 1	17067202470000	32.8634311	-91.9614298	110	43.33	119.85	48.81	2550	0.78
Morehouse	ALLISON NO. N-235	17067203440000	32.75483501	-91.9996302	102	38.89	111.13	43.96	2373	0.72
Morehouse	RICH LAND SEED CO INC ETAL F NO. 2	17067203580000	32.5615408	-91.9019284	104	40.00	113.32	45.18	2420	0.74
Morehouse	RICH LAND SEED CO INC ETAL F NO. 2	17067203580000	32.5615408	-91.9019284	111	43.89	122.72	50.40	3010	0.92
Morehouse	VIRGINIA SMITH HARPER NO. 1	17067205930000	32.52254155	-91.8487271	150	65.56	173.75	78.75	6386	1.95
Morehouse	BALL NO. N-247	17067204330000	32.92212912	-92.0285314	109	42.78	117.66	47.59	2261	0.69
Morehouse	BALL NO. N-250	17067204400000	32.9032296	-92.0340318	103	39.44	111.66	44.25	2260	0.69
Morehouse	PERRY NO. 6	17067204540000	32.77623396	-91.9865302	104	40.00	113.39	45.22	2437	0.74
Morehouse	MOTT PADGETT NO. 8	17067206140000	32.59843944	-91.8961284	104	40.00	113.17	45.10	2385	0.73
Morehouse	MERL PADGETT NO. 3	17067205820000	32.60243955	-91.8815277	104	40.00	113.13	45.07	2375	0.72
Morehouse	GEORGIA PACIFIC NO. M-4	17067205310000	32.77493408	-91.9583295	119	48.33	128.67	53.70	2505	0.76
Morehouse	GEORGIA PACIFIC NO. 15	17067205650000	32.84133187	-91.9737298	105	40.56	114.59	45.88	2486	0.76
Morehouse	GEORGIA PACIFIC NO. M-5	17067206000000	32.78413375	-91.9561295	114	45.56	123.61	50.89	2490	0.76
Morehouse	O E MONTGOMERY NO. 3	17067206300000	32.91542943	-91.9123284	121	49.44	137.25	58.47	4180	1.27
Morehouse	FRANK BURGESS NO. 1	17067206890000	32.58113997	-91.8433271	108	42.22	118.87	48.26	2800	0.85
Morehouse	B B HANDY JR NO. 3	17067207170000	32.64303816	-91.8961283	104	40.00	113.03	45.02	2350	0.72
Morehouse	GEORGIA PACIFIC NO. A010	17067206410000	32.84493169	-91.9867304	106	41.11	116.06	46.70	2600	0.79
Morehouse	GEORGIA PACIFIC NO. A017	17067206590000	32.79543324	-91.98823	106	41.11	115.91	46.62	2565	0.78
Morehouse	GEORGIA PACIFIC NO. 2	17067207720000	32.89282957	-91.9995308	105	40.56	114.65	45.92	2500	0.76
Morehouse	E B AND J C SMITH NO. 2	17067207930000	32.53404093	-91.845227	104	40.00	117.50	47.50	3460	1.05
Morehouse	INTERNATIONAL PAPER B NO. 2	17067206810000	32.57594022	-91.9251292	104	40.00	113.36	45.20	2430	0.74
Morehouse	O E MONTGOMERY NO. 6	17067208150000	32.88633026	-91.896628	118	47.78	132.93	56.07	3830	1.17
Morehouse	BALL NO. N-111	17067208560000	32.92052944	-92.0699329	103	39.44	111.91	44.39	2320	0.71
Morehouse	MILES NO. 1	17067208630000	32.77123417	-92.0076308	103	39.44	111.82	44.35	2300	0.70
Morehouse	B B HANDY JR NO. 6	17067207310000	32.64693831	-91.887028	104	40.00	113.07	45.04	2360	0.72
Morehouse	INTERNATIONAL PAPER BR NO. 4	17067207450000	32.66643779	-91.9076282	102	38.89	110.66	43.70	2260	0.69

Morehouse	PIPES ET AL NO. 4	17067207520000	32.63193848	-91.8961283	104	40.00	113.07	45.04	2360	0.72
Morehouse	VANCE TRICHEL NO. 8	17067207590000	32.64233849	-91.9080283	104	40.00	113.07	45.04	2360	0.72
Morehouse	E B & J C SMITH NO. 1	17067207610000	32.52504117	-91.8434272	113	45.00	126.11	52.28	3360	1.02
Morehouse	GEORGIA PACIFIC 19 NO. 1	17067209900000	32.79953338	-91.9847302	105	40.56	114.44	45.80	2450	0.75
Morehouse	BALL C NO. 5	17067208840000	32.90283008	-92.0487322	103	39.44	111.93	44.40	2325	0.71
Morehouse	SEAY ET AL NO. 2	17067208220000	32.63303848	-91.9066283	103	39.44	112.07	44.48	2360	0.72
Morehouse	ROBINSON NO. 3	17067208290000	32.72993584	-91.9998303	102	38.89	110.95	43.86	2330	0.71
Morehouse	SEAY ET AL NO. 3	17067208360000	32.63303846	-91.9002284	103	39.44	112.07	44.48	2360	0.72
Morehouse	INTERNATIONAL PAPER BR NO. 5	17067207460000	32.66793747	-91.9038284	103	39.44	111.58	44.21	2240	0.68
Morehouse	BALL NO. N-104	17067208490000	32.90833013	-92.0693328	103	39.44	111.87	44.37	2310	0.70
Morehouse	TENSAS DELTA NO. F-98	17067208700000	32.87213128	-92.0572321	103	39.44	111.60	44.22	2245	0.68
Morehouse	GEORGIA PACIFIC NO. M-18	17067208910000	32.7850337	-91.9628297	103	39.44	112.79	44.88	2534	0.77
Morehouse	BALL NO. N-122	17067209050000	32.9250291	-92.0570325	103	39.44	111.93	44.40	2325	0.71
Morehouse	BALL NO. N-117	17067209120000	32.91612951	-92.0414318	103	39.44	111.91	44.39	2320	0.71
Morehouse	BALL NO. N-133	17067209230000	32.91732942	-92.0382319	103	39.44	111.95	44.42	2330	0.71
Morehouse	ALLISON NO. 3	17067209290000	32.76303472	-92.0031303	104	40.00	113.48	45.26	2458	0.75
Morehouse	ALLISON NO. 4	17067209300000	32.7618348	-92.0073307	103	39.44	112.44	44.69	2450	0.75
Morehouse	BALL NO. N-137	17067209360000	32.92502904	-92.0518321	171	77.22	195.09	90.61	6500	1.98
Morehouse	PIPES ET AL NO. 9	17067209470000	32.6339384	-91.883628	104	40.00	113.09	45.05	2365	0.72
Morehouse	GEORGIA PACIFIC NO. 5	17067209760000	32.94292825	-91.8947283	117	47.22	131.53	55.29	3725	1.14
Morehouse	REYNOLDS NO. 2	17067209830000	32.73653585	-91.8521267	106	41.11	116.83	47.13	2790	0.85
Morehouse	GEORGIA PACIFIC 46 NO. 2	17067209970000	32.81233492	-91.9778671	105	40.56	114.65	45.92	2500	0.76
Morehouse	GEORGIA PACIFIC 43 NO. 8	17067210670000	32.82213256	-91.9789301	102	38.89	110.72	43.73	2275	0.69
Morehouse	MRS CHERRIE BERNSTEIN ET AL NO. 21	17067210750000	32.93472881	-92.039632	103	39.44	111.93	44.40	2325	0.71
Morehouse	GEORGIA PACIFIC 9 NO. 5	17067210180000	32.8221326	-91.9669299	103	39.44	112.65	44.80	2500	0.76
Morehouse	GEORGIA PACIFIC 8 NO. 7	17067210250000	32.82213259	-91.9698299	105	40.56	114.65	45.92	2500	0.76
Morehouse	PENNZOIL SCHOOL BOARD A NO. 2	17067210390000	32.80783329	-92.0573323	102	38.89	110.67	43.70	2262	0.69
Morehouse	SPEIR NO. 2	17067210460000	32.67823044	-91.8932251	103	39.44	111.82	44.35	2300	0.70
Morehouse	GEORGIA PACIFIC 8 NO. 10	17067210530000	32.81673277	-91.9756301	105	40.56	114.65	45.92	2500	0.76

Morehouse	HARRELL SU996;BROWN-MILNER NO. 12	17067210600000	32.63513867	-91.8992284	103	39.44	111.94	44.41	2327	0.71
Morehouse	TENSAS DELTA A NO. 3	17067210810000	32.88843064	-92.0522323	102	38.89	110.51	43.62	2224	0.68
Morehouse	MARY MCENERY NO. 3	17067211310000	32.62058213	-91.8919363	116	46.67	127.74	53.19	3015	0.92
Morehouse	GEORGIA PACIFIC NO. 7	17067210610000	32.93024408	-91.8752759	119	48.33	134.20	56.78	3900	1.19
Morehouse	MOTT-PADGETT NO. 17	17067211450000	32.58366901	-91.8920833	98	36.67	107.20	41.78	2390	0.73
Morehouse	VUA;PIPES NO. 2	17067211800000	32.64607444	-91.8832229	104	40.00	113.44	45.25	2450	0.75
Morehouse	PERRY HEIRS NO. 2	17067211520000	32.70435556	-91.9927055	103	39.44	112.09	44.50	2365	0.72
Morehouse	GEORGIA-PACIFIC NO. 1	17067211590000	32.84877769	-91.9779041	110	43.33	119.64	48.69	2499	0.76
Morehouse	PERRY HEIRS NO. 11	17067212170000	32.70937152	-91.9893293	102	38.89	110.72	43.73	2275	0.69
Morehouse	RICH LAND SEED CO INC ET AL NO. 21	17067210990000	32.57640535	-91.8964165	104	40.00	113.24	45.13	2400	0.73
Morehouse	TENSAS DELTA NO. F-106	17067211970000	32.88420216	-92.074504	103	39.44	111.55	44.20	2235	0.68
Morehouse	TENSAS DELTA NO. F-112	17067212030000	32.85816071	-92.0617306	102	38.89	110.51	43.62	2225	0.68
Morehouse	PERRY HEIRS NO. 6	17067212100000	32.70872265	-91.9851392	103	39.44	111.89	44.39	2317	0.71
Morehouse	JANES BROTHERS INC ET AL NO. 5	17067212310000	32.58009901	-91.8699667	106	41.11	116.06	46.70	2600	0.79
Morehouse	BALL NO. N-96	17067212450000	32.91069903	-92.0756841	102	38.89	110.60	43.67	2246	0.68
Morehouse	RICH LAND SEED CO INC ET AL NO. 32	17067212520000	32.55502898	-91.8921753	110	43.33	120.53	49.18	2715	0.83
Morehouse	MRS CHERRIE BERNSTEIN ET AL NO. 27	17067212590000	32.9344451	-92.0520443	103	39.44	111.89	44.38	2315	0.71
Morehouse	KENO NO. 5	17067212690000	32.74358157	-92.0084238	103	39.44	112.11	44.51	2370	0.72
Morehouse	WHITAKER NO. 8	17067212730000	32.71379344	-92.0167111	102	38.89	110.55	43.64	2234	0.68
Morehouse	GEORGIA PACIFIC B NO. 7	17067213300000	32.86369487	-92.0041309	102	38.89	110.72	43.73	2275	0.69
Morehouse	GEORGIA PACIFIC D NO. 5	17067213710000	32.7989445	-92.0038957	106	41.11	116.14	46.74	2620	0.80
Morehouse	J W SPIER A NO. 1	17067213840000	32.66048905	-91.8916381	105	40.56	114.65	45.92	2500	0.76
Morehouse	MARY DEAN NAFF PUGH ET AL NO. 2	17067213910000	32.60826317	-91.8517173	127	52.78	136.71	58.17	2515	0.77
Morehouse	WHITAKER NO. 13	17067212800000	32.71128456	-92.0075239	103	39.44	112.03	44.46	2350	0.72
Morehouse	SANDIDGE A NO. 6	17067214010000	32.7040449	-92.0190381	103	39.44	112.07	44.48	2360	0.72
Morehouse	SANDIDGE A NO. 13	17067214080000	32.72862506	-92.0364027	102	38.89	110.62	43.68	2250	0.69
Morehouse	KENO A NO. 6	17067214110000	32.73999254	-92.0112398	102	38.89	110.37	43.54	2190	0.67
Morehouse	SANDIDGE A NO. 14	17067214180000	32.74013962	-92.0286694	102	38.89	110.70	43.72	2270	0.69
Morehouse	RICH LAND SEED CO INC ET AL NO. 41	17067214300000	32.56520673	-91.8879533	105	40.56	114.80	46.00	2538	0.77

Morehouse	TENSAS DELTA NO. F-316	17067214380000	32.87533984	-92.038948	102	38.89	110.50	43.61	2221	0.68
Morehouse	JANES BROTHERS INC ET AL NO. 8	17067214430000	32.57302647	-91.8794941	104	40.00	113.57	45.31	2480	0.76
Morehouse	GEORGIA PACIFIC D NO. 20	17067214750000	32.77171355	-92.0345904	102	38.89	111.72	44.29	2518	0.77
Morehouse	FRED MARLATT NO. 1	17067214970000	32.69532696	-91.9004432	104	40.00	113.09	45.05	2365	0.72
Morehouse	CHAPMAN ET AL NO. 1	17067215100000	32.69628998	-91.8776838	104	40.00	113.57	45.31	2480	0.76
Morehouse	J 2 RANCH NO. 2	17067215450000	32.78643696	-91.9691498	102	38.89	110.76	43.76	2285	0.70
Morehouse	DUNN ET AL NO. 1	17067215520000	32.64093966	-91.9134687	102	38.89	111.61	44.23	2490	0.76
Morehouse	SPYKER 80 NO. 12	17067215600000	32.74319646	-91.9653317	103	39.44	111.91	44.39	2320	0.71
Morehouse	SPYKER 80 NO. 24	17067215660000	32.73386767	-91.9843471	102	38.89	110.91	43.84	2320	0.71
Morehouse	TENSAS DELTA NO. F-324	17067215730000	32.84708212	-92.0527972	102	38.89	110.58	43.65	2240	0.68
Morehouse	SPYKER 80 NO. 29	17067215800000	32.74609135	-91.977059	103	39.44	111.91	44.39	2320	0.71
Morehouse	MOTT-PADGETT NO. 1	17067216020000	32.58947994	-91.8903263	238	114.44	270.97	132.76	12805	3.90
Morehouse	GEORGIA PACIFIC 19 NO. 3	17067209920000	32.79497724	-92.1914582	103	39.44	112.03	44.46	2350	0.72
Morehouse	YOUNG 80 NO. 1	17067216090000	32.72695395	-91.9864582	103	39.44	111.89	44.38	2315	0.71
Morehouse	HARRELL SU914;AMBROSE MEEKS NO. 1	17067216210000	32.61595726	-91.9092857	89	31.67	98.65	37.03	2500	0.76
Morehouse	RUTH K WROTEN ET AL NO. 1	17067216230000	32.88942467	-91.6978773	140	60.00	162.89	72.72	6106	1.86
Morehouse	W B WILLIAMS NO. 5	17067216370000	32.68066038	-91.9139316	108	42.22	117.32	47.40	2420	0.74
Morehouse	GEORGIA PACIFIC S NO. 1	17067216490000	32.93009846	-92.0009469	162	72.22	189.25	87.36	7652	2.33
Morehouse	GEORGIA PACIFIC 12 NO. 3	17067216550000	32.90896545	-92.0168783	103	39.44	111.93	44.40	2325	0.71
Morehouse	TENSAS DELTA NO. F-345	17067216610000	32.87473435	-92.0717498	103	39.44	111.58	44.21	2240	0.68
Morehouse	W T & C E CARPENTER NO. 1	17067216670000	32.94092116	-91.883872	120	48.89	135.08	57.27	3870	1.18
Morehouse	ANNONA RA SUA;ROBERT HODGES NO. 1	17067216750000	32.61100939	-91.9068516	100	37.78	109.65	43.14	2500	0.76
Morehouse	J 2 RANCH B NO. 3	17067216810000	32.8270595	-91.9405212	108	42.22	117.98	47.76	2580	0.79
Morehouse	PRATT NO. 5	17067217160000	32.65481609	-91.886145	103	39.44	112.83	44.91	2545	0.78
Morehouse	GEORGIA PACIFIC S NO. 2	17067217010000	32.9229469	-91.9766656	169	76.11	195.86	91.03	7495	2.28
Morehouse	PIPES NO. 10	17067217090000	32.64222455	-91.882891	104	40.00	113.46	45.26	2455	0.75
Morehouse	GEORGIA PACIFIC S NO. 3	17067217170000	32.93002957	-91.9769903	148	64.44	172.80	78.22	6740	2.05
Morehouse	MONTEREY NO. 1	17067217190000	32.72418686	-91.6238774	135	57.22	159.13	70.63	6514	1.99
Morehouse	VANCE TRICHEL NO. 13	17067217240000	32.64226181	-91.9023495	105	40.56	114.24	45.69	2400	0.73

Morehouse	SIMS NO. 1	17067217310000	32.74030563	-91.756213	210	98.89	237.81	114.34	7881	2.40
Morehouse	ERNEST SMITH NO. 8	17067217320000	32.52813276	-91.8447889	104	40.00	113.63	45.35	2495	0.76
Morehouse	HARRELL SU404;GEORGIA PACIFICN NO. 18	17067217390000	32.8561763	-91.9794247	110	43.33	119.65	48.69	2500	0.76
Morehouse	TENSAS DELTA E NO. 49	17067217670000	32.87001265	-91.9964107	103	39.44	111.82	44.35	2300	0.70
Morehouse	GEORGIA PACIFIC W NO. 1	17067218010000	32.88821969	-91.8857905	170	76.67	195.75	90.97	7080	2.16
Morehouse	BRYAN R WHITE NO. 5	17067218020000	32.68564755	-91.9613156	105	40.56	114.73	45.96	2521	0.77
Morehouse	SIMS NO. 1	17067218500000	32.74032452	-91.7594647	161	71.67	182.69	83.72	5730	1.75
Morehouse	NAVARRO-MILES B NO. 4	17067218570000	32.76718687	-92.0147374	104	40.00	113.09	45.05	2365	0.72
Morehouse	TENSAS DELTA F NO. 13	17067219040000	32.82750134	-92.0437625	103	39.44	111.64	44.24	2255	0.69
Morehouse	STEWART S NO. 1	17067219110000	32.68452448	-91.8761449	105	40.56	114.24	45.69	2400	0.73
Morehouse	TENSAS DELTA F NO. 26	17067219180000	32.83113293	-92.048686	103	39.44	111.69	44.27	2268	0.69
Morehouse	TENSAS DELTA D NO. 9	17067219250000	32.87811457	-92.0719203	105	40.56	113.66	45.37	2260	0.69
Morehouse	TENSAS DELTA C NO. 3	17067219320000	32.85807159	-92.0404219	104	40.00	113.13	45.07	2375	0.72
Morehouse	PAGGETT ETAL NO. 1	17067219540000	32.67430645	-91.8987446	107	41.67	116.65	47.03	2500	0.76
Morehouse	BALL NO. 9	17067219750000	32.9190418	-92.0763328	102	38.89	110.72	43.73	2275	0.69
Morehouse	MONTEREY O&G TRANS NO. 1	17067219890000	32.76921703	-91.6607045	107	41.67	117.48	47.49	2704	0.82
Morehouse	SHEPARD NO. 1	17067219960000	32.608297	-91.821027	112	44.44	124.47	51.37	3200	0.98
Morehouse	H SU477;CROSSETT J NO. 175	17067220010000	32.81179958	-91.9873525	105	40.56	114.68	45.93	2507	0.76
Morehouse	CROSSETT TBR & DEV CO INC JO NO. 1	17067220030000	32.8119331	-92.00530337	107	41.67	116.65	47.03	2500	0.76
Morehouse	CROSSETT TBR & DEV CO INC JO NO. 2	17067220040000	32.82526554	-92.00280344	107	41.67	116.63	47.02	2496	0.76
Morehouse	SWD NO. 2	17067880010000	32.91251896	-92.0532921	97	36.11	103.27	39.60	1690	0.52
Union	FROST LUMBER IND NO. 4	17111009850000	32.82723441	-92.2364372	102	38.89	111.72	44.29	2518	0.77
Union	FROST LUMBER IND NO. 4	17111009850000	32.82723441	-92.2364372	129	53.89	141.55	60.86	3220	0.98
Union	FROST LBR IND B LD NO. 1	17111009640000	32.8061372	-92.3385406	150	65.56	175.50	79.72	6987	2.13
Union	FROST LBR IND B LD NO. 1	17111009640000	32.8061372	-92.3385406	176	80.00	205.73	96.51	8756	2.67
Union	CARL HOLLIS NO. 1	17111000880000	32.94193599	-92.4840471	110	43.33	118.52	48.07	2226	0.68
Union	ROBERT L ANDREWS NO. 1	17111001560000	32.93373132	-92.2438375	130	54.44	150.30	65.72	5312	1.62
Union	ROBERT L ANDREWS NO. 1	17111001560000	32.93373132	-92.2438375	150	65.56	176.48	80.27	7350	2.24
Union	ROBERT L ANDREWS NO. 1	17111001560000	32.93373132	-92.2438375	160	71.11	188.63	87.02	8235	2.51

Union	ROBERT L ANDREWS NO. 1	17111001560000	32.93373132	-92.2438375	95	35.00	101.39	38.55	1718	0.52
Union	BENNETT NO. 1	17111000230000	32.8725429	-92.7220547	118	47.78	130.94	54.97	3318	1.01
Union	BENNETT NO. 1	17111000230000	32.8725429	-92.7220547	215	101.67	246.70	119.28	9950	3.03
Union	BENNETT NO. 1	17111000230000	32.8725429	-92.7220547	226	107.78	258.77	125.98	10985	3.35
Union	BENNETT NO. 1	17111000230000	32.8725429	-92.7220547	233	111.67	266.02	130.01	11420	3.48
Union	OLIN GAS TRANSMISSION NO. D-1	17111022030000	32.67863916	-92.1982364	110	43.33	119.27	48.48	2408	0.73
Union	OLIN GAS TRANSMISSION NO. D-1	17111022030000	32.67863916	-92.1982364	158	70.00	183.90	84.39	7133	2.17
Union	OLIN GAS TRANSMISSION NO. D-1	17111022030000	32.67863916	-92.1982364	195	90.56	227.35	108.53	10498	3.20
Union	M S BAUGHMAN UNIT NO. 1	17111022700000	32.73113837	-92.2825389	110	43.33	118.20	47.89	2150	0.66
Union	M S BAUGHMAN UNIT NO. 1	17111022700000	32.73113837	-92.2825389	164	73.33	190.29	87.94	7280	2.22
Union	M S BAUGHMAN UNIT NO. 1	17111022700000	32.73113837	-92.2825389	199	92.78	230.47	110.26	9777	2.98
Union	M S BAUGHMAN UNIT NO. 1	17111022700000	32.73113837	-92.2825389	212	100.00	244.79	118.21	11015	3.36
Union	M S BAUGHMAN UNIT NO. 1	17111022700000	32.73113837	-92.2825389	236	113.33	269.16	131.75	11995	3.66
Union	T L JAMES & CO INC NO. 1	17111024390000	32.73064025	-92.3953422	130	54.44	147.56	64.20	4534	1.38
Union	T L JAMES & CO INC NO. 1	17111024390000	32.73064025	-92.3953422	212	100.00	244.77	118.21	10994	3.35
Union	FROST LBR IND NO. D014		32.82394522	-92.1803649	100	37.78	108.81	42.67	2296	0.70
Union	HARRELL SU138;UNION PROD CO NO. 1	17111017630000	32.75293586	-92.1010332	100	37.78	108.99	42.77	2340	0.71
Union	OLIN GAS TRANSMISSION CO NO. 57	17111201610000	32.73543737	-92.2182367	142	61.11	163.31	72.95	5615	1.71
Union	JOINER NO. 1	17111206660000	32.72014164	-92.4523439	232	111.11	265.14	129.52	11823	3.60
Union	JENNY ESTATE NO. 4	17111209320000	32.74753585	-92.1124335	178	81.11	210.65	99.25	10829	3.30
Union	JENNY ESTATE NO. 4	17111209320000	32.74753585	-92.1124335	186	85.56	218.97	103.87	11320	3.45
Union	JENNY ESTATE NO. 4	17111209320000	32.74753585	-92.1124335	210	98.89	243.16	117.31	12070	3.68
Union	JENNY ESTATE NO. 4	17111209320000	32.74753585	-92.1124335	226	107.78	258.87	126.04	12982	3.96
Union	JENNY ESTATE NO. 4	17111209320000	32.74753585	-92.1124335	240	115.56	272.49	133.60	13455	4.10
Union	JENNY ESTATE NO. 4	17111209320000	32.74753585	-92.1124335	244	117.78	276.27	135.71	13655	4.16
Union	PENNZOIL FEE 51 A GRU NO. 1	17111213030000	32.83873221	-92.0595324	187	86.11	195.64	90.91	11290	3.44
Union	OLINKRAFT NO. 4	17111221590000	32.8731892	-92.2861462	103	39.44	111.87	44.37	2310	0.70
Union	JOHN WALTER GRAFTON NO. 1	17111227360000	32.86394927	-92.6195821	222	105.56	254.35	123.53	10500	3.20
Union	ROYE NO. 1	17111228630000	32.60800062	-92.3686292	225	107.22	258.01	125.56	11416	3.48

Union	ROYE NO. 1	17111228630000	32.60800062	-92.3686292	290	143.33	322.54	161.41	13396	4.08
Union	T L JAMES A NO. 1	17111229800000	32.77918205	-92.495927	211	99.44	242.96	117.20	10155	3.10
Union	T L JAMES A NO. 1	17111229800000	32.77918205	-92.495927	223	106.11	255.22	124.01	10376	3.16
Union	MLGC FEE GAS NO. 1107	17111235430000	32.74937379	-92.2058556	100	37.78	108.33	42.41	2181	0.66
Union	REPPOND HEIRS NO. 1	17111238860000	32.91090739	-92.1440377	112	44.44	123.50	50.83	2955	0.90
Union	DANIEL B GREEN ET AL NO. 1	17111238810000	32.91398893	-92.2498516	105	40.56	113.82	45.46	2300	0.70
Union	DANIEL B GREEN ET AL NO. 1	17111238810000	32.91398893	-92.2498516	183	83.89	213.26	100.70	9037	2.75
Union	VUA;HAMMONS A NO. 1	17111241380000	32.63666864	-92.2884191	168	75.56	191.66	88.70	6355	1.94
Union	VUA;HAMMONS A NO. 1	17111241380000	32.63666864	-92.2884191	208	97.78	239.57	115.32	9852	3.00
Union	VUA;HAMMONS A NO. 1	17111241380000	32.63666864	-92.2884191	230	110.00	263.16	128.42	12000	3.66
Union	VUA;HAMMONS A NO. 1	17111241380000	32.63666864	-92.2884191	282	138.89	314.95	157.20	12841	3.91
Union	PRIMOS-FROST LUMBER NO. 1	17111244540000	32.88957953	-92.124251	163	72.78	190.20	87.89	7630	2.33
Union	NEWT MANNING NO. 1	17111245780000	32.99393321	-92.6714194	121	49.44	132.68	55.93	3000	0.91
Union	NEWT MANNING NO. 1	17111245780000	32.99393321	-92.6714194	222	105.56	254.30	123.50	10450	3.19
Union	NEWT MANNING NO. 1	17111245780000	32.99393321	-92.6714194	231	110.56	264.10	128.94	11661	3.55
Union	NEWT MANNING NO. 1	17111245780000	32.99393321	-92.6714194	303	150.56	331.19	166.22	15725	4.79
Union	NEWT MANNING NO. 1	17111245780000	32.99393321	-92.6714194	310	154.44	331.72	166.51	17500	5.33
Union	EXXON FEE NO. 1	17111248970000	32.94165486	-92.1544614	188	86.67	216.92	102.73	8365	2.55
Union	SMK B RA SUB;GRAFTON NO. 002-ALT	17111250240000	32.80324147	-92.6154147	228	108.89	260.79	127.10	11018	3.36
Union	H COOK ETAL NO. 1	17111254110000	32.81443297	-92.6746765	245	118.33	278.16	136.75	12000	3.66
Union	PARDUE NO. 1	17111255680000	32.9094011	-92.5092376	182	83.33	212.86	100.48	9380	2.86
Union	EXXON-MOBILE NO. 1	17111255880000	32.92542742	-92.34842716	196	91.11	226.64	108.13	9250	2.82
Union	EXXONMOBIL ETAL 17 NO. 1	17111256110000	32.80955446	-92.18145825	218	103.33	249.78	120.99	10008	3.05

Appendix B. Temperature profiles

Parish	API #	Tc (°C)	Tc depth (km)	Linear gradient (°C/km)	lat (°)	lon (°)	plot #
Union	17111009850000	44.29	0.77	37.85	32.82723441	-92.2364372	1
Union	17111009850000	60.86	0.98		32.82723441	-92.2364372	
Union	17111009640000	79.72	2.13	28.43	32.8061372	-92.3385406	2
Union	17111009640000	96.51	2.67		32.8061372	-92.3385406	
Union	17111001560000	65.72	1.62	27.22	32.93373132	-92.2438375	3
Union	17111001560000	80.27	2.24		32.93373132	-92.2438375	
Union	17111001560000	87.02	2.51		32.93373132	-92.2438375	
Union	17111001560000	38.55	0.52		32.93373132	-92.2438375	
Union	17111000230000	54.97	1.01	32.02	32.8725429	-92.7220547	4
Union	17111000230000	119.28	3.03		32.8725429	-92.7220547	
Union	17111000230000	125.98	3.35		32.8725429	-92.7220547	
Union	17111000230000	130.01	3.48		32.8725429	-92.7220547	
Union	17111022030000	48.48	0.73	28.65	32.67863916	-92.1982364	5
Union	17111022030000	84.39	2.17		32.67863916	-92.1982364	
Union	17111022030000	108.53	3.20		32.67863916	-92.1982364	
Union	17111022700000	47.89	0.66	30.26	32.73113837	-92.2825389	6
Union	17111022700000	87.94	2.22		32.73113837	-92.2825389	
Union	17111022700000	110.26	2.98		32.73113837	-92.2825389	
Union	17111022700000	118.21	3.36		32.73113837	-92.2825389	
Union	17111022700000	131.75	3.66		32.73113837	-92.2825389	
Union	17111024390000	64.20	1.38	29.70	32.73064025	-92.3953422	7
Union	17111024390000	118.21	3.35		32.73064025	-92.3953422	
Union	17111209320000	99.25	3.30	26.42	32.74753585	-92.1124335	8
Union	17111209320000	103.87	3.45		32.74753585	-92.1124335	
Union	17111209320000	117.31	3.68		32.74753585	-92.1124335	
Union	17111209320000	126.04	3.96		32.74753585	-92.1124335	

Union	17111209320000	133.60	4.10		32.74753585	-92.1124335	
Union	17111209320000	135.71	4.16		32.74753585	-92.1124335	
Union	17111228630000	125.56	3.48	32.83	32.60800062	-92.3686292	9
Union	17111228630000	161.41	4.08		32.60800062	-92.3686292	
Union	17111229800000	117.20	3.10	32.16	32.77918205	-92.495927	10
Union	17111229800000	124.01	3.16		32.77918205	-92.495927	
Union	17111238810000	45.46	0.70	29.72	32.91398893	-92.2498516	11
Union	17111238810000	100.70	2.75		32.91398893	-92.2498516	
Union	17111241380000	88.70	1.94	32.63	32.63666864	-92.2884191	12
Union	17111241380000	115.32	3.00		32.63666864	-92.2884191	
Union	17111241380000	128.42	3.66		32.63666864	-92.2884191	
Union	17111241380000	157.20	3.91		32.63666864	-92.2884191	
Union	17111245780000	55.93	0.91	29.75	32.99393321	-92.6714194	13
Union	17111245780000	123.50	3.19		32.99393321	-92.6714194	
Union	17111245780000	128.94	3.55		32.99393321	-92.6714194	
Union	17111245780000	166.22	4.79		32.99393321	-92.6714194	
Union	17111245780000	166.51	5.33		32.99393321	-92.6714194	
Morehouse	17067001970000	43.48	0.44	39.62	32.58583952	-91.770325	14
Morehouse	17067001970000	61.39	0.98		32.58583952	-91.770325	
Morehouse	17067001970000	69.53	1.35		32.58583952	-91.770325	
Morehouse	17067000150000	79.88	1.85	34.03	32.94352853	-91.8913283	15
Morehouse	17067000150000	87.99	1.91		32.94352853	-91.8913283	
Morehouse	17067000610000	50.43	1.00	29.24	32.87023013	-91.5848201	16
Morehouse	17067000610000	82.70	2.28		32.87023013	-91.5848201	
Morehouse	17067000610000	81.65	1.97		32.87023013	-91.5848201	
Morehouse	17067000720000	71.84	1.71	29.95	32.81653333	-91.8019256	17
Morehouse	17067000720000	82.33	2.10		32.81653333	-91.8019256	
Morehouse	17067201430000	78.94	1.88	30.16	32.85483124	-91.6285212	18
Morehouse	17067201430000	75.85	1.92		32.85483124	-91.6285212	

Morehouse	17067202550000	87.37	2.00	31.77	32.70253675	-91.8975279	19
Morehouse	17067202550000	109.48	2.90		32.70253675	-91.8975279	
Morehouse	17067203300000	100.77	2.48	31.96	32.64823784	-91.7233239	20
Morehouse	17067203300000	103.73	2.67		32.64823784	-91.7233239	
Morehouse	17067002030000	54.22	0.91	31.54	32.62513895	-91.893028	21
Morehouse	17067002030000	69.31	1.66		32.62513895	-91.893028	
Morehouse	17067000140000	60.45	1.16	30.61	32.95082799	-91.8915283	22
Morehouse	17067000140000	75.17	1.90		32.95082799	-91.8915283	
Morehouse	17067001820000	45.14	0.73	36.08	32.72333589	-91.8889276	23
Morehouse	17067001820000	125.05	2.90		32.72333589	-91.8889276	
Morehouse	17067001960000	40.73	0.45	30.15	32.59543899	-91.7652251	24
Morehouse	17067001960000	79.12	2.01		32.59543899	-91.7652251	
Morehouse	17067203580000	45.18	0.74	33.53	32.5615408	-91.9019284	25
Morehouse	17067203580000	50.40	0.92		32.5615408	-91.9019284	
Morehouse	17067000450000	58.98	0.80	48.903	32.84883164	-91.8851276	26
Morehouse	17067000450000	58.92	0.79		32.84883164	-91.8851276	

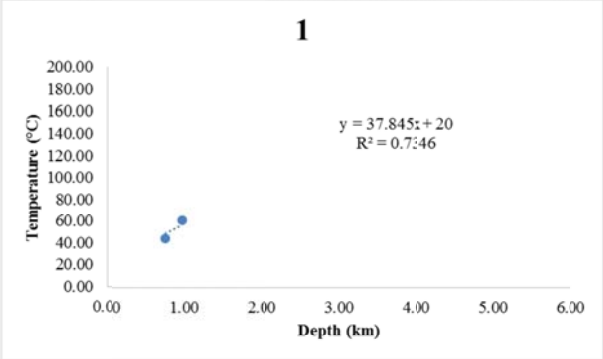
1
y = 37.845x + 20
R² = 0.7146
Temperature (°C)
Depth (km)

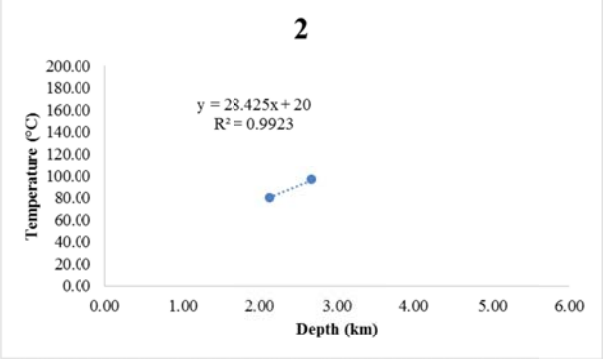
2
y = 28.425x + 20
R² = 0.9923
Temperature (°C)
Depth (km)

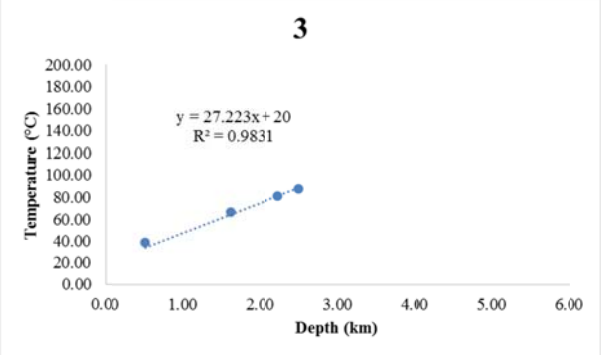
3
y = 27.223x + 20
R² = 0.9831
Temperature (°C)
Depth (km)

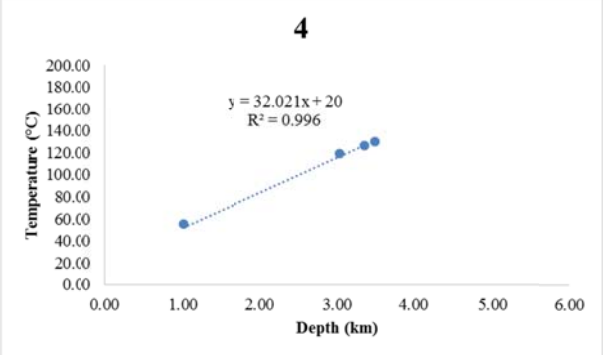
4
y = 32.021x + 20
R² = 0.996
Temperature (°C)
Depth (km)

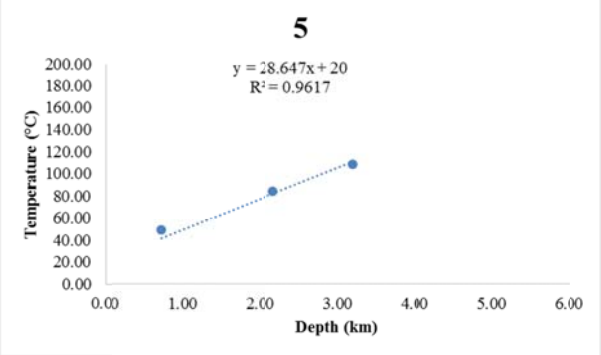
5
y = 28.647x + 20
R² = 0.9617
Temperature (°C)
Depth (km)

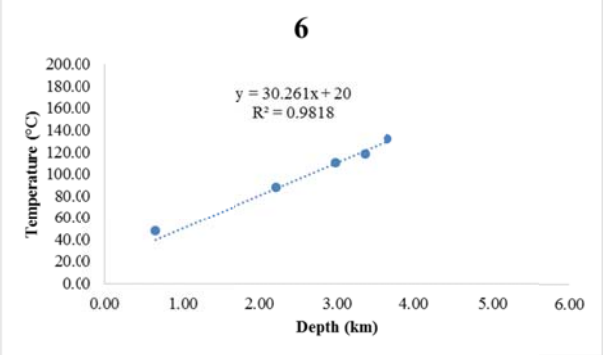
6
y = 30.261x + 20
R² = 0.9818
Temperature (°C)
Depth (km)

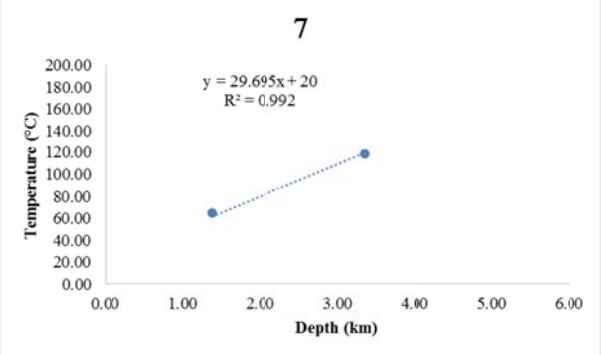
7
y = 29.695x + 20
R² = 0.992
Temperature (°C)
Depth (km)

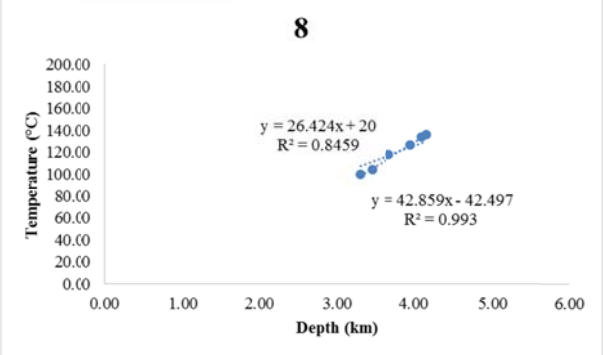
8
y = 26.424x + 20
R² = 0.8459
y = 42.859x - 42.497
R² = 0.993
Temperature (°C)
Depth (km)

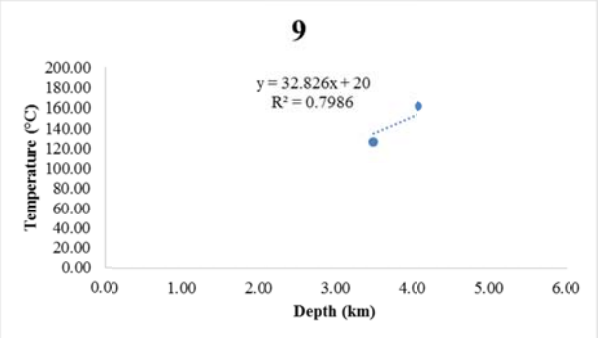
9
y = 32.826x + 20
R² = 0.7986
Temperature (°C)
Depth (km)

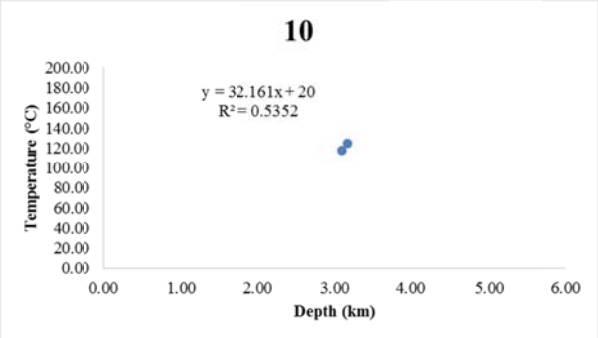
10
y = 32.161x + 20
R² = 0.5352
Temperature (°C)
Depth (km)

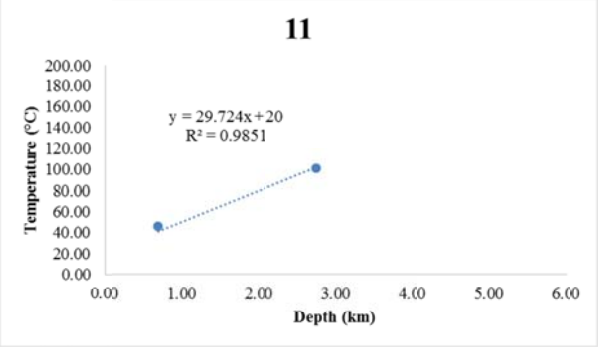
11
y = 29.724x + 20
R² = 0.9851
Temperature (°C)
Depth (km)

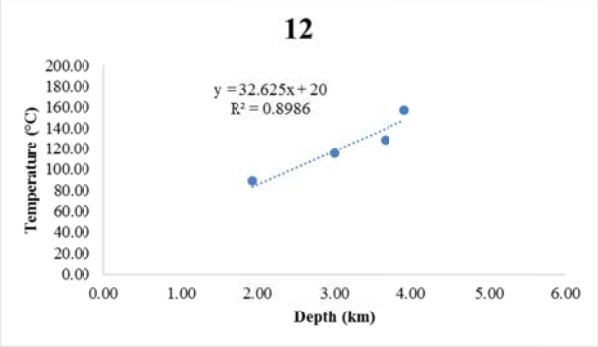
12
y = 32.625x + 20
R² = 0.8986
Temperature (°C)
Depth (km)

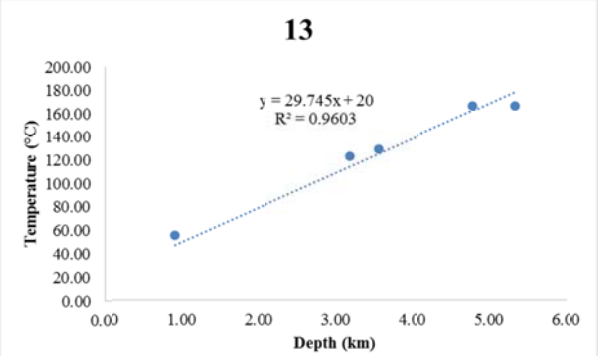
13
y = 29.745x + 20
R² = 0.9603
Temperature (°C)
Depth (km)

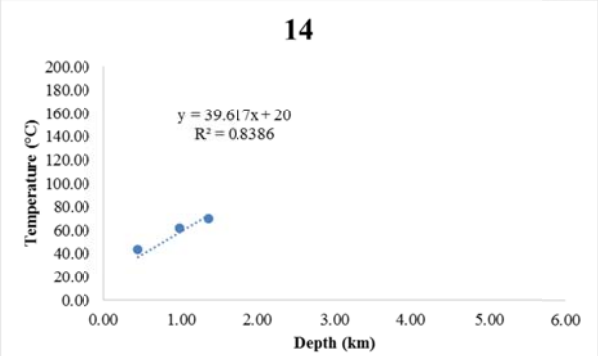
14
y = 39.617x + 20
R² = 0.8386
Temperature (°C)
Depth (km)

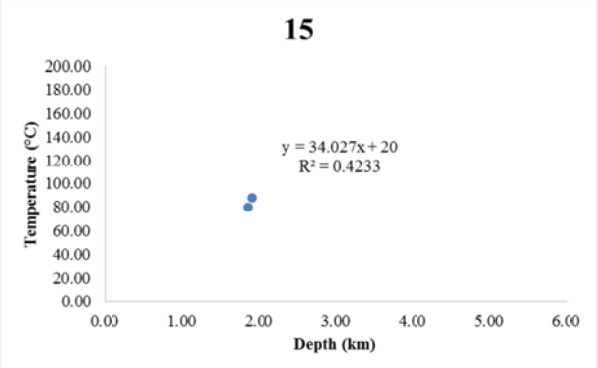
15
y = 34.027x + 20
R² = 0.4233
Temperature (°C)
Depth (km)

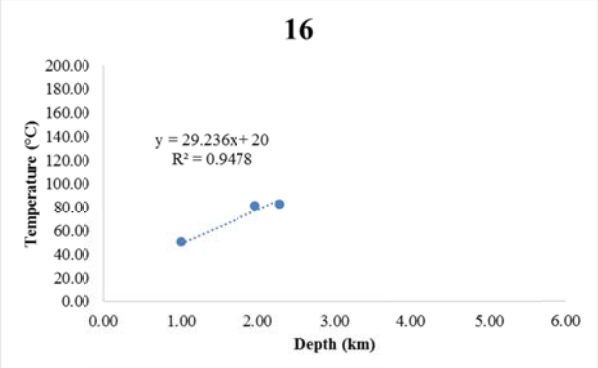
16
y = 29.236x + 20
R² = 0.9478
Temperature (°C)
Depth (km)

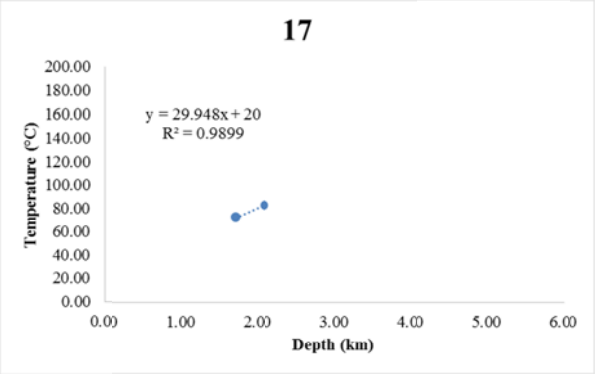
17
y = 29.948x + 20
R² = 0.9899
Temperature (°C)
Depth (km)

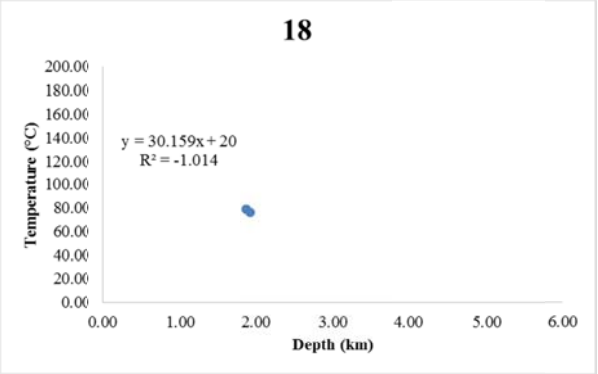
18
y = 30.159x + 20
R² = -1.014
Temperature (°C)
Depth (km)

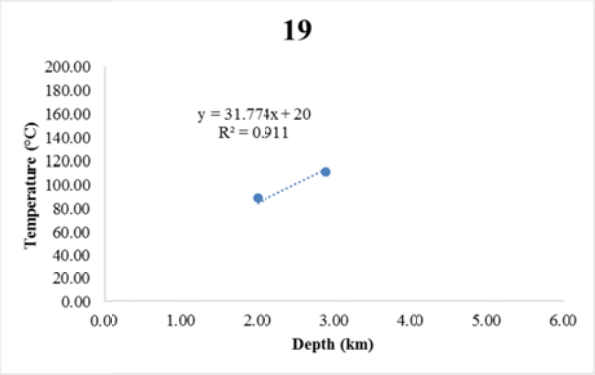
19
y = 31.774x + 20
R² = 0.911
Temperature (°C)
Depth (km)

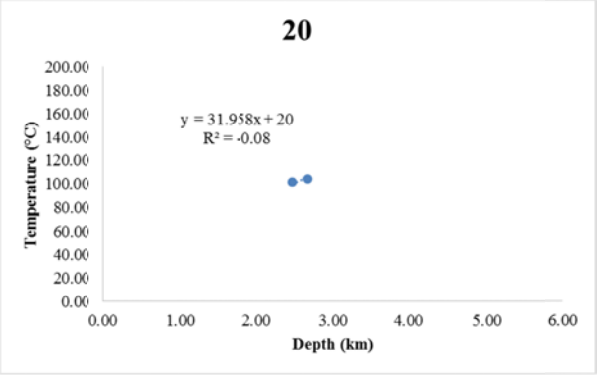
20
y = 31.958x + 20
R² = -0.08
Temperature (°C)
Depth (km)

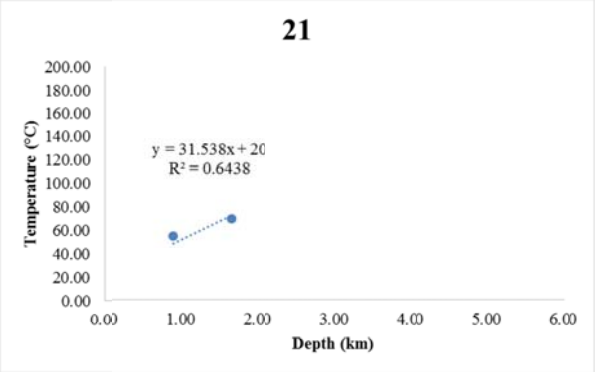
21
y = 31.538x + 20
R² = 0.6438
Temperature (°C)
Depth (km)

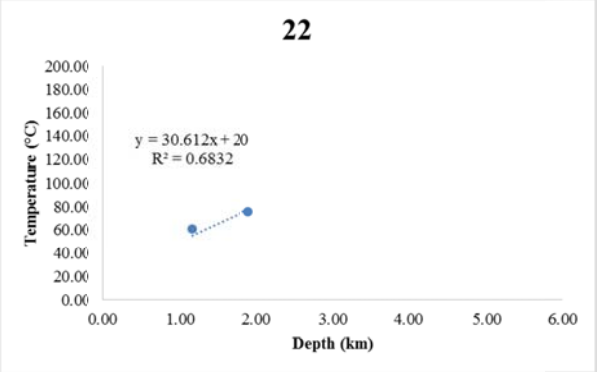
22
y = 30.612x + 20
R² = 0.6832
Temperature (°C)
Depth (km)

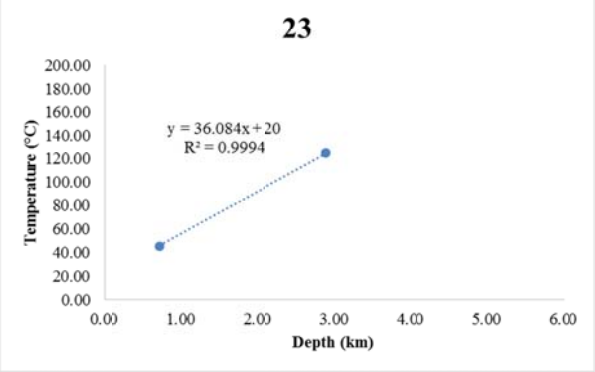
23
y = 36.084x + 20
R² = 0.9994
Temperature (°C)
Depth (km)

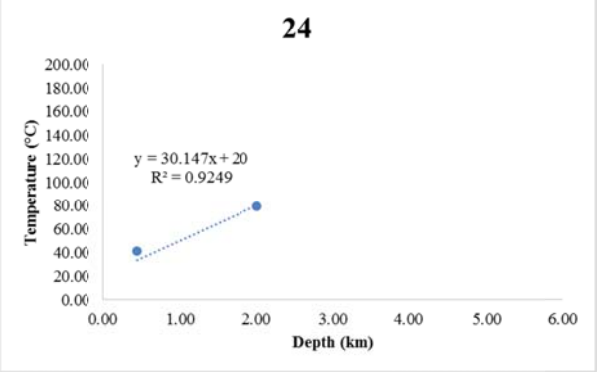
24
y = 30.147x + 20
R² = 0.9249
Temperature (°C)
Depth (km)

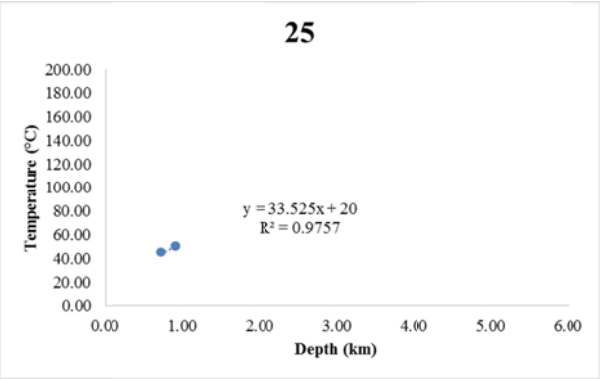
25
Temperature (°C)
200.00
180.00
160.00
140.00
120.00
100.00
80.00
60.00
40.00
20.00
0.00
y = 33.525x + 20
R² = 0.9757
0.00
1.00
2.00
3.00
4.00
5.00
6.00
Depth (km)

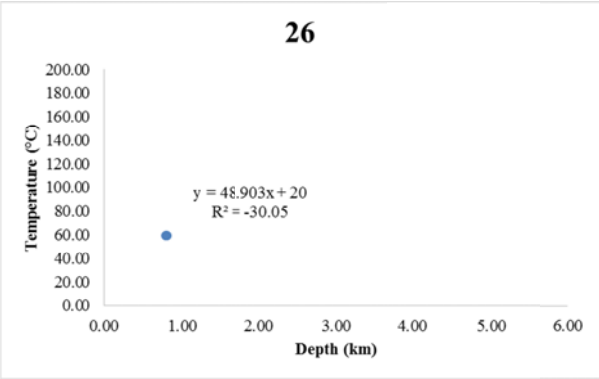
26
Temperature (°C)
200.00
180.00
160.00
140.00
120.00
100.00
80.00
60.00
40.00
20.00
0.00
y = 48.903x + 20
R² = -30.05
0.00
1.00
2.00
3.00
4.00
5.00
6.00
Depth (km)

Appendix C. Geothermal gradient and data derived from geothermal gradient

Interpolated

API from NGD	lat	lon	dT/dZ	Depth to 100 °C	Depth to 150 °C	Temp (°C) at 5 km	Heat flow (mW/m^2)
17067203300000	32.6482378	-91.723324	31.96	2.50	4.07	179.79	78.94
17067001800000	32.733536	-91.833926	41.00	1.95	3.17	225.02	101.28
17067216210000	32.6159573	-91.909286	22.34	3.58	5.82	131.72	55.19
17067217670000	32.8700127	-91.996411	34.73	2.30	3.74	193.64	85.78
17111000230000	32.8725429	-92.722055	32.02	2.50	4.06	180.11	79.09
17111022030000	32.6786392	-92.198236	28.65	2.79	4.54	163.24	70.76
17111022700000	32.7311384	-92.282539	30.26	2.64	4.30	171.31	74.74
17111024390000	32.7306403	-92.395342	29.70	2.69	4.38	168.48	73.35
17111206660000	32.7201416	-92.452344	30.39	2.63	4.28	171.96	75.07
17111209320000	32.7475358	-92.112433	26.42	3.03	4.92	152.12	65.27
17111227360000	32.8639493	-92.619582	32.35	2.47	4.02	181.74	79.90
17111228630000	32.6080006	-92.368629	32.83	2.44	3.96	184.13	81.08
17111229800000	32.7791821	-92.495927	32.16	2.49	4.04	180.81	79.44
17111238810000	32.9139889	-92.249852	29.72	2.69	4.37	168.62	73.42
17111241380000	32.6366686	-92.288419	32.63	2.45	3.98	183.13	80.58
17111245780000	32.9939332	-92.671419	29.75	2.69	4.37	168.73	73.47
17111248970000	32.9416549	-92.154461	32.45	2.47	4.01	182.24	80.15
17111250240000	32.8032415	-92.615415	31.89	2.51	4.08	179.46	78.77
17111254110000	32.814433	-92.674677	31.92	2.51	4.07	179.60	78.84
17111255680000	32.9094011	-92.509238	28.15	2.84	4.62	160.74	69.52
17111255880000	32.9254274	-92.348427	31.26	2.56	4.16	176.29	77.21
17111256110000	32.8095545	-92.181458	33.11	2.42	3.93	185.53	81.77

Extrapolated

API from NGD	lat	lon	dT/dZ	Depth to 100 °C	Depth to 150 °C	temp at 5 km	Heat flow (mW/m^2)

17067000080000	32.940928	-91.597021	17.02	4.70	7.64	105.12	42.05
17067001970000	32.5858395	-91.770325	39.62	2.02	3.28	218.09	97.85
17067000050000	32.9790275	-91.662422	41.11	1.95	3.16	225.54	101.54
17067000090000	32.9720283	-91.748025	25.24	3.17	5.15	146.22	62.35
17067000150000	32.9435285	-91.891328	34.03	2.35	3.82	190.14	84.05
17067000620000	32.8224316	-91.58462	28.76	2.78	4.52	163.82	71.04
17067000640000	32.7605342	-91.627921	35.56	2.25	3.66	197.80	87.83
17067000610000	32.8702301	-91.58482	29.24	2.74	4.45	166.18	72.21
17067002260000	32.9584281	-92.046732	32.24	2.48	4.03	181.19	79.63
17067000720000	32.8165333	-91.801926	29.95	2.67	4.34	169.74	73.97
17067201430000	32.8548312	-91.628521	30.16	2.65	4.31	170.80	74.49
17067202550000	32.7025368	-91.897528	31.77	2.52	4.09	178.87	78.48
17067206960000	32.8881309	-91.723124	27.60	2.90	4.71	158.01	68.18
17067207440000	32.6696377	-91.906228	34.44	2.32	3.77	192.20	85.07
17067000360000	32.9291289	-91.869327	39.25	2.04	3.31	216.25	96.95
17067000600000	32.9143286	-91.524219	28.05	2.85	4.63	160.25	69.28
17067000590000	32.9280286	-91.58832	31.69	2.52	4.10	178.46	78.28
17067000540000	32.885631	-91.726924	32.38	2.47	4.01	181.91	79.98
17067002070000	32.5883395	-91.835027	22.63	3.54	5.75	133.13	55.89
17067000410000	32.9192291	-91.891028	30.09	2.66	4.32	170.46	74.33
17067000030000	32.9970268	-91.640822	27.07	2.96	4.80	155.34	66.86
17067002030000	32.625139	-91.893028	31.54	2.54	4.12	177.69	77.90
17067000140000	32.950828	-91.891528	30.61	2.61	4.25	173.06	75.61
17067000010000	33.0050272	-91.737224	29.70	2.69	4.38	168.49	73.35
17067000570000	32.8664309	-91.636822	29.89	2.68	4.35	169.44	73.82
17067000180000	32.9328287	-91.882628	32.19	2.49	4.04	180.95	79.51
17067002990000	32.9173297	-92.062433	24.24	3.30	5.36	141.19	59.87
17067000170000	32.9401287	-91.882828	37.49	2.13	3.47	207.43	92.59
17067002080000	32.5865398	-91.828526	29.66	2.70	4.38	168.31	73.27

17067001820000	32.7233359	-91.888928	36.08	2.22	3.60	200.42	89.13
17067002140000	32.5673403	-91.834427	39.92	2.00	3.26	219.62	98.61
17067001920000	32.7539355	-91.786225	47.16	1.70	2.76	255.81	116.49
17067000060000	32.9527284	-91.669923	36.50	2.19	3.56	202.49	90.15
17067001960000	32.595439	-91.765225	30.15	2.65	4.31	170.74	74.46
17067001450000	32.7183362	-91.98383	32.59	2.45	3.99	182.96	80.50
17067002320000	32.9549284	-92.060533	32.57	2.46	3.99	182.85	80.45
17067002230000	32.9613286	-92.073233	32.57	2.46	3.99	182.85	80.45
17067002250000	32.9639795	-92.065722	32.36	2.47	4.02	181.81	79.93
17067002190000	32.9732282	-92.072132	31.67	2.53	4.11	178.34	78.22
17067002370000	32.9568282	-92.074433	33.94	2.36	3.83	189.68	83.82
17067000770000	32.8318323	-91.943429	29.92	2.67	4.35	169.58	73.89
17067001390000	32.747335	-91.97253	29.40	2.72	4.42	166.99	72.61
17067005530000	32.7220362	-92.013231	40.12	1.99	3.24	220.60	99.10
17067001600000	32.6893371	-91.929729	31.30	2.56	4.15	176.49	77.30
17067002900000	32.9280291	-92.066133	32.88	2.43	3.95	184.40	81.21
17067000750000	32.7722348	-91.837727	43.00	1.86	3.02	235.02	106.22
17067000450000	32.8488316	-91.885128	48.90	1.64	2.66	264.52	120.79
17067000980000	32.8058333	-91.943829	33.79	2.37	3.85	188.95	83.46
17067001740000	32.6749376	-91.944329	31.82	2.51	4.09	179.11	78.60
17067000830000	32.8376321	-91.95393	31.34	2.55	4.15	176.72	77.42
17067004850000	32.7767344	-92.029231	33.20	2.41	3.92	186.00	82.00
17067004740000	32.7965337	-92.022831	33.43	2.39	3.89	187.17	82.58
17067004090000	32.8470317	-92.014231	32.20	2.48	4.04	181.02	79.55
17067004020000	32.8543314	-92.031532	38.03	2.10	3.42	210.15	93.93
17067001300000	32.812733	-91.951629	31.07	2.57	4.18	175.37	76.75
17067000270000	32.8615311	-91.97103	31.49	2.54	4.13	177.47	77.79
17067200230000	32.8020334	-92.046432	35.81	2.23	3.63	199.07	88.46
17067200410000	32.8600313	-91.95323	31.62	2.53	4.11	178.10	78.10

17067201330000	32.8326319	-92.005631	31.48	2.54	4.13	177.38	77.75
17067201120000	32.7657347	-91.97233	41.98	1.91	3.10	229.91	103.70
17067201190000	32.7544348	-92.009531	40.91	1.96	3.18	224.57	101.06
17067201400000	32.785434	-91.956829	41.57	1.92	3.13	227.86	102.68
17067201470000	32.8448317	-91.97373	41.92	1.91	3.10	229.59	103.54
17067201540000	32.8594312	-91.97773	41.30	1.94	3.15	226.50	102.01
17067203090000	32.7356358	-92.024031	31.82	2.51	4.09	179.12	78.60
17067203370000	32.6709377	-91.944429	31.68	2.53	4.10	178.40	78.25
17067203230000	32.7240362	-92.016031	31.82	2.51	4.09	179.12	78.60
17067202470000	32.8634311	-91.96143	37.06	2.16	3.51	205.31	91.55
17067203440000	32.754835	-91.99963	33.12	2.42	3.92	185.62	81.82
17067203580000	32.5615408	-91.901928	33.53	2.39	3.88	187.63	82.81
17067205930000	32.5225416	-91.848727	30.18	2.65	4.31	170.91	74.55
17067204330000	32.9221291	-92.028531	40.03	2.00	3.25	220.17	98.89
17067204400000	32.9032296	-92.034032	35.21	2.27	3.69	196.05	86.97
17067204540000	32.776234	-91.98653	33.95	2.36	3.83	189.74	83.85
17067206140000	32.5984394	-91.896128	34.52	2.32	3.77	192.62	85.27
17067205820000	32.6024396	-91.881528	34.64	2.31	3.75	193.19	85.55
17067205310000	32.7749341	-91.95833	44.14	1.81	2.94	240.71	109.03
17067205650000	32.8413319	-91.97373	34.16	2.34	3.81	190.79	84.37
17067206000000	32.7841338	-91.95613	40.70	1.97	3.19	223.52	100.54
17067206300000	32.9154294	-91.912328	30.20	2.65	4.31	170.98	74.59
17067206890000	32.58114	-91.843327	33.11	2.42	3.93	185.57	81.79
17067207170000	32.6430382	-91.896128	34.93	2.29	3.72	194.63	86.27
17067206410000	32.8449317	-91.98673	33.69	2.37	3.86	188.45	83.21
17067206590000	32.7954332	-91.98823	34.05	2.35	3.82	190.24	84.10
17067207720000	32.8928296	-91.999531	34.01	2.35	3.82	190.05	84.00
17067207930000	32.5340409	-91.845227	26.07	3.07	4.99	150.37	64.40
17067206810000	32.5759402	-91.925129	34.02	2.35	3.82	190.12	84.04

17067208150000	32.8863303	-91.896628	30.90	2.59	4.21	174.49	76.32
17067208560000	32.9205294	-92.069933	34.49	2.32	3.77	192.47	85.20
17067208630000	32.7712342	-92.007631	34.73	2.30	3.74	193.64	85.78
17067207310000	32.6469383	-91.887028	34.81	2.30	3.73	194.05	85.98
17067207450000	32.6664378	-91.907628	34.40	2.33	3.78	192.02	84.98
17067207520000	32.6319385	-91.896128	34.81	2.30	3.73	194.05	85.98
17067207590000	32.6423385	-91.908028	34.81	2.30	3.73	194.05	85.98
17067207610000	32.5250412	-91.843427	31.52	2.54	4.12	177.60	77.85
17067209900000	32.7995334	-91.98473	34.55	2.32	3.76	192.75	85.34
17067208840000	32.9028301	-92.048732	34.44	2.32	3.78	192.18	85.06
17067208220000	32.6330385	-91.906628	34.04	2.35	3.82	190.19	84.07
17067208290000	32.7299358	-91.99983	33.60	2.38	3.87	187.98	82.98
17067208360000	32.6330385	-91.900228	34.04	2.35	3.82	190.19	84.07
17067207460000	32.6679375	-91.903828	35.46	2.26	3.67	197.28	87.58
17067208490000	32.9083301	-92.069333	34.61	2.31	3.76	193.06	85.49
17067208700000	32.8721313	-92.057232	35.39	2.26	3.67	196.97	87.42
17067208910000	32.7850337	-91.96283	32.21	2.48	4.04	181.07	79.57
17067209050000	32.9250291	-92.057033	34.44	2.32	3.78	192.18	85.06
17067209120000	32.9161295	-92.041432	34.49	2.32	3.77	192.47	85.20
17067209230000	32.9173294	-92.038232	34.38	2.33	3.78	191.89	84.92
17067209290000	32.7630347	-92.00313	33.72	2.37	3.86	188.61	83.29
17067209300000	32.7618348	-92.007331	33.06	2.42	3.93	185.31	81.66
17067209360000	32.925029	-92.051832	35.64	2.24	3.65	198.19	88.03
17067209470000	32.6339384	-91.883628	34.75	2.30	3.74	193.76	85.84
17067209760000	32.9429283	-91.894728	31.08	2.57	4.18	175.42	76.78
17067209830000	32.7365359	-91.852127	31.90	2.51	4.08	179.50	78.79
17067209970000	32.8123349	-91.977867	34.01	2.35	3.82	190.05	84.00
17067210670000	32.8221326	-91.97893	34.23	2.34	3.80	191.13	84.54
17067210750000	32.9347288	-92.039632	34.44	2.32	3.78	192.18	85.06

17067210180000	32.8221326	-91.96693	32.55	2.46	3.99	182.76	80.40
17067210250000	32.8221326	-91.96983	34.01	2.35	3.82	190.05	84.00
17067210390000	32.8078333	-92.057332	34.38	2.33	3.78	191.90	84.92
17067210460000	32.6782304	-91.893225	34.73	2.30	3.74	193.64	85.78
17067210530000	32.8167328	-91.97563	34.01	2.35	3.82	190.05	84.00
17067210600000	32.6351387	-91.899228	34.41	2.32	3.78	192.07	85.00
17067210810000	32.8884306	-92.052232	34.84	2.30	3.73	194.19	86.05
17067211310000	32.6205821	-91.891936	36.11	2.22	3.60	200.56	89.20
17067210610000	32.9302441	-91.875276	30.94	2.59	4.20	174.68	76.41
17067211450000	32.583669	-91.892083	29.89	2.68	4.35	169.46	73.83
17067211800000	32.6460744	-91.883223	33.81	2.37	3.85	189.03	83.50
17067211520000	32.7043556	-91.992706	33.98	2.35	3.83	189.91	83.93
17067211590000	32.8487777	-91.977904	37.67	2.12	3.45	208.33	93.04
17067212170000	32.7093715	-91.989329	34.23	2.34	3.80	191.13	84.54
17067210990000	32.5764054	-91.896417	34.35	2.33	3.78	191.77	84.86
17067211970000	32.8842022	-92.074504	35.52	2.25	3.66	197.60	87.73
17067212030000	32.8581607	-92.061731	34.83	2.30	3.73	194.13	86.02
17067212100000	32.7087226	-91.985139	34.53	2.32	3.76	192.65	85.29
17067212310000	32.580099	-91.869967	33.69	2.37	3.86	188.45	83.21
17067212450000	32.910699	-92.075684	34.57	2.31	3.76	192.85	85.39
17067212520000	32.555029	-91.892175	35.26	2.27	3.69	196.31	87.10
17067212590000	32.9344451	-92.052044	34.55	2.32	3.76	192.76	85.34
17067212690000	32.7435816	-92.008424	33.93	2.36	3.83	189.63	83.80
17067212730000	32.7137934	-92.016711	34.72	2.30	3.74	193.58	85.75
17067213300000	32.8636949	-92.004131	34.23	2.34	3.80	191.13	84.54
17067213710000	32.7989445	-92.003896	33.49	2.39	3.88	187.44	82.72
17067213840000	32.6604891	-91.891638	34.01	2.35	3.82	190.05	84.00
17067213910000	32.6082632	-91.851717	49.79	1.61	2.61	268.97	122.99
17067212800000	32.7112846	-92.007524	34.15	2.34	3.81	190.75	84.35

17067214010000	32.7040449	-92.019038	34.04	2.35	3.82	190.19	84.07
17067214080000	32.7286251	-92.036403	34.52	2.32	3.77	192.61	85.27
17067214110000	32.7399925	-92.01124	35.26	2.27	3.69	196.31	87.10
17067214180000	32.7401396	-92.028669	34.29	2.33	3.79	191.43	84.68
17067214300000	32.5652067	-91.887953	33.61	2.38	3.87	188.06	83.02
17067214380000	32.8753398	-92.038948	34.87	2.29	3.73	194.37	86.14
17067214430000	32.5730265	-91.879494	33.49	2.39	3.88	187.44	82.72
17067214750000	32.7717136	-92.03459	31.65	2.53	4.11	178.24	78.17
17067214970000	32.695327	-91.900443	34.75	2.30	3.74	193.76	85.84
17067215100000	32.69629	-91.877684	33.49	2.39	3.88	187.44	82.72
17067215450000	32.786437	-91.96915	34.11	2.35	3.81	190.55	84.25
17067215520000	32.6409397	-91.913469	31.92	2.51	4.07	179.60	78.84
17067215600000	32.7431965	-91.965332	34.49	2.32	3.77	192.47	85.20
17067215660000	32.7338677	-91.984347	33.71	2.37	3.86	188.54	83.26
17067215730000	32.8470821	-92.052797	34.64	2.31	3.75	193.22	85.57
17067215800000	32.7460914	-91.977059	34.49	2.32	3.77	192.47	85.20
17067216020000	32.5894799	-91.890326	28.89	2.77	4.50	164.46	71.36
17067209920000	32.7949772	-92.191458	34.15	2.34	3.81	190.75	84.35
17067216090000	32.726954	-91.986458	34.55	2.32	3.76	192.76	85.34
17067216230000	32.8894247	-91.697877	28.32	2.82	4.59	161.62	69.96
17067216370000	32.6806604	-91.913932	37.15	2.15	3.50	205.73	91.75
17067216490000	32.9300985	-92.000947	28.88	2.77	4.50	164.41	71.34
17067216550000	32.9089654	-92.016878	34.44	2.32	3.78	192.18	85.06
17067216610000	32.8747343	-92.07175	35.46	2.26	3.67	197.28	87.58
17067216670000	32.9409212	-91.883872	31.59	2.53	4.11	177.97	78.04
17067216750000	32.6110094	-91.906852	30.36	2.63	4.28	171.82	75.00
17067216810000	32.8270595	-91.940521	35.31	2.27	3.68	196.53	87.20
17067217160000	32.6548161	-91.886145	32.11	2.49	4.05	180.54	79.31
17067217010000	32.9229469	-91.976666	31.09	2.57	4.18	175.46	76.80

17067217090000	32.6422246	-91.882891	33.75	2.37	3.85	188.77	83.37
17067217170000	32.9300296	-91.97699	28.34	2.82	4.59	161.70	70.00
17067217190000	32.7241869	-91.623877	25.50	3.14	5.10	147.50	62.98
17067217240000	32.6422618	-91.90235	35.11	2.28	3.70	195.57	86.73
17067217310000	32.7403056	-91.756213	39.27	2.04	3.31	216.37	97.01
17067217320000	32.5281328	-91.844789	33.33	2.40	3.90	186.66	82.33
17067217390000	32.8561763	-91.979425	37.65	2.12	3.45	208.27	93.01
17067218010000	32.8882197	-91.88579	32.89	2.43	3.95	184.44	81.23
17067218020000	32.6856475	-91.961316	33.79	2.37	3.85	188.94	83.46
17067218500000	32.7403245	-91.759465	36.48	2.19	3.56	202.41	90.11
17067218570000	32.7671869	-92.014737	34.75	2.30	3.74	193.76	85.84
17067219040000	32.8275013	-92.043763	35.27	2.27	3.69	196.36	87.12
17067219110000	32.6845245	-91.876145	35.11	2.28	3.70	195.57	86.73
17067219180000	32.8311329	-92.048686	35.11	2.28	3.70	195.56	86.73
17067219250000	32.8781146	-92.07192	36.82	2.17	3.53	204.11	90.95
17067219320000	32.8580716	-92.040422	34.64	2.31	3.75	193.19	85.55
17067219540000	32.6743065	-91.898745	35.47	2.26	3.67	197.34	87.60
17067219750000	32.9190418	-92.076333	34.23	2.34	3.80	191.13	84.54
17067219890000	32.769217	-91.660704	33.35	2.40	3.90	186.77	82.38
17067219960000	32.608297	-91.821027	32.17	2.49	4.04	180.83	79.45
17067220010000	32.8117996	-91.987353	33.94	2.36	3.83	189.68	83.82
17067220030000	32.8119331	-92.005303	35.47	2.26	3.67	197.34	87.60
17067220040000	32.8252655	-92.002803	35.51	2.25	3.66	197.56	87.72
17067880010000	32.912519	-92.053292	38.04	2.10	3.42	210.20	93.96
17111009850000	32.8272344	-92.236437	37.85	2.11	3.44	209.23	93.48
17111009640000	32.8061372	-92.338541	28.43	2.81	4.57	162.13	70.21
17111000880000	32.941936	-92.484047	41.36	1.93	3.14	226.82	102.17
17111001560000	32.9337313	-92.243837	27.22	2.94	4.78	156.12	67.24
	32.8239452	-92.180365	32.39	2.47	4.01	181.97	80.01

17111017630000	32.7529359	-92.101033	31.93	2.51	4.07	179.64	78.86
17111201610000	32.7354374	-92.218237	30.94	2.59	4.20	174.69	76.42
17111221590000	32.8731892	-92.286146	34.61	2.31	3.76	193.06	85.49
17111235430000	32.7493738	-92.205856	33.70	2.37	3.86	188.52	83.25
17111238860000	32.9109074	-92.144038	34.23	2.34	3.80	191.15	84.55
17111244540000	32.8895795	-92.124251	29.19	2.74	4.45	165.95	72.10

Appendix D. Mud weights and pressure data

Parish	APINo	lat	lon	Depth (m)	MW (lbs/gal)	hydrostatic pressure (kPa)	geostatic ratio (kPa/m)
Morehouse	17067000080000	32.940928	-91.597021	1498.70	9.8	17247.25	11.51
Morehouse	17067001970000	32.5858395	-91.770325	442.57	10.0	5197.09	11.74
Morehouse	17067001970000	32.5858395	-91.770325	1347.83	10.7	16935.43	12.56
Morehouse	17067000050000	32.9790275	-91.662422	1127.46	10.2	13504.49	11.98
Morehouse	17067000090000	32.9720283	-91.748025	2011.07	10.9	25741.42	12.80
Morehouse	17067000150000	32.9435285	-91.891328	1851.66	10.0	21744.02	11.74
Morehouse	17067000150000	32.9435285	-91.891328	1908.96	10.0	22416.93	11.74
Morehouse	17067000620000	32.8224316	-91.58462	1873.91	9.9	21785.26	11.63
Morehouse	17067000640000	32.7605342	-91.627921	917.45	9.5	10234.90	11.16
Morehouse	17067000610000	32.8702301	-91.58482	997.92	9.1	10663.84	10.69
Morehouse	17067000610000	32.8702301	-91.58482	2284.17	10.7	28700.61	12.56
Morehouse	17067000610000	32.8702301	-91.58482	1968.09	10.0	23111.30	11.74
Morehouse	17067002260000	32.9584281	-92.046732	2168.65	11.7	29795.76	13.74
Morehouse	17067000720000	32.8165333	-91.801926	1711.76	10.9	21910.25	12.80
Morehouse	17067000720000	32.8165333	-91.801926	2097.02	10.8	26595.36	12.68
Morehouse	17067201430000	32.8548312	-91.628521	1880.62	9.7	21421.53	11.39
Morehouse	17067201430000	32.8548312	-91.628521	1923.59	9.7	21911.07	11.39
Morehouse	17067202550000	32.7025368	-91.897528	1999.49	9.2	21601.57	10.80
Morehouse	17067202550000	32.7025368	-91.897528	2899.56	10.1	34390.03	11.86
Morehouse	17067203300000	32.6482378	-91.723324	2477.72	9.6	27932.00	11.27
Morehouse	17067203300000	32.6482378	-91.723324	2666.09	9.5	29742.43	11.16
Morehouse	17067206960000	32.8881309	-91.723124	1922.37	10.2	23025.90	11.98
Morehouse	17067207440000	32.6696377	-91.906228	749.81	10.1	8893.04	11.86
Morehouse	17067216020000	32.5894799	-91.890326	3902.96	10.2	46749.12	11.98
Morehouse	17067216490000	32.9300985	-92.000947	2332.33	9.6	26292.98	11.27
Morehouse	17067217190000	32.7241869	-91.623877	1985.47	9.0	20983.79	10.57

Morehouse	17067217310000	32.7403056	-91.756213	2402.13	9.2	25951.52	10.80
Morehouse	17067218010000	32.8882197	-91.88579	2157.98	9.2	23313.89	10.80
Morehouse	17067218500000	32.7403245	-91.759465	1746.50	9.4	19278.63	11.04
Morehouse	17067220010000	32.8117996	-91.987353	764.13	9.6	8636.72	11.30
Morehouse	17067220030000	32.8119331	-92.005303	762.00	9.7	8679.71	11.39
Morehouse	17067220040000	32.8252655	-92.002803	760.78	9.3	8308.47	10.92
Union	17111009850000	32.8272344	-92.236437	767.49	9.5	8561.96	11.16
Union	17111009850000	32.8272344	-92.236437	981.46	9.8	11294.72	11.51
Union	17111009640000	32.8061372	-92.338541	2129.64	10.1	25258.40	11.86
Union	17111009640000	32.8061372	-92.338541	2668.83	10.2	31966.83	11.98
Union	17111000880000	32.941936	-92.484047	678.48	10.2	8126.79	11.98
Union	17111001560000	32.9337313	-92.243837	1619.10	10.5	19963.70	12.33
Union	17111001560000	32.9337313	-92.243837	2240.28	10.9	28675.27	12.80
Union	17111001560000	32.9337313	-92.243837	2510.03	11.0	32422.76	12.92
Union	17111001560000	32.9337313	-92.243837	523.65	10.0	6149.17	11.74
Union	17111000230000	32.8725429	-92.722055	1011.33	9.4	11163.44	11.04
Union	17111000230000	32.8725429	-92.722055	3032.76	12.4	44160.95	14.56
Union	17111000230000	32.8725429	-92.722055	3348.23	12.4	48754.58	14.56
Union	17111000230000	32.8725429	-92.722055	3480.82	12.5	51093.98	14.68
Union	17111022030000	32.6786392	-92.198236	733.96	9.5	8187.92	11.16
Union	17111022030000	32.6786392	-92.198236	2174.14	10.4	26552.12	12.21
Union	17111022030000	32.6786392	-92.198236	3199.79	10.3	38702.36	12.10
Union	17111022700000	32.7311384	-92.282539	655.32	10.2	7849.32	11.98
Union	17111022700000	32.7311384	-92.282539	2218.94	11.0	28662.74	12.92
Union	17111022700000	32.7311384	-92.282539	2980.03	11.0	38493.90	12.92
Union	17111022700000	32.7311384	-92.282539	3357.37	12.0	47310.70	14.09
Union	17111022700000	32.7311384	-92.282539	3656.08	12.0	51519.92	14.09
Union	17111024390000	32.7306403	-92.395342	1381.96	10.0	16228.38	11.74
Union	17111024390000	32.7306403	-92.395342	3350.97	10.6	41711.45	12.45

Union	17111017630000	32.7529359	-92.101033	713.23	9.5	7956.70	11.16
Union	17111206660000	32.7201416	-92.452344	3603.65	10.1	42740.81	11.86
Union	17111227360000	32.8639493	-92.619582	3200.40	9.4	35327.33	11.04
Union	17111228630000	32.6080006	-92.368629	3479.60	10.6	43312.52	12.45
Union	17111228630000	32.6080006	-92.368629	4083.10	14.4	69044.85	16.91
Union	17111229800000	32.7791821	-92.495927	3095.24	10.4	37801.32	12.21
Union	17111229800000	32.7791821	-92.495927	3162.60	10.4	38623.97	12.21
Union	17111238810000	32.9139889	-92.249852	701.04	9.3	7656.04	10.92
Union	17111238810000	32.9139889	-92.249852	2754.48	9.6	31051.97	11.27
Union	17111241380000	32.6366686	-92.288419	1937.00	9.1	20699.06	10.69
Union	17111241380000	32.6366686	-92.288419	3002.89	9.5	33499.76	11.16
Union	17111241380000	32.6366686	-92.288419	3657.60	12.4	53259.44	14.56
Union	17111241380000	32.6366686	-92.288419	3913.94	14.5	66643.91	17.03
Union	17111244540000	32.8895795	-92.124251	2325.62	9.5	25944.29	11.16
Union	17111245780000	32.9939332	-92.671419	914.40	9.3	9986.14	10.92
Union	17111245780000	32.9939332	-92.671419	3185.16	10.7	40021.53	12.56
Union	17111245780000	32.9939332	-92.671419	3554.27	11.0	45911.57	12.92
Union	17111245780000	32.9939332	-92.671419	4792.98	11.3	63600.82	13.27
Union	17111245780000	32.9939332	-92.671419	5334.00	11.4	71406.30	13.39
Union	17111248970000	32.9416549	-92.154461	2549.65	9.9	29641.13	11.63
Union	17111250240000	32.8032415	-92.615415	3358.29	10.5	41408.14	12.33
Union	17111254110000	32.814433	-92.674677	3657.60	11.9	51111.88	13.97
Union	17111255680000	32.9094011	-92.509238	2859.02	9.9	33237.75	11.63
Union	17111255880000	32.9254274	-92.348427	2819.40	11.3	37412.25	13.27
Union	17111256110000	32.8095545	-92.181458	3050.44	10.1	36179.48	11.86

Appendix E. Pressure profiles

Parish	APINo	lat	lon	Depth (m)	MW (lbs/gal)	hydrostatic pressure (kPa)	geostatic ratio (kPa/m)	Plot #
Morehouse	17067000150000	32.9435285	-91.891328	1851.66	10	21744.02458	11.74298985	1
Morehouse	17067000150000	32.9435285	-91.891328	1908.962	10	22416.92608	11.74298985	
Morehouse	17067000610000	32.8702301	-91.58482	997.9152	9.1	10663.84234	10.68612076	2
Morehouse	17067000610000	32.8702301	-91.58482	2284.171	10.7	28700.60915	12.56499914	
Morehouse	17067000610000	32.8702301	-91.58482	1968.094	10	23111.30316	11.74298985	
Morehouse	17067000720000	32.8165333	-91.801926	1711.757	10.9	21910.24557	12.79985893	3
Morehouse	17067000720000	32.8165333	-91.801926	2097.024	10.8	26595.35806	12.68242903	
Morehouse	17067001970000	32.5858395	-91.770325	442.5696	10	5197.090319	11.74298985	4
Morehouse	17067001970000	32.5858395	-91.770325	1347.826	10.7	16935.4275	12.56499914	
Morehouse	17067201430000	32.8548312	-91.628521	1880.616	9.7	21421.53295	11.39070015	5
Morehouse	17067201430000	32.8548312	-91.628521	1923.593	9.7	21911.0688	11.39070015	
Morehouse	17067202550000	32.7025368	-91.897528	1999.488	9.2	21601.5699	10.80355066	6
Morehouse	17067202550000	32.7025368	-91.897528	2899.562	10.1	34390.02714	11.86041974	
Morehouse	17067203300000	32.6482378	-91.723324	2477.719	9.6	27931.99815	11.27327025	7
Morehouse	17067203300000	32.6482378	-91.723324	2666.086	9.5	29742.42532	11.15584035	
Union	17111000230000	32.8725429	-92.722055	1011.326	9.4	11163.43591	11.03841046	8
Union	17111000230000	32.8725429	-92.722055	3032.76	12.4	44160.95066	14.56130741	
Union	17111000230000	32.8725429	-92.722055	3348.228	12.4	48754.57718	14.56130741	
Union	17111000230000	32.8725429	-92.722055	3480.816	12.5	51093.98368	14.67873731	
Union	17111001560000	32.9337313	-92.243837	1619.098	10.5	19963.69901	12.33013934	9
Union	17111001560000	32.9337313	-92.243837	2240.28	10.9	28675.26797	12.79985893	
Union	17111001560000	32.9337313	-92.243837	2510.028	11	32422.75665	12.91728883	
Union	17111001560000	32.9337313	-92.243837	523.6464	10	6149.174358	11.74298985	
Union	17111009640000	32.8061372	-92.338541	2129.638	10.1	25258.39584	11.86041974	10
Union	17111009640000	32.8061372	-92.338541	2668.829	10.2	31966.83009	11.97784964	

Union	17111009850000	32.8272344	-92.236437	767.4864	9.5	8561.955752	11.15584035	11
Union	17111009850000	32.8272344	-92.236437	981.456	9.8	11294.72329	11.50813005	
Union	17111022030000	32.6786392	-92.198236	733.9584	9.5	8187.922737	11.15584035	12
Union	17111022030000	32.6786392	-92.198236	2174.138	10.4	26552.12056	12.21270944	
Union	17111022030000	32.6786392	-92.198236	3199.79	10.3	38702.35936	12.09527954	
Union	17111022700000	32.7311384	-92.282539	655.32	10.2	7849.324428	11.97784964	13
Union	17111022700000	32.7311384	-92.282539	2218.944	11	28662.74055	12.91728883	
Union	17111022700000	32.7311384	-92.282539	2980.03	11	38493.90307	12.91728883	
Union	17111022700000	32.7311384	-92.282539	3357.372	12	47310.70237	14.09158782	
Union	17111022700000	32.7311384	-92.282539	3656.076	12	51519.91601	14.09158782	
Union	17111024390000	32.7306403	-92.395342	1381.963	10	16228.37983	11.74298985	14
Union	17111024390000	32.7306403	-92.395342	3350.971	10.6	41711.44602	12.44756924	
Union	17111228630000	32.6080006	-92.368629	3479.597	10.6	43312.52208	12.44756924	15
Union	17111228630000	32.6080006	-92.368629	4083.101	14.4	69044.84818	16.90990538	
Union	17111229800000	32.7791821	-92.495927	3095.244	10.4	37801.31562	12.21270944	16
Union	17111229800000	32.7791821	-92.495927	3162.605	10.4	38623.9735	12.21270944	
Union	17111238810000	32.9139889	-92.249852	701.04	9.3	7656.04421	10.92098056	17
Union	17111238810000	32.9139889	-92.249852	2754.478	9.6	31051.97039	11.27327025	
Union	17111241380000	32.6366686	-92.288419	1937.004	9.1	20699.05866	10.68612076	18
Union	17111241380000	32.6366686	-92.288419	3002.89	9.5	33499.75698	11.15584035	
Union	17111241380000	32.6366686	-92.288419	3657.6	12.4	53259.43798	14.56130741	
Union	17111241380000	32.6366686	-92.288419	3913.937	14.5	66643.91415	17.02733528	
Union	17111245780000	32.9939332	-92.671419	914.4	9.3	9986.144621	10.92098056	19
Union	17111245780000	32.9939332	-92.671419	3185.16	10.7	40021.53265	12.56499914	
Union	17111245780000	32.9939332	-92.671419	3554.273	11	45911.56834	12.91728883	
Union	17111245780000	32.9939332	-92.671419	4792.98	11.3	63600.82448	13.26957853	
Union	17111245780000	32.9939332	-92.671419	5334	11.4	71406.30294	13.38700842	

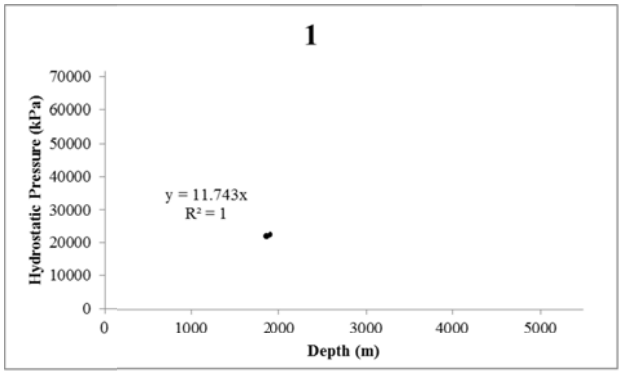
1
Hydrostatic Pressure (kPa)
70000
60000
50000
40000
30000
20000
10000
0
y = 11.743x
R² = 1
0
1000
2000
3000
4000
5000
Depth (m)

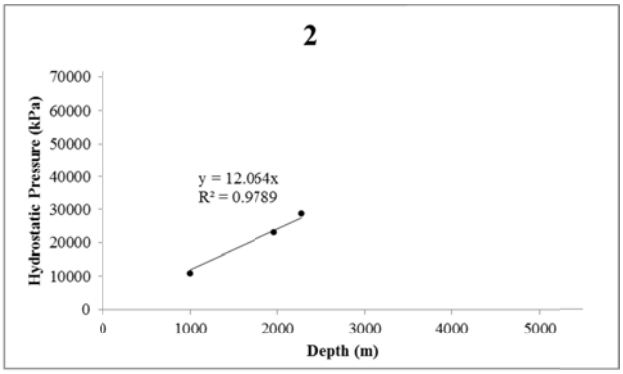
2
Hydrostatic Pressure (kPa)
70000
60000
50000
40000
30000
20000
10000
0
y = 12.064x
R² = 0.9789
0
1000
2000
3000
4000
5000
Depth (m)

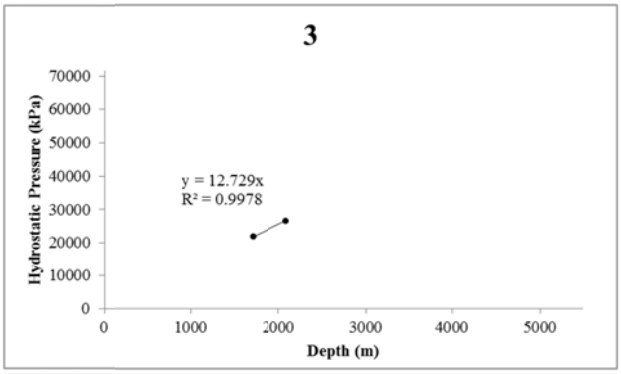
3
Hydrostatic Pressure (kPa)
70000
60000
50000
40000
30000
20000
10000
0
y = 12.729x
R² = 0.9978
0
1000
2000
3000
4000
5000
Depth (m)

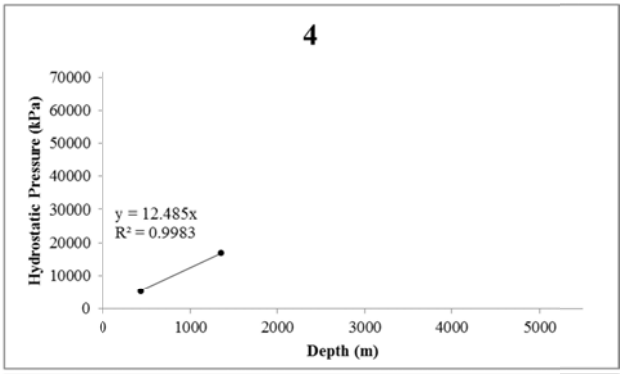
4
Hydrostatic Pressure (kPa)
70000
60000
50000
40000
30000
20000
10000
0
y = 12.485x
R² = 0.9983
0
1000
2000
3000
4000
5000
Depth (m)

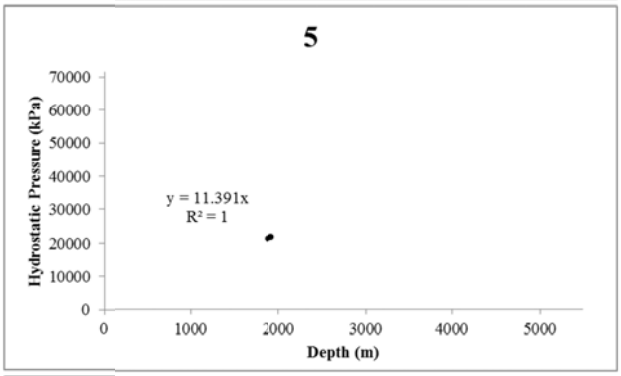
5
Hydrostatic Pressure (kPa)
70000
60000
50000
40000
30000
20000
10000
0
y = 11.391x
R² = 1
0
1000
2000
3000
4000
5000
Depth (m)

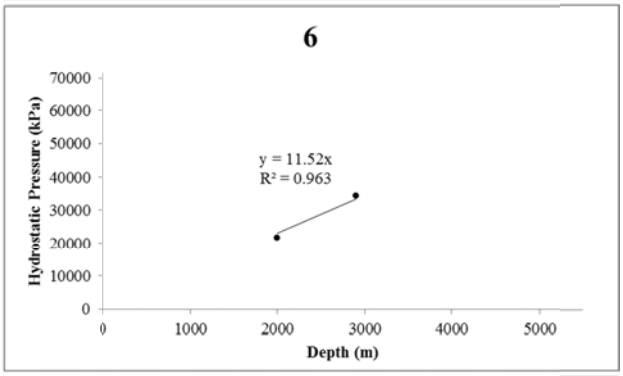
6
Hydrostatic Pressure (kPa)
70000
60000
50000
40000
30000
20000
10000
0
y = 11.52x
R² = 0.963
0
1000
2000
3000
4000
5000
Depth (m)

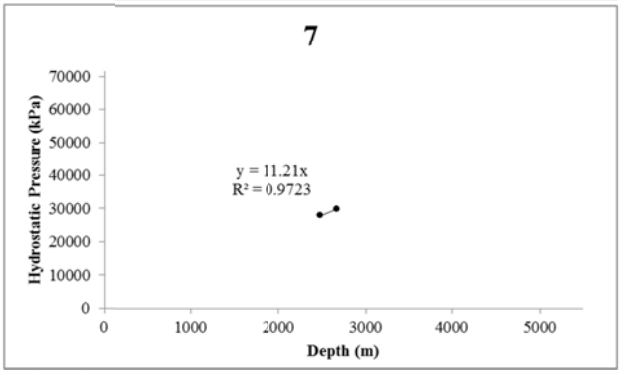
7
Hydrostatic Pressure (kPa)
70000
60000
50000
40000
30000
20000
10000
0
y = 11.21x
R² = 0.9723
0
1000
2000
3000
4000
5000
Depth (m)

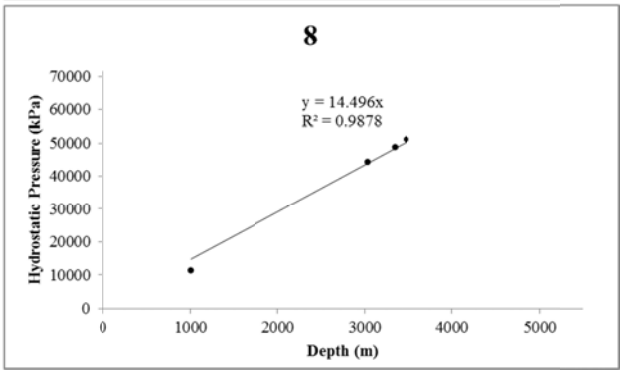
8
Hydrostatic Pressure (kPa)
70000
60000
50000
40000
30000
20000
10000
0
y = 14.496x
R² = 0.9878
0
1000
2000
3000
4000
5000
Depth (m)

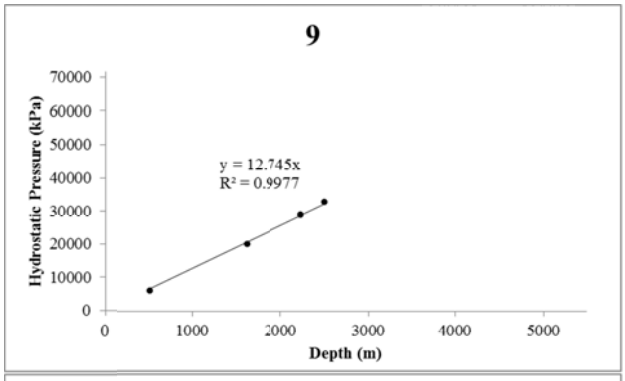
9
Hydrostatic Pressure (kPa)
Depth (m)
y = 12.745x
R² = 0.9977

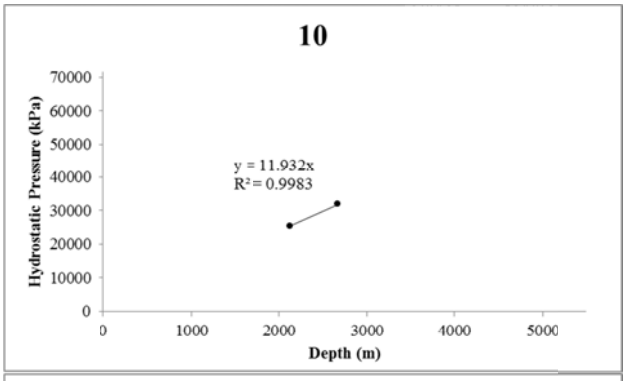
10
Hydrostatic Pressure (kPa)
Depth (m)
y = 11.932x
R² = 0.9983

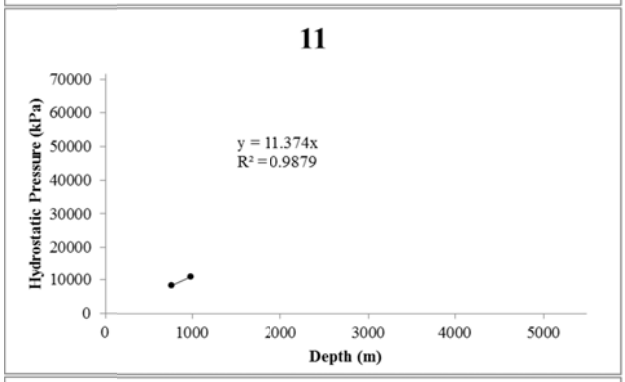
11
Hydrostatic Pressure (kPa)
Depth (m)
y = 11.374x
R² = 0.9879

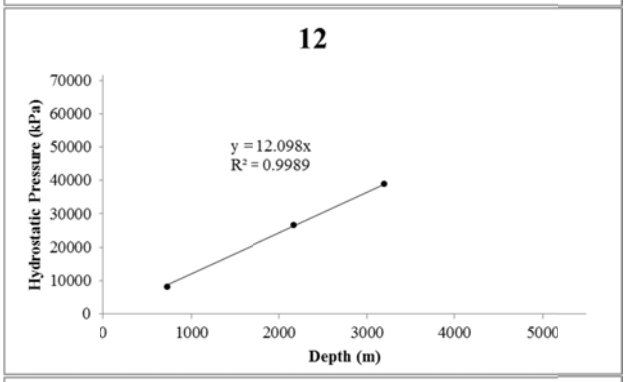
12
Hydrostatic Pressure (kPa)
Depth (m)
y = 12.098x
R² = 0.9989

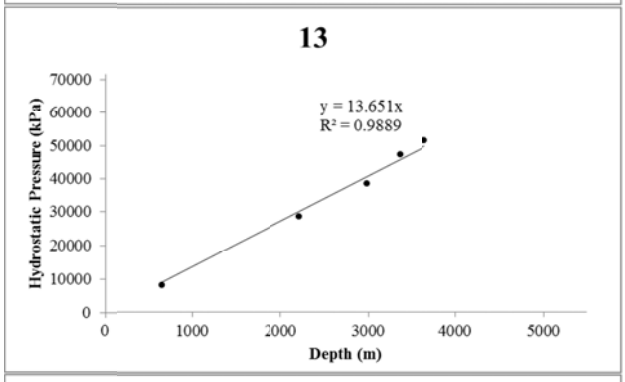
13
Hydrostatic Pressure (kPa)
Depth (m)
y = 13.651x
R² = 0.9889

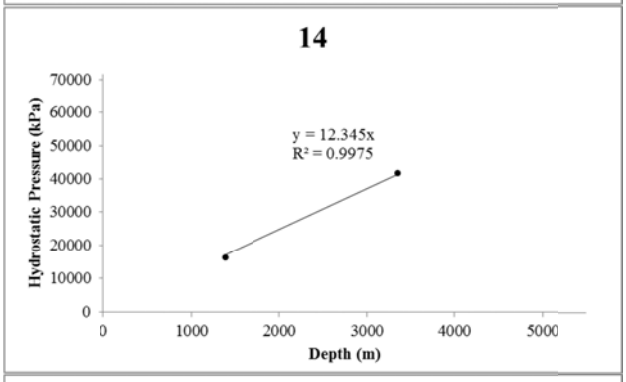
14
Hydrostatic Pressure (kPa)
Depth (m)
y = 12.345x
R² = 0.9975

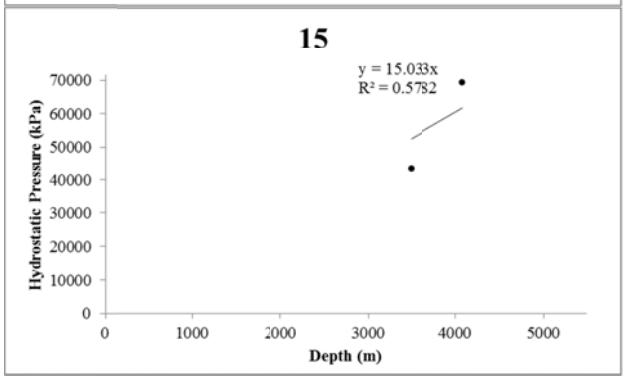
15
Hydrostatic Pressure (kPa)
Depth (m)
y = 15.033x
R² = 0.5782

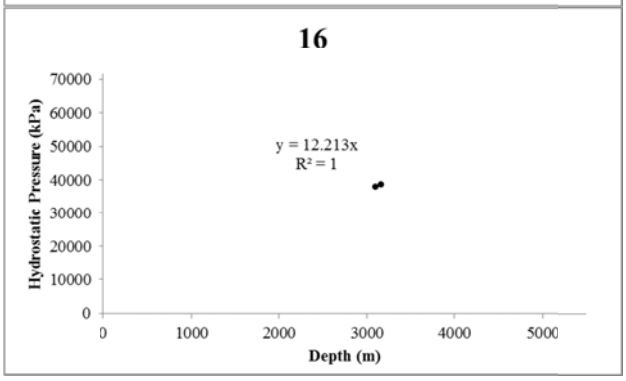
16
Hydrostatic Pressure (kPa)
Depth (m)
y = 12.213x
R² = 1

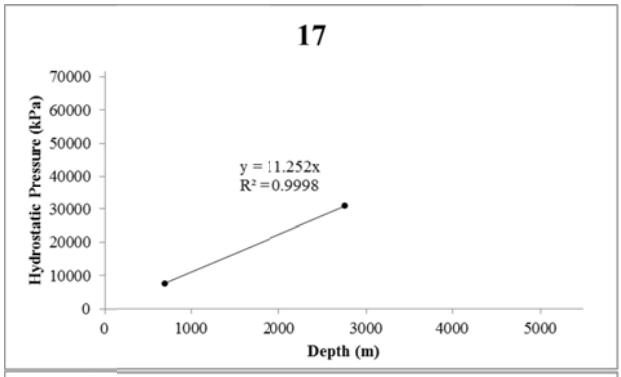
17
Hydrostatic Pressure (kPa)
70000
60000
50000
40000
30000
20000
10000
0
y = 11.252x
R² = 0.9998
0
1000
2000
3000
4000
5000
Depth (m)

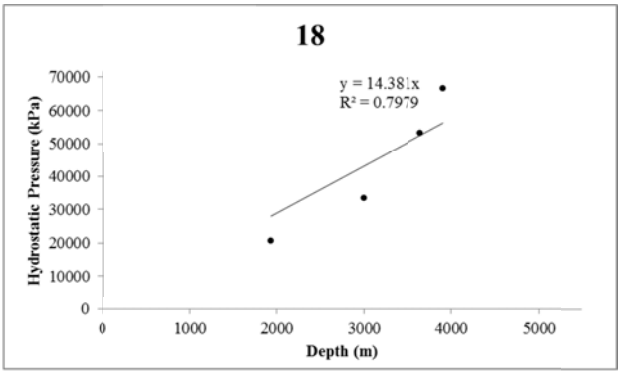
18
Hydrostatic Pressure (kPa)
70000
60000
50000
40000
30000
20000
10000
0
y = 14.381x
R² = 0.7979
0
1000
2000
3000
4000
5000
Depth (m)

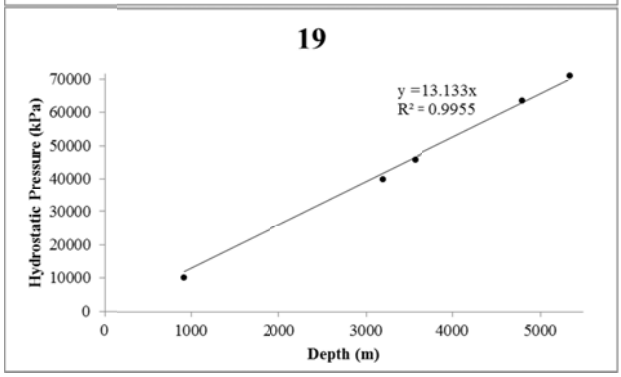
19
Hydrostatic Pressure (kPa)
70000
60000
50000
40000
30000
20000
10000
0
y = 13.133x
R² = 0.9955
0
1000
2000
3000
4000
5000
Depth (m)

Appendix F. Fluid chemistry of produced brines

a.

API	IDUSGS	LAT	LONG_	COUNTY	DEPTHSAMP	Depth (km)	ELEVATION	SPGRAV	pH	TDS
17111200530000	12987	32.7789	-92.5529	UNION	7900	2.41	230 DF	1.1	4.9	143108
17111024560000	13049	32.6498	-92.3552	UNION	7575	2.31	216 ES	1.2169		323785
17111024570000	13050	32.6504	-92.3519	UNION	8505	2.59	214 ES	1.1297		187816
17111009610000	17060	32.8383	-92.4034	UNION	3600	1.10	231 DF	1.0487	6.81	68445
17111007360000	17062	32.8846	-92.4304	UNION	2150	0.66	131 ES	1.044	7.05	60737
17111007520000	17063	32.8614	-92.4432	UNION	2161	0.66	180 ES	1.043	7	58449
17111008250000	17064	32.8454	-92.4497	UNION	2162	0.66	182 ES	1.042	7.24	57606
17111001560000	17066	32.9336	-92.2437	UNION	8235	2.51	200 DF	1.1697	6.38	230833

b.

API	HCO3	Ca	Cl	FeTot	FeAl2O3	KNa	Mg	Na	SO4	Si	CBE
17111200530000	37	14600	88700				1520	38011	240		-0.00923
17111024560000	131.43	37103	201082.99		-1	81699.02	3356.21		412.53		-45.515
17111024570000	136.69	19033	116259.69		-1	50233.24	1861.75		291.46		-49.7561
17111009610000	596	1290	41202	4			472	24667	194	20	0.008698
17111007360000	159	767	36906	12			282	22585	26		-0.01232
17111007520000	174	796	35488	15			270	21665	41		-0.01875
17111008250000	176	758	34974	11			262	21392	33		-0.0088
17111001560000	109	32332	143072	181			1404	53185	548		-0.07823

Fluid chemistry of brines produced by wells in Union Parish, LA (modified from Blondes et al. 2015), split into a and b for ease of viewing. The wells highlighted in gray have CBE greater than 5%.

Vita

Born and raised by two Clinical Psychologists in a village nestled against the city of Chicago, Tessa set out for the Liberal enclave of Oberlin College in 2005. A first-generation American on her mother's side, she graduated from Oberlin in 2009 with a Bachelor of Arts in Geology and a Minor in Japanese Language and Literature. After this, she completed a year-long Field Geologist Development Program with Horizon Well Logging, LLC, mud logging and geosteering across West Virginia and Pennsylvania. Promotion to a full-time remote geosteering position on the main corporate campus of Chesapeake Energy caused Tessa to put her plans for a Master of Science degree on hold, and allowed her to enjoy the urban lifestyle of Oklahoma City for nearly two years. In 2013 she left her geosteering position to move her life to Baton Rouge in order to work with Drs. Dutrow and Nunn on the research presented in this thesis and earn the degree of Master of Science in Geology.